# Atmospheric Imaging Assembly for the Solar Dynamics Observatory

Concept Study Report

Appendix A

AIA Science Plan

V. February 19, 2004
AIA Science Team

# Contents

## Overview

The Atmospheric Imaging Assembly (AIA) on the Solar Dynamics Observatory (SDO) is designed to provide an unprecedented view of the solar corona, taking images that span at least 1.3 solar diameters in multiple wavelengths nearly simultaneously, at a resolution of $\sim 1$ arcsec and at a cadence of 10 s or better. The primary goal of the AIA Science Investigation is to use these data, together with data from other SDO instruments and from other observatories, to significantly improve our understanding of the physics behind the activity displayed by the Sun's atmosphere, which drives space weather in the heliosphere and in planetary environments. The AIA will produce data required for quantitative studies of the evolving coronal magnetic field, and the plasma that it holds, both in quiescent phases and during flares and eruptions; the AIA science investigation aims to utilize these data in a comprehensive research program to provide new understanding of the observed processes and, ultimately, to guide development of advanced forecasting tools needed by the user community of the Living With a Star (LWS) program.

Solar activity is driven by the evolving magnetic field. Although the coronal magnetic field cannot be measured directly, much of the magnetic field within a few times $10^5$ km from the surface contains hot plasma that is dense enough to emit detectable levels of light. This plasma is (mostly) frozen onto the field lines, so that the emission from (or absorption by) the plasma outlines the magnetic field. The coronal plasma has a wide range of temperatures, emitting brightest at EUV and soft X-ray wavelengths. The brightness of that emission is a combination of local temperature and density, both of which exhibit very large contrasts with steep gradients perpendicular to the magnetic field. The contrasts in temperature and density exist down to the current best resolution of $\sim 1$ arcsec. A suitably designed imager with narrow thermal responses, such as the AIA, can use these contrasts to dissect the corona into complementary sets of high-contrast images for further analysis.

The AIA is designed to provide, for the first time, multiple near-simultaneous, high-resolution images of the corona covering a wide and continuous temperature range, with the aim to resolve the fundamental observational ambiguity between magnetic field evolution (evidenced by moving loops) and thermal and density changes in adjacent loop atmospheres that outline the magnetic field. To achieve this goal, the AIA images as much of the emitting coronal plasma as is feasible subject to physical and fiscal constraints, by providing the required

1. global coverage of the solar corona, with
2. observations at a wide and continuous range of temperatures,
3. at a cadence that enables the study of impulsive and explosive phenomena, with
4. adequate continuity to study gradual phenomena on time scales up to several weeks.

Achieving the primary investigation goal of understanding the physics of the solar atmosphere requires that the AIA science investigation *focus on the evolution of the observed plasma and inferred magnetic field through quantitative analyses of the observations and comparisons with models*.

The AIA Science Investigation includes the following elements:

- The AIA design is based on science requirements (as detailed in the AIA proposal LMSSC-P20017) that are compatible with the requirements formulated by the SDO Science Definition Team and the LWS Science Architecture Team. This design provides the following instrument capabilities:
  - Seven EUV and three UV-visible channels (listed in Table A1). Four of the EUV wavelength bands open new perspectives on the solar corona, having never been imaged or imaged only during brief rocket flights. The set of six EUV channels that observe ionized iron allow the construction of relatively narrow-band temperature maps of the solar corona from below 1 MK to above 20 MK.

- A field of view exceeding 41 arcmin (1.28 solar radii in the EW and NS directions), with 0.6 arcsec pixels.
- A detector full well $> 150,000$ electrons and $\sim 15$ e/photon, with a camera readout noise $\leq 25$ electrons.
- A sustained 10-s cadence during most of the mission.
- A capability to adjust the observing program to changing solar conditions in order to implement observing programs that are optimized to meet the requirements of specific scientific objectives. This allows, for example, a 2 second cadence in a reduced field of view for flare studies.[1]

These capabilities derive from requirements first formulated in the original proposal. They continue to be the consensus of the AIA science team, which met on October 30 and 31, 2003, to re-evaluate the proposed science after selection of the Investigation. The science requirements upon which these instrument requirements are based are discussed in some detail in the body of this report. We note that the instrument has significant heritage from the Transition Region and Coronal Explorer (TRACE), expanded and modified to allow observations of the global solar corona with nearly complete temperature coverage.

- AIA will obtain images in multiple EUV and UV pass bands. The basic observables are full-Sun intensities at a range of wavelengths. Together, these will comprise the data archive, which is freely accessible to the research community and, with limitations dictated by resources, to other interested parties. Derived data products, such as coronal thermal charts, maps of variability, and comparisons to HMI magnetograms and to (non-)potential field extrapolations will be made available regularly through the data-processing pipeline for a subset of the data for use in evaluation of the data and to aid the discovery of phenomena and cataloging of events. Software will be made available to researchers to create these data products for other datasets; a core library of easy-to-use, publicly-available software will be developed as part of the SolarSoft IDL environment to enable and support the investigations that are required to meet the primary AIA science goals.
- The data stream to be provided by the AIA must be analyzed and interpreted with advanced tools that permit
  1. quick and easy visual inspection of near real-time solar and space-weather data,
  2. rapid archiving and publication of summary results on the World-Wide Web,

[1] Note that during any special-mode observing, the regular full-Sun cadence will always be better than 30 s in order not to compromise the SDO science objectives, or the needs of the HMI, EVE, or other LWS programs, and that special observing modes will only be run in consultation with these programs.

Table A1: AIA wavelength bands.

| Channel name | Primary ion(s) | Region of atmosphere* | Char. $\log(T)$ |
|---|---|---|---|
| white light | continuum | photosphere | 3.7 |
| 1700Å | continuum | temperature minimum, photosphere | 3.7 |
| 304Å† | He II | chromosphere, transition region | 4.7 |
| 1600Å† | C IV+cont. | transition region + upper photosphere | 5.0 |
| 171Å† | Fe IX | quiet corona, upper transition region | 5.8 |
| 193Å† | Fe XII, XXIV | corona and hot flare plasma | 6.1, 7.3 |
| 211Å† | Fe XIV | active-region corona | 6.3 |
| 335Å† | Fe XVI | active-region corona | 6.4 |
| 94Å† | Fe XVIII | flaring regions (partial readout possible) | 6.8 |
| 131Å† | Fe VIII, XX, XXIII | flaring regions (partial readout possible) | 5.6, 7.0, 7.2 |

* Absorption allows imaging of chromospheric material within the corona; † in baseline program

3. convenient preliminary comparison with magnetic field measurements by the SDO HMI including field extrapolations based on those data, and
4. efficient searching of an up-to-date meta-data archive. This archive will be built up by a combination of continuously running automated feature-recognition software and of manually entered summaries of visual inspections within 12-24 hours of the receipt of the data.

The AIA investigation will provide catalog-search software, and interface capabilities to utilize the data and meta-data archives for scientific study (compatible with web use, in the context of, e.g., the Virtual Solar Observatory - VSO - and the Collaborative Sun-Earth Connector - COSEC).

- Some of the higher level AIA data products will be useful for the monitoring and forecasting of solar activity and resulting space weather. Some of these products are identified in this report; others are to be identified during the phase B in consultation with the full AIA science team and interested LWS partners. Meta-data products include filament and sigmoid developments, flares, field emergence, dimming, and other reconfigurations of the coronal magnetic field.
- This AIA science investigation plan identifies a broad range of science objectives that focus on the following five core research themes or objectives. The themes structure the AIA science investigation, and address the overarching questions formulated in the SDO Science Definition Team report [Table SFO-I in the original AIA proposal]:

  1. *Energy input, storage, and release: the 3D dynamic coronal structure, including reconnection and the effects of coronal currents.*
  2. *Coronal heating and irradiance: origins of the thermal structure and coronal emission, to understand the basic properties of the solar coronal plasma and field, and the spatially-resolved input to solar spectral irradiance.*
  3. *Transients: sources of radiation and energetic particles.*
  4. *Connections to geospace: material and magnetic field output of the Sun.*
  5. *Coronal seismology: a new diagnostic to access coronal physics.*

  These core themes encompass the broad range of investigations for which the AIA data are essential to advance scientific understanding, and to provide advanced warning of coronal and inner-heliospheric disturbances of interest to the LWS program, i.e., global change, space weather, human exploration of space, and technological infrastructure in space and on Earth. AIA also provides input data for accomplishing the objectives of the other SDO instruments, including, e.g., information on the coronal field configuration compared to that inferred from HMI data, and information on the sources of irradiance changes observed by EVE. The AIA investigation will carry out a set of the highest-priority studies throughout the mission, in close collaboration with other LWS colleagues, and present these results to the scientific community. The AIA team will, when possible, stimulate other research projects by pooling resources, organizing joint observations and analyses, and by optimizing the baseline for AIA observations.
- The international science team of AIA brings extensive heritage from Yohkoh, SOHO, TRACE, Solar-B, and STEREO, including experts in normal incidence optics, detector systems, image stabilization, instrument control, high-volume telemetry, and data archiving and access. The team includes investigators from Solar-B, STEREO, GOES, RHESSI, TRACE, SOHO, and IMAGE, as well as the ground-based SOLIS and the the new Swedish solar telescope. This ensures the coordination needed to follow events from Sun to Earth. The team's observational and theoretical expertise extends from the solar interior to the solar corona and beyond into heliospheric, geomagnetic, and ionospheric physics, irradiance modeling, and stellar activity.
- The real-time, continuous AIA images will be of great interest to the public at large, and data products

will be provided on the web and through suitable channels, including popular science magazines, press releases, posters, and movies supplied to museums and planetaria. A highly leveraged collaborative Education and Public Outreach (E/PO) program is a key part of the AIA investigation.

The breadth of the scientific problems to be addressed within the AIA investigation as part of the LWS program far exceeds what can be addressed by the AIA science team with the available funding. This document therefore also serves to identify core needs that the team intends to address to catalyze community research, while in parallel identifying the highest priorities for resources needed to let the investigation proceed most efficiently. These resources will have to be pursued separately by both the AIA team and the broader LWS community, in coordination with the mission teams within LWS.

Among the highest priority non-core projects needed to allow LWS scientists to make optimal use of AIA data we identify (1) methods for magnetic field modeling using both photospheric and coronal observations, (2) modeling of the coronal-heliospheric coupling, (3) the theory of coronal reconnection, and (4) field-instability modeling for flares and CMEs. These projects are too demanding for the AIA budget; the AIA science team recommends that LWS management consult their science community on how to best complement the SDO investigation with these theoretical and numerical programs.

This document summarizes the AIA science investigation. The following two sections describe and summarize the science investigation, and formulate the top-level requirements. The final four sections then describe the overall plans and requirements in more detail, separating the requirements for instrument design (including flight software), operations, data systems, and science infrastructure. The sections titles are:

1. Scientific goals and objectives
2. Implementation of the AIA science investigation
3. Summary of AIA science requirements on instrument design
4. Observing plans, and requirements on ground operations
5. Coordination with other instruments
6. Observations, data bases, and products, and requirements on data systems
7. Required science infrastructure and a science operations center concept

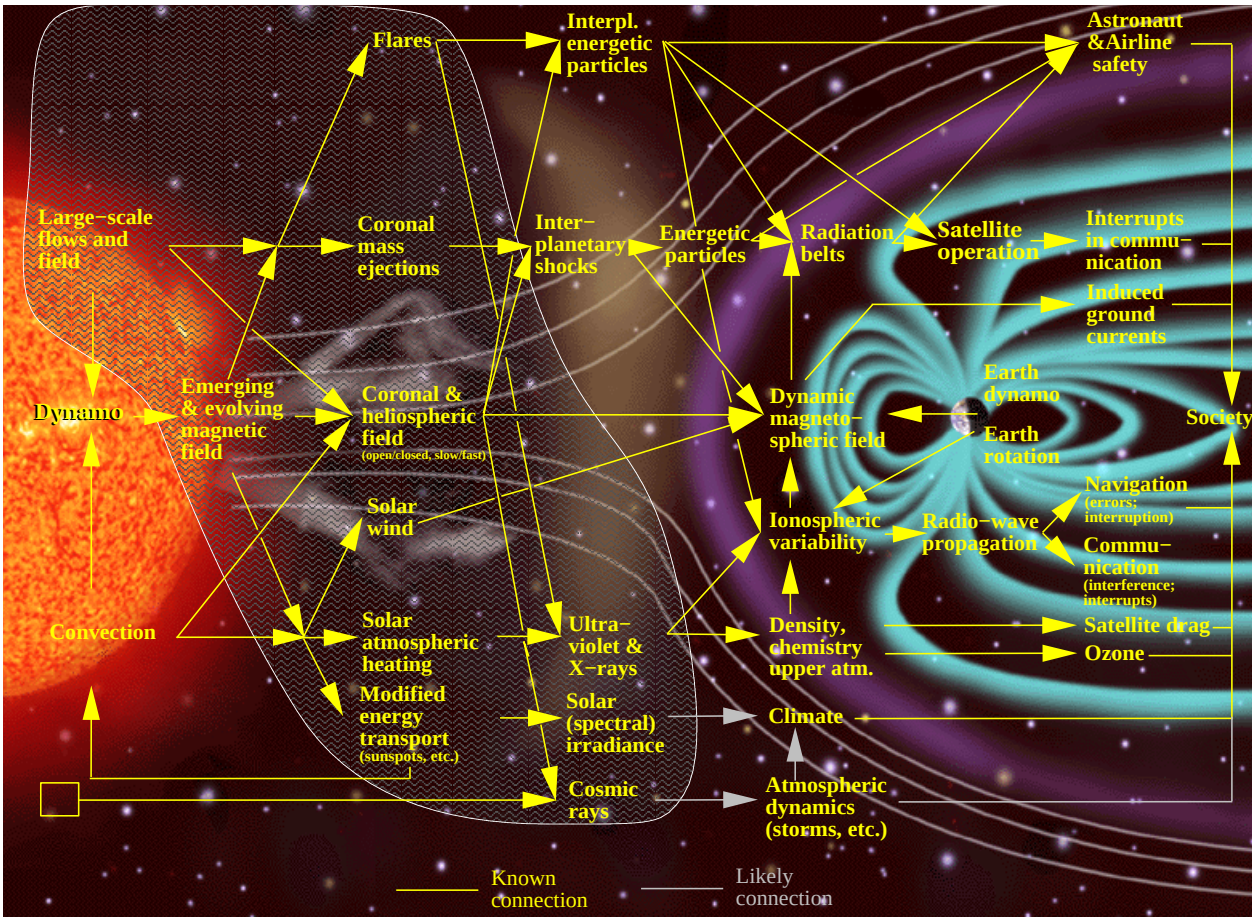


Figure A1: *Space weather involves a multitude of physical processes, some confirmed, some as yet speculative. The part of the web to which the AIA investigation contributes directly is outlined by a shaded area surrounded by a white contour: AIA contributions span the entire interface between the Sun and the Earth.*

## A1 Scientific goals and objectives

The primary goal of SDO is to understand the physics of solar variations that influence life and society. It achieves that goal by targeted basic research focused on determining how and why the Sun varies, and on improving our understanding of how the Sun drives global change and space weather. As one of the crucial instruments required to meet this goal, the AIA focuses on the evolution of the magnetic environment in the Sun's atmosphere, and its interaction with embedded and surrounding plasma. The science areas within the LWS program to which AIA contributes directly are highlighted in Fig. A1. By its crucial contribution to part of the mesh of linked science questions, AIA plays a key role within the entire LWS program.

The images of the corona taken by YOHKOH, SOHO/EIT, and TRACE have shown that all coronal structures evolve in density, temperature, and position on time scales as short as minutes. Conditions within coronal loop volumes and open magnetic structures appear to depend primarily on 'local' conditions, i.e., on conditions determined by the path of the field line, or loop, from end to end in the photosphere. This sensitive dependence, combined with the marked temporal evolutions of the atmospheres contained within loops and open-field regions on relatively short time scales, causes images to be dissimilar for different

band passes, even if their characteristic temperature intervals are rather small [1]. Added to the relatively slow thermal evolution, there is an abundance of waves, flows, and impulsive phenomena that occur on significantly shorter time scales of minutes or less.

The time scales on which the field itself evolves range from seconds to years. Slowest is the evolution of the largest-scale field. On shorter time scales, electrical currents that are induced in, and carried with, the magnetic field may build up over weeks or months, while release of those stresses may take only a fraction of a minute. YOHKOH and SOHO have shown, moreover, that there are no purely local field topologies: the short and long-term evolution of the corona is affected by both nearby and distant magnetic sources.

In view of these properties of the solar corona, the SDO Science Definition Team formulated requirements that the AIA must meet in order to understand the properties of the Sun's dynamic magnetic field and the coronal response to it. After matching these with feasible designs, the AIA team concluded that SDO must record both the surface magnetic field, using the HMI, and image the corona completely and accurately in space, time, and temperature. To achieve this, *the AIA provides the following essential capabilities*:

1. A view of the entire corona at the best feasible resolution compatible with SDO's constraints, providing coverage of the full thermal range of the corona, at a thermal resolution limited only by atomic physics, in order to have minimal line-of-sight confusion,
2. A S/N ratio for standard exposures that reaches 100 in optimal conditions, with a dynamic range of up to 10,000, and
3. Essentially uninterrupted viewing for at least months at a time at a temporal resolution of $\sim$10 s, and sometimes faster during energetic transient phenomena.

*These capabilities are met by our design* that includes

1. Four 20-cm, dual-channel normal incidence telescopes, that observe a 46 arcmin field of view in up to ten (E)UV channels,
2. Detectors with a full well of at least 150,000 electrons, with typically 15 e/photon, and a readout noise of 25 e, and data compression that is nearly lossless,
3. A standard baseline observing program running most of the time, while observing continuously from SDO's geo-synchronous orbit.

With these capabilities, AIA will, for the first time, enable us to observe the changing topology of the magnetic field even as the coronal plasma is changing in temperature. In its standard operating mode, the AIA images each area on the Sun 10$\times$ faster per wavelength than TRACE at twice the number of coronal channels, with a 16-fold increase in the number of imaged pixels. Compared with the full-disk SOHO/EIT, AIA runs at 700$\times$ their usual image frequency, with 16 times more pixels per image, in typically 8 instead of 4 channels. The AIA thus represents an increase in the information rate for coronal observations by a factor of 400 to 22,000.

The five broad research AIA themes that structure our science investigation and address the overarching questions formulated in the SDO Science Definition Team report are:

1. *Energy input, storage, and release: the 3D dynamic coronal structure.*
2. *Coronal heating and irradiance: thermal structure and emission.*
3. *Transients: sources of radiation and energetic particles.*
4. *Connections to geospace: material and magnetic field output of the Sun.*
5. *Coronal seismology: a new diagnostic to access coronal physics.*

Later sections in this Chapter describe the science rationale, research methodology, and required data and infrastructure. A summary is provided in Table A2. Note that this science plan describes all efforts needed to

fully exploit the scientific potential of the AIA instrument, including research efforts that are clearly beyond the scope of the limited AIA budget. We differentiate where necessary in the main text, and explicitly in the final column of Table A2 where 'core' and 'external' resources are listed separately.

This AIA Science Plan outlines how we envision the optimization of the observations, data products, and science investigation to achieve the SDO and LWS science goals. The subsequent subsections focus on high-priority tasks within each of the AIA Science Themes; subsequent sections take a higher level view of the integrated investigation and its expectations, requirements, and implementation.

## A1.1 Science overview

This Section discusses the objectives of the AIA science investigation. Each is broken up into four primary tasks, for which we discuss the major goals and significance, the technical approach and methodology, the science data requirements, the science team roles and responsibilities, and the required resources. In the latter category, we differentiate between 'core' resources that the AIA team will either pursue or strongly stimulate, and 'external' resources that are either developed by other teams or that will require investigations in parallel to the AIA core investigation. A summary of this section is given in Table A2.

### A1.1.1 Objective 1: Energy input, storage, and release; *the 3-D dynamic coronal structure*

All coronal activity relies on energy dissipation within the plasma contained in the Sun's magnetic field. One of the primary objectives of the LWS program in general, and of the AIA science investigation in particular, is to understand how energy is brought into the coronal field, how it is stored there, and how it is released. One key part of that objective is to understand the geometry of the magnetic field, and its evolution subject to external forcing and internal energy dissipation.

Plasma motions in and below the solar photosphere force the embedded magnetic field to move with the flows. These motions apply stress to the outer-atmospheric field on a broad range of spatial and temporal scales. This stress propagates throughout the outer atmosphere in the form of a variety of wave types and frequencies, as well as a broad spectrum of slower changes associated with evolving induced currents. How are these perturbations imposed upon the corona? How do they propagate? How do the electric currents close either within the atmosphere or through the photosphere?

TRACE observations reveal that the stresses that are applied to the coronal field by the photospheric motions lead to a magnetic field that is only moderately tangled on scales of the granular motions up to the largest scales, despite theoretical expectations that field-line braids should persist for long times in a coronal environment where reconnection was expected to proceed only slowly. Instead of a highly tangled field, however, TRACE images show that small-scale braids, driven by convective motions from the arcsecond scale of the granulation upward, are only seen around filaments and fibrils. Even then, the images suggest that loop twists rarely exceed about half a turn. This implies rapid dissipation of the induced currents, which is mimicked by some recent numerical simulations; the fidelity of these simulations does not approach the real corona yet, however, with anticipated (but maybe not realized) magnetic Reynolds numbers for the bulk of the coronal volume many orders of magnitude larger than in the simulated volume. In contrast to the apparently efficient smoothing out of the small-scale complexity, many filament configurations erupt, requiring substantial amounts of stored energy. Why do small-scale twists dissipate readily, whereas large-scale stresses persist for long times in filament and sigmoid field configurations which can eventually lead to instabilities?

W have identified the following **main tasks for Objective 1:**

1. **3D configurations of the solar corona**
2. **Mapping magnetic free energy**
3. **Evolution of the corona towards unstable configurations**
4. **The life-cycle of atmospheric field.**

Co-investigators Metcalf and Schrijver are responsible for coordinating this research objective.

**Task 1A: 3D configurations of the solar corona**

**Major goals and significance** At the core of all research of coronal activity lies the requirement to know the geometry of the magnetic field. How are photospheric flux concentrations of one polarity connected to their counterparts of opposite polarity? How much twist, writhe, and braiding exists between the two photospheric foot points? How does the mean field strength vary with height? Where are the separator structures between domains of connectivity and between open and closed field lines? Are there coronal null points, and what role do they play? What is the role of quasi-separatrix layers?

The study of the coronal field topology and connectivity relies in part on the ability to observe as much of the tracer emission as possible. Yet at the same time, we must utilize the thermal contrasts within the corona to keep the images less crowded in order to minimize line-of-sight confusion: multi-thermal imaging is essential. These observations will be complemented with stereoscopic methods and measurements of flow trajectories to determine the 3-D structure.

**Technical approach and methodology** Sets of EUV images will be combined to reconstruct temperature maps for temperature intervals with a range of about a factor of two (limited by the ionization intervals of the emitting iron ions; see Sect. A3.2). These temperature maps can be overlaid or blinked in sets to estimate the end-to-end connectivity of loops, in comparison with HMI magnetograms. The images can be used to quantify braids and twists within bundles of coronal structures. This provides a first assessment of the field topology, albeit subject to the line-of-sight confusion introduced by the projection onto the plane of the sky.

One way to incorporate the line-of-sight information unambiguously is to attempt full forward modeling of the solar corona, i.e., a combination of field extrapolation and loop-atmosphere modeling. This step clearly requires a better understanding of coronal heating and of the response of the solar atmosphere to that heating; this type of full forward model therefore requires significant advances in Objective 1 as well as 2.

Additional field information is derived by correlation tracking of irregularities in flows observed with AIA combined with spectroscopic line-of-sight velocity measurements made with SOLAR-B/EIS ("Doppler tracking"). If enough such measurements of vector velocities can be made along structures within the time scale on which the field evolves, we can establish the 3-D geometry independent of other measurements.

One approach that we will apply to reconstruct the true 3-D field geometry can be applied in the case of relatively slow changes: dynamic stereoscopy [2] relies on solar rotation to provide different perspectives. The AIA images can also be combined with true stereoscopic data from the STEREO/EUVI instrument which includes the same EUV wavelengths as SOHO/EIT. This will be pursued primarily by the STEREO team but, for high structures, will require deep exposures from AIA.

Coronal field strengths can also be measured by combining coronal images with microwave images at different wavelengths [3, 4, 5], obtained with the Very Large Array, the Owens Valley Radio Observatory, and the future Frequency Agile Solar Radio-telescope. The well-calibrated, multi-thermal AIA images will provide a major improvement to this technique, by allowing accurate determination of plasma parameters needed to calculate the expected free-free radio flux, which is subtracted from the observed flux to determine the field strength.

The inferred geometry is to be compared to field extrapolations (see below) in order to establish, e.g., the topology of the separatrices and the existence of coronal null points.

**Science data requirements** Required are full sets of the continuously acquired EUV images so that the full thermal range of the coronal plasma is visible. The large-scale coronal field is controlled by widely distributed sources. In order to establish the resulting field geometry, the AIA is designed to image the entire low corona (Table 1, Figs. A2). In combination with HMI (vector-)magnetograms and available coronagraph

images, these observations provide the information needed to improve our understanding of coronal field topology.

For dynamic stereoscopy, sequences of such images are needed that are continuous for up to a few days, at a cadence of at least one set per minute. Flow mapping requires the full 10 s cadence to map flows up to some 50 km/s without motion blurring or imaging gaps; higher speeds require higher cadences, up to 2 s for sonic motions at 5 MK. Combination with spectroscopic velocities requires coordination with Solar-B, while WL images are needed for co-alignment between SDO, Solar-B, and other instruments.

Combination with (space- or ground-based) H$\alpha$ images will complement the geometrical information derived from AIA data for filament configurations in order to help constrain the field direction and strength within and around filaments.

**Science team roles and responsibilities** J. Brosius (radio data as field proxies), P. Démoulin (force-free field extrapolations), A. Gary (field approximations, current determination), C. Keller (chromospheric magnetograms, H$\alpha$ images), T. Metcalf (field extrapolation), E. Priest (plasma physics, field topology).

**Required resources:**

1. Inversion codes to transform filtergrams into a complementing set 'thermal maps,' i.e., images as expected if the filters had response curves tuned to a single spectral line.
2. Field modeling codes, including force-free field models.
3. Field rendering and visualization codes.
4. Loop atmosphere modeling.
5. Global surface field model to properly deal with the large-scale structures.
6. Procedure to quantify the quality of the correspondence between a field extrapolation and loops seen in AIA images.
7. Calculations of null points and separatrices from magnetic field surface maps.
8. Codes for analysis of stereoscopic images (using either time delays between AIA observations or STEREO images).

We anticipate that items $1-6$ will be addressed by the AIA Co-I team (funded by AIA and other funds; note that item 4 is addressed primarily by Objective 2, and item 5 already exists for SOHO/MDI data), while the last two items need to be addressed in associated investigations.

## Task 1B: Mapping of magnetic free energy

**Major goals and significance** Eruptions within the coronal magnetic field tap into the available magnetic free energy, i.e. they are powered from the difference in total energy content of the corona between the actual and potential field configurations. Sites where major eruptions are likely to occur are indicated by sigmoids, filaments, field emergence into pre-existing active regions, and regions of field cancellation. All such configurations carry helicity, contain currents, and are consequently strongly non-potential.

Understanding where flares and coronal mass ejections are likely to occur requires that we are able to locate configurations with considerable non-potential energy within the coronal field by detailed comparison of models with observations, and to study their evolution. How much free energy emerges within active regions? How much free energy is built up by the photospheric stressing motions? How much survives reconnection? What role does the possible cascading of helicity between large and small scales play?

**Technical approach and methodology** To determine where magnetic free energy resides in the corona, the observed coronal configurations need to be compared to potential-field or linear force-free field models. The extent to which the helicity in the observed coronal field systems can be dissipated or transported out of the system determines whether a linear force-free or potential field model is more appropriate as the minimum energy state. Hence, quantifying the free energy will be the subject of both theoretical and observational efforts. A potential field model, with a heliospheric source surface [6], will serve as a first element in the field extrapolation to establish where significant current systems exist in the corona that affect the field configuration on the largest scales.

To quantify the free energy, we must apply detailed non-potential and MHD models. Non-potential modeling in part relies on vector field information that will come from SDO's vector-magnetograph, or from other observatories, including SOLAR-B's Solar Optical Telescope, the Advanced Stokes Polarimeter of the High-Altitude Observatory, and SOLIS and ATST of the National Solar Observatory. A complicating factor is that the non-force-free nature of the photospheric and lower chromospheric field causes significant effects in the coronal field [7]. The H$\alpha$ images obtained by SOLAR-B and SOLIS, and the SOLIS chromospheric magnetograms, will provide additional information to help us understand the transition of field from photosphere to corona through the non-force-free environment of the lower atmosphere.

Our team will develop and evaluate several approaches to determine the current systems responsible for the observed coronal structure in non-potential situations. A semi-empirical generalization towards non-potential fields will be made by volume transformations of the field to match observed structures [8]. Advanced MHD modeling, proceeding on a parallel research track with separate funding, will be applicable by combining HMI, Solar-B, or SOLIS vector-magnetogram sequences with MHD modeling of the coronal field and subsequent visualization techniques to made the model results comparable to AIA observations. Evolution of magnetic helicity will also be a research goal as we compare temporal changes in the helicity determined from the coronal field models with energy and helicity fluxes across the photospheric boundary derived from HMI data.

**Science data requirements** Sequences of vector-magnetograms and photospheric flow maps are to be used as input to MHD models. Complete sets of AIA EUV images are needed to compare to model results. Complementary H$\alpha$ images (from, e.g., Solar-B or SOLIS) will aid the analysis in case filament configurations are studied; if these are not available, the bound-free absorption in the H and He continua seen in the 171 Å and 193 Å images for filaments sufficiently far from disk center also provide information.

**Science team roles and responsibilities** A. van Ballegooijen (surface-field and MHD modeling, including filaments), P. Démoulin (force-free field extrapolations), A. Gary (field approximations, current determination), N. Hurlburt (field modeling), C. Keller (chromospheric magnetograms, H$\alpha$ images), A. Kosovichev (flow fields), P. Martens (filament evolution), Z. Mikic (MHD modeling of coronal field), T. Metcalf (field extrapolation, evolution of helicity and free energy).

**Required resources** Once the field geometry has been established in Task 1A, this task requires multiple force-free and non-force-free models of the lower-atmospheric magnetic field to derive reference field configurations. For relatively large-scale structures, these field extrapolations need to be based on a global model for the surface magnetic field (including data assimilation) combined with source-surface modeling to study the coupling of the coronal field to distant areas and to the heliosphere. This global surface field model exists for MDI assimilation [9], and will be converted to HMI data when these become available.

Parallel research efforts will be stimulated to develop more general (non-linear) force-free extrapolations as well as comprehensive MHD models. Co-I's in Europe [10] and in the U.S. [7, 8, 11, 12], are dedicated

to optimizing their models for the AIA investigation.

Visualization tools will be employed to compare model and observation.

H$\alpha$ images from Solar-B, SOLIS, or other observatories are useful as additional constraints to the field geometry.

**Task 1C: Evolution of the corona towards unstable configurations**

**Major goals and significance** A key ingredient in our ability to forecast solar activity and space weather is adequate understanding of how stresses can develop in certain field configurations, even as reconnection and dissipation of currents counteracts the buildup of such stresses. Reconnection occurs unexpectedly fast in the solar corona, as witnessed, for example, by the lack of small-scale tangles or braids in the coronal loop configurations (discussed in Task 1A, p. 12). Observations by TRACE, EIT, and SXT reveal that connections between distant active regions form within hours of emergence of new magnetic flux, with no photospheric motions forcing oppositely-directed fields together. Reconnection occurs readily when field emerges within, or adjacent to, an active region and appears to be especially efficient at coronal null points. Many of these phenomena have been observed at relatively cool coronal temperatures (including the 171, 195, and 284 Å channels of SOHO/EIT and TRACE).

An example of reconnection in the high corona was discovered by Yohkoh/SXT observations of flows among the cusped structures above post-eruption arcades, interpreted as reconnected magnetic fields downstream of large-scale current sheets [13, 14]. Their extent is $\sim 10 - 30$ Mm, with a temperature above 10 MK, and downward velocities that may exceed 500 km/s. The two high-temperature channels of AIA will image these structures and the outflows at unprecedented spatial and temporal resolution, and may shed light on the patchiness of reconnection in the sheet, suggested by the strong intermittency of hard X-ray and radio emission [15, 16]. Moreover, AIA will have an excellent opportunity to observe any inflows into the current sheet region that may occur at much lower temperatures [17].

Under what conditions does reconnection most readily occur? What determines how stresses and currents are dissipated at a range of scales? Why do certain stressed configurations survive for a long time whereas others disappear or do not even build up as reconnection relaxes stresses?

The twists and linkages of the coronal magnetic field, measured by the magnetic helicity, present important aspects of this study. Helicity is a globally quasi-conserved quantity but it can be redistributed through the coronal field during reconnections. The realistic magnetic field models produced using AIA data will enable new understanding of the properties of helicity transport and evolution. Knowledge of the helicity of the coronal field (often measured relative to a potential field configuration) therefore allows us to better understand and forecast how changes in one field configuration are associated with sometimes distant other changes that together conserve total relative helicity.

How does helicity evolve within the solar corona? Magnetic helicity is injected into the corona mainly by emerging flux, but also by shearing flows [18, 19]. It then somehow cascades to large scales to form magnetic structures like sigmoids [20] and filaments. Helicity is ultimately removed by flux retraction, coronal mass ejections (CMEs), filament eruptions, and redistribution during reconnection of opposite helicity regions. Helicity studies require the continuous, full-Sun observation of the evolving coronal field linkage at the spatio-temporal resolution offered by AIA, in combination with the HMI measurements of the flux of magnetic helicity and energy through the photosphere.

**Technical approach and methodology** Quantitative empirical constraints including topological change, speed of field lines, intermittency of reconnection vs. smooth evolution, and amounts of dissipated energy will help test the various reconnection theories [21].

Large-scale helicity evolution will be studied by observing quiet-Sun and intra-region filaments in absorption in the EUV, as well as in the He II 304Å channel, and sigmoids in the hotter (335Å and 94Å) coronal channels. We expect that the large field of view and high cadence of AIA will reveal field geometries like those associated with filaments but that are not traced out by chromospheric material. This expectation is based on TRACE data that occasionally provide tantalizing glimpses of such fields by fleeting brightenings that move so fast that their motions are generally blurred; AIA observations will be much better suited to studying these phenomena.

**Science data requirements** At present, studies of reconnection are hampered by the continual thermal evolution of plasma. This causes structures to fade from a band pass in typically minutes to tens of minutes in quiescent states [1] and much faster in transients. The wide thermal coverage by AIA will distinguish between correlated thermal evolution of adjacent loops and true geometric evolution of the magnetic field. Combining that with AIA's large field of view and dynamic range, we will be able to map a much larger fraction of the field than is possible now.

Forecasting of solar transients requires understanding of the evolution of the coronal field towards unstable configurations by stresses induced at the solar surface. Continuous photospheric (vector)magnetograms and photospheric flow fields (from HMI, ground-based SOLIS, or - for part of the disk -SOLAR-B) in combination with AIA coronal imaging will enable us to map both the magnetic shear and magnetic neutral lines over the full disk at HMI's 1-min cadence, and to estimate the work applied to the coronal field and the injection of field into the corona. Field models (described above) can then be compared with these observations to study the rate at which magnetic free energy is injected and removed; these comparisons will be even more valuable if chromospheric vector magnetograms are available [22].

**Science team roles and responsibilities** A. van Ballegooijen (surface-field and MHD modeling, including filaments), N. Hurlburt (field modeling), A. Kosovichev (flow fields), P. Martens (filament evolution), Z. Mikic (MHD modeling of coronal field), E. Priest (plasma physics, field topology), N. Weiss (theoretical modeling of field-flow interactions). T. Metcalf (helicity and energetics of the coronal field).

**Required resources** This task requires the same tools as those mentioned under tasks 1A and 1B. In addition, we need to be able to study the evolution of the field, both in observations (by analyzing image sequences), and in models. This type of modeling needs to explicitly include the field evolution, and thus must use, e.g., MHD or magneto-frictional methods. Such high-fidelity models are being developed for programs such as Solar-B and under research grants (e.g., the SAIC coronal MHD model).

### Task 1D: The life-cycle of atmospheric field

**Major goals and significance** Dynamo-generated field can leave the solar solar atmosphere either by retraction or by expulsion. The retraction of flux (and its helicity) with a preferential orientation may be essential for a Babcock-Leighton type dynamo [23]; its study is thus important in answering the question why the Sun varies. It remains unclear where and how much flux subducts: after decades of study, observational limitations still have not allowed us to determine how much flux retracts within an active region relative to what disperses away into the large-scale field pattern that determines the global appearance of the corona and the heliospheric field. How does buoyant field manage to subduct? How important is reconnection in this process?

Expulsion of field and helicity from the Sun affects the heliospheric field [24, 25, 26]. What role does the expulsion of flux play to both the dynamo and to the heliospheric field? Are flux and its helicity expelled only during eruptive processes, or also during the more gradual quiescent field evolution?

**Technical approach and methodology** While SOLAR-B will study field evolution on active-region scales, the combination of AIA and HMI is uniquely suited for the study of flux disappearance from the entire Sun by allowing us to track the field's 3-D evolution in detail. AIA data will be used to study the evolving connections within the solar atmosphere. They will show us the atmospheric processes as photospheric footpoints are brought together by surface flows. If atmospheric loops form between them, and decrease in size as the footpoint separation decreases, we can infer that flux retracted. If the footpoints appear to remain unconnected as flux concentrations of opposite polarity approach each other, a case can be made that the field is actually expelled. In the latter case, we should see substantiating evidence in the behavior of the surrounding field. The diagnostic techniques to map helicity as part of task 1B can be used here also to study the evolution of helicity within the field.

**Science data requirements** Required are full EUV wavelength sets at a 10 s cadence to follow the evolution of the field as it reconnects in response to the changing boundary conditions in the photosphere. Co-temporal (vector-)magnetograms should be obtained at a cadence not less than once every few minutes, compatible with the standard HMI observing mode. Supplementing H$\alpha$ observations will aid the evolution of field connections close to the solar surface.

**Science team roles and responsibilities** N. Hurlburt (field modeling), P. Martens (filament evolution), Z. Mikic (MHD modeling of coronal field), A. Title (observational studies).

**Required resources** Resources as under 1B: field-extrapolation

### A1.1.2 Objective 2: Coronal heating and irradiance: *thermal structure and emission*

Solar radiation at UV, EUV, and SXR wavelengths plays a significant role in the determining the physical properties of the Earth's upper atmosphere. Variations in solar radiation at these wavelengths drive changes in the density and ionization of the Earth's thermosphere and ionosphere, impacting the performance of ground-based communications systems and spacecraft in low-Earth orbit. Long term observations of the solar irradiance with the required accuracy have proven difficult, however, and much of our knowledge of the solar irradiance and its variability remains uncertain.

As is illustrated in Figure A2, observations over the past several decades have clearly established that solar variability at UV, EUV, and SXR wavelengths is tied to the variability of the Sun's surface magnetic fields. Past studies of the Sun and Sun-like stars has revealed that the primary determinant of the radiation leaving the corona is the total magnetic flux threading the photosphere [27].At present, however, we do not possess a detailed understanding of how magnetic energy is released within the solar corona. Thus we cannot use our knowledge of the Sun's magnetic fields to model and predict changes in the solar irradiance. Such calculations are an invaluable aid to interpreting and extending direct measurements of the solar irradiance. One of the primary objectives of the SDO mission is to develop a physical understanding of solar irradiance and its variability, specifically at (E)UV wavelengths. We propose to address this objective with the following tasks.

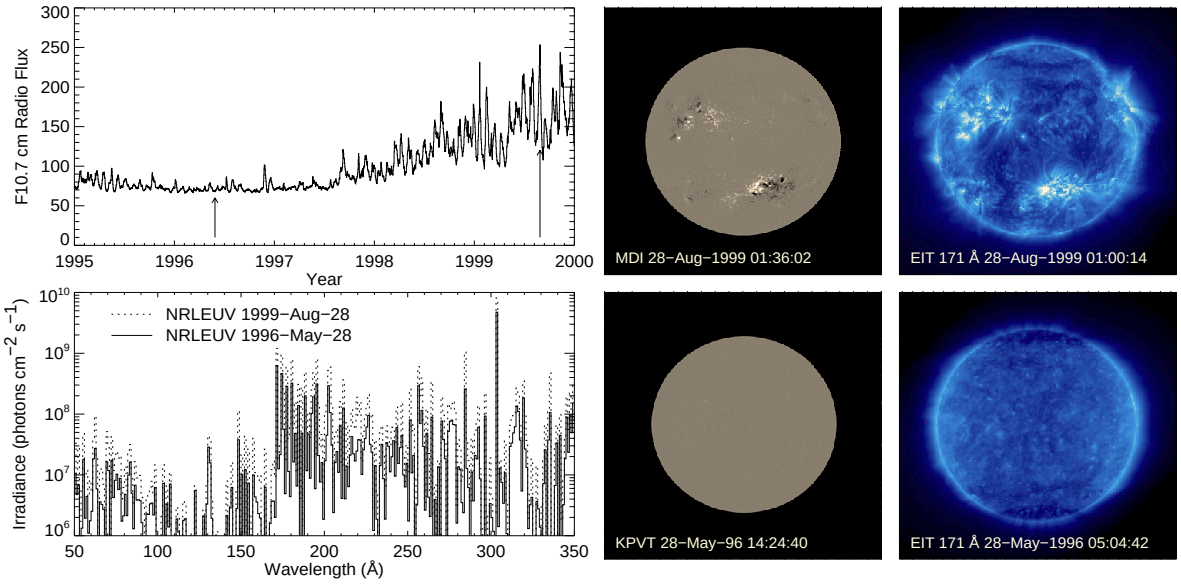


Figure A2: The Sun at solar maximum and solar minimum. (*top left*) The F10.7 cm radio flux during the rising phase of the current solar cycle. (*right panels*) EIT 171 Å images and full-disk magnetograms for August 28, 1999 and May 28, 1996. The images have been corrected for changes in instrumental response and are scaled the same way. (*bottom left*) Irradiance spectra at 1 Å resolution calculated with the NRLEUV irradiance model for these dates.

**Main tasks for Objective 2:**

1. **Identify the solar features that drive changes in the solar irradiance**
2. **Characterize the physical properties of coronal structures**
3. **Develop physical models of loop atmospheres**
4. **Construct physical models of the solar (E)UV irradiance with predictive capability**

Co-investigators Warren and Martens are responsible for coordinating this research objective.

**Task 2A: Contributions to solar (E)UV irradiance by types of features**

**Major goals and significance** Solar active regions are the primary driver of changes in the solar irradiance at UV, EUV, and soft X-ray wavelengths. Thus the solar irradiance at these wavelengths is modulated primarily by the Sun's 11-year solar activity cycle and the Sun's 27-day rotational period. Solar active regions, however, are highly complex, evolving over many different spatial and temporal scales. The contribution of an active region to the solar irradiance changes as the active region evolves.

Other solar features can also have important consequences for irradiance variability. For example, [28] demonstrated that the contribution of active regions alone was not sufficient to account for the observed variability in the hydrogen Lyman $\alpha$ line. They determined that an enhanced, or "active," network component, formed from the fragments of decaying active regions, was also required to reproduce the variability over both solar rotational and solar cycle time scales. This "active network" component is broadly dispersed over the solar disk so it contributes more significantly to longer term (solar cycle) variations than to solar rotational modulations in the irradiance. This effect has not been extensively studied at other wavelengths

and temperature regimes. Other features, such as coronal holes or bright points, also contribute to irradiance variability, but the nature of their contributions have not been studied in sufficient detail. The AIA He II 304 Å and UV channels will will be used for studying the evolution of chromospheric and transition region structures such as the network. He II 304 Å is the strongest emission line in the EUV and is particularly important for understanding the conditions in the thermosphere and ionosphere.

During flares short-lived ($< 1$ day) but enormous surges in solar EUV emission occur that have a significant impact on the Earth's atmosphere [29].AIA's high temporal resolution permits the accurate measurement of these surges, and its high spatial resolution the precise determination of their locations.Since EUV flare emissions regularly surpass the EUV output of the rest of the Sun, absolute calibration with the help of EVE data will by relatively straightforward.Measurement and analysis of EUV flare emissions will be a routine AIA task, automated to a high degree through the use of threshold-based flare flags, which have been successful on Yohkoh-SXT and TRACE.

**Technical approach and methodology** The broad temperature coverage of the AIA coupled with simultaneous EUV irradiance measurements from EVE will provide an unprecedented opportunity to study the origins of solar (E)UV irradiance variability at many different spatial and temporal scales. The first step in this analysis will be to convolve the EVE MEGS-A irradiance spectra, which cover the wavelength range of 50–370 Å, with the relevant AIA spectral responses. This will allow us to cross-calibrate the AIA and EVE at the wavelengths where they overlap.

The AIA UV channels will not overlap with the EVE MEGS-B channel, which covers the wavelength range of 350–1050 Å. MEGS-B, however, will observe emission that is formed at similar temperatures to the emission seen in the AIA UV channels, and it will be possible to study relative irradiance variability with these channels and the EVE measurements. Absolute calibration of the AIA UV channels may be possible through direct comparisons with observations from the SOLSTICE instrument on SORCE. SOLSTICE covers the wavelength range from 1150 Å to 3200 Å with a spectral resolution of 10 Å. SORCE was successfully launched in January of 2003. A six-year SORCE mission would provide for some overlap with the operation of the AIA. It should also be possible to calibrate the AIA UV channels indirectly using empirical models derived from the SOLSTICE UARS data.

Comparisons between the absolutely calibrated EVE irradiance measurements and the spatially resolved AIA images will allow us to study the origins of irradiance variability in detail. We will analyze the AIA images using both intensity distributions, or histograms, as well as feature identification and tracking techniques. Histogramming methods involve decomposing intensity distributions into their constituent components and tracking the evolution of these components. [30] and [31], for example, have used histograms derived from Ca II K-line images to model photospheric, chromospheric, and transition region emission. In these studies, intensity histograms were decomposed into a single Gaussian component, which represented the quiet Sun, and a high-intensity "tail," which accounted for solar activity.

We will also attempt to identify and track individual features, such as active regions, bright points, and coronal holes. These identifications will be based on intensity thresholds and feature continuity. We will compare the variability of these features with the variability determined from the histograms and the EVE irradiance measurements. These studies will provide essential information on which solar features contribute strongly to irradiance variability. With this knowledge we can turn to the problem of developing physical models for these features.

**Science data requirements** For this task we will require full-resolution, full-disk AIA images in all in all bandpasses at a cadence of at least several per day. These images must be complemented by fully calibrated, simultaneous EVE MEGS-A and MEGS-B irradiance measurements.

In order to understand the origin of changes in coronal radiation, we must characterize the evolving thermal structure of the corona with adequate spatio-temporal resolution. AIA will identify sources of variation in the full-Sun spectra observed by SDO's SIE and by the XUV Photometer System, XPS, on the SORCE satellite of the NASA Earth Science Enterprise. AIA's wavelength set allows accurate determination of the amount of material at all coronal temperatures from about 0.7 MK up to 20 MK (i.e., it allows the determination of the differential emission measure, see Fig. A5; [32]). To achieve this goal, the temperature coverage is made as complete as atomic physics and technologically feasible passbands allow. The 10-s cadence is essential to following the evolution of flare plasma.

The lower-temperature channels are also important for irradiance studies: the broad band UV channel is a proxy for chromospheric variability, while the He II 304Å line is the strongest emission line below 1200Å and thus crucial for the study of irradiance variations driven by the transition region.

**Science team roles and responsibilities** B. De Pontieu (chromosphere-corona interface), P. Martens (thermal analysis, modeling, prediction), C. Schrijver (radiative loss modeling, sun-as-a-star studies), R. Shine (image processing, object tracking), and H. Warren (irradiance modeling, spectroscopy).

**Required Resources** Completing this task will require a comprehensive understanding of the AIA spectral response and how it changes with time. Proper flat-fielding and scattered light corrections will also be important. This task will also require the development of software tools for feature recognition and tracking in the AIA images.

**Task 2B: Physical properties of irradiance-modulating features**

**Major goals and significance** Once we have identified the structures that give rise to global irradiance variations – loops in Active Regions, the EUV background of Active Regions, coronal holes, and/or the active network – the AIA complement of bandpasses provides a unique opportunity to characterize the emitting plasma of these structures with unprecedented thermal resolution. The AIA's sequence of bandpasses of coronal iron lines leaves no significant gaps in the thermal coverage of the coronal plasma, and hence a reliable per-pixel thermal structure (summarized in the DEM, or differential emission measure) of each can be determined.In the absence of stereoscopic observations these per-pixel DEM's will provide the most complete characterization of the coronal plasma ever obtained. With the help of STEREO observations an even better 3D description can be derived, although not with the same spatial, temporal, and thermal resolution.

The per-pixel thermal-structure studies possible with AIA will represent a significant improvement over previous efforts to study coronal heating. Current instrumentation results in separate intensity distributions for active regions and quiet Sun that are largely disjoint in energy range [33, 34, 35], so it is unclear whether they form a single continuous distribution. Moreover, the detailed shapes of these distributions are quite sensitive to corrections for instrumental limitations.As a result, extrapolations of the frequency distributions remain too uncertain to establish the relative importance of small events to the total heating. With a precision limited essentially only by photon noise, the AIA will measure flares at smaller energies than ever before and trace thermal variations with unprecedented accuracy.

To fully characterize the physical properties of the corona we must also identify the local magnetic topologies that are associated with various solar features. Of particular importance is the evolution of non-potential fields that give rise to coronal heating. This task will make extensive use of the magnetic field modeling results from Objective 1.

**Technical approach and methodology** The AIA team will analyze regular sequences of nearly simultaneous full disk images in all AIA's passbands to locate and categorize the various EUV emitting structures.This repetitive task will be automated as much as possible using feature recognition software such as the loop tracking code described in more detail further on. Once the locations of the EUV emitting features have been determined in all passbands, and their overlap verified, our automatic DEM fitting, also described below, will determine the best per-pixel DEM fits for the selected features.

While the analysis steps to be taken and the basic software tools to be developed are quite transparent at this point, the development of a completely automated sequence for the DEM measurement of the relevant features must rely on a trial-and-error approach employed in the initial phases of the mission.

**Science Data Requirements** For this task we will require full-resolution AIA images in all in all bandpasses at a cadence of approximately 60 s. These data must be complemented by simultaneous, full resolution HMI observations at a comparable cadence.

**Science team roles and responsibilities** J. Brosius (spectroscopy), B. De Pontieu (chromosphere-corona interface), A. Fludra (spectroscopy), L. Golub (spectroscopy, coronal physics), J. Gurman (coronal physics), D. Hassler (spectroscopic constraints), J. Lemen (coronal physics), P. Martens (thermal analysis, modeling, prediction), A. Nordlund (MHD modeling), C. Schrijver (radiative loss modeling, sun-as-a-star studies), R. Shine (image processing, object tracking), and H. Warren (irradiance modeling, spectroscopy).

**Required Resources** To make this type of characterization a routine analysis tool the AIA team will develop a thermal analysis tool (a spectral inversion code to reconstruct the contributions from each temperature to the overall signal). For an identified structure observed in all AIA passbands, this program will produce for each pixel the differential emission measure, DEM, that best fits the background subtracted emission and calculate its accuracy, according to a selectable criterion.A prototype of such a code has already been demonstrated at the October 2003 AIA science meeting.

A second tool will be used for isolating the pertinent physical structures, loops in particular: a loop tracking code, described in more detail in Section 6.5.1 will interactively find the outline of coronal loops for each AIA passband and determine their overlap (or lack thereof).

Finally, we will utilize the magnetic field-line modeling and mapping tools developed for Task 1 to study the relationship between coronal heating events and the topological evolution of the magnetic field.

**Task 2C: Physical models of the irradiance-modulating features**

**Major goals and significance** With the best obtainable physical characterization of the EUV variable coronal structures in hand, the next logical step that the AIA science team will take is the comparison with the predictions of physics based models for such structures.The basic idea is to use local magnetic field extrapolations combined with time dependent MHD and hydrodynamic simulations to reproduce the topology, morphology, and thermal and density structure of the coronal structures under study.

**Technical approach and methodology** The AIA images will be compared with MHD computations of coronal heating, that are even now approaching the fidelity required for detailed loop-to-loop comparisons [36, 37, 38].The observations will thus enable us to deduce which coronal heating mechanism are most consistent with observations. Moreover, AIA observations will be compared with Solar-B and SOLIS

observations of the chromosphere to elucidate the puzzling lack of correlation between chromospheric and transition-region brightness patterns on small scales [39].

**Science Data Requirements** This task will not require additional data.

**Science team roles and responsibilities** J. Brosius (spectroscopy), B. De Pontieu (chromosphere-corona interface), A. Fludra (spectroscopy), L. Golub (spectroscopy, coronal physics), J. Gurman (coronal physics), D. Hassler (spectroscopic constraints), J. Lemen (coronal physics), P. Martens (thermal analysis, modeling, prediction), A. Nordlund (MHD modeling), C. Schrijver (radiative loss modeling, sun-as-a-star studies), R. Shine (image processing, object tracking), and H. Warren (irradiance modeling, spectroscopy).

**Required Resources** To facilitate this task the AIA team will develop a suit of software tools that can be used independently or in combination to complete elements of the modeling task described above.These tools include hydro-dynamical field line (or loop) modeling codes, time-dependent MHD codes, and a number of magnetic field models (potential, nonlinear, time dependent, and prominence specific), described in more detail in Section 6.5.2.

**Task 2D: Physics-based predictive capability for the spectral irradiance**

**Major goals and significance** Once we have developed a physical understanding of the coronal heating mechanism and the relevant magnetic topologies we will be able to calculate solar irradiances using global models of the Sun's magnetic fields. Furthermore, we will be able to extend this irradiance model to allow for near-term forecasts of solar (E)UV irradiances.

**Technical approach and methodology** We will combine physical models of coronal heating with global models of the solar magnetic field to calculate the temperature and density everywhere in the corona. These parameters will be combined with a database of atomic physics parameters, such as CHIANTI [40], to calculate the line intensity for optically thin emission. Spectral irradiances are then determined by the integration along a line of sight. Optically thick emission will need to be treated with radiative transfer models or by making empirical adjustments to the calculated irradiances.

Future irradiances can be calculated with this physics based model in several different ways. The simplest method is to simply change the line of sight to account for solar rotation. This method represents a simple extrapolation of the available magnetic field data. This approach can be modified to incorporate the evolution and emergence of active regions detected with far-side helioseismology. A more sophisticated approach to predicting near-term irradiance variability is to use statistical models of magnetic flux transport and emergence to make short term projections of how the coronal magnetic field may evolve. The feasibility of these projected irradiance models will depend upon how what type of magnetic field data is required for the global magnetic field models. Global magnetic field models that rely heavily on vector magnetograms, for example, may be be difficult to forecast or model in a statistical way.

**Science Data Requirements** This task will require extended time series of irradiance observations and corresponding magnetic field measurements for model testing and validation.

**Science team roles and responsibilities** J. Brosius (spectroscopy), B. De Pontieu (chromosphere-corona interface), A. Fludra (spectroscopy), L. Golub (spectroscopy, coronal physics), J. Gurman (coronal physics), D. Hassler (spectroscopic constraints), J. Lemen (coronal physics), P. Martens (thermal analysis, modeling, prediction), A. Nordlund (MHD modeling), C. Schrijver (radiative loss modeling, sun-as-a-star studies), R. Shine (image processing, object tracking), and H. Warren (irradiance modeling, spectroscopy).

**Required Resources** In addition to the coronal heating models and local magnetic field models described in Tasks 2B and 2C, this task will require global models of the magnetic field, such as the potential-field source-surface model developed by members of our team at LMATC.

### A1.1.3 Objective 3: Transients:
*sources of radiation and energetic particles*

Most of the time, the coronal field appears to evolve smoothly. At times, however, massive explosions or eruptions rock the coronal field. Many are not strong enough to rupture the encapsulating coronal magnetic field, and only the energetic radiation escapes towards Earth. Some, however, are associated with opening magnetic fields into the heliosphere; these coronal eruptions appear to be the counterparts of coronal mass ejections. What triggers the eruptions or explosions? What determines whether the field confines the eruption to the corona or allows coupling into the heliosphere?

Flares, CMEs, filament destabilizations, sprays, and other transients are sources of radiation and energetic particles, and therefore prime drivers of violent solar weather. Transients result from the sudden conversion of magnetic energy into bulk, thermal, and non-thermal energy as magnetic field reconnects. Theories of 3-D reconnection [41, 21] are still in their infancy, and advances in its understanding are hampered by observational limitations.

AIA is designed to make the next leap forward in understanding transient initiation and evolution. Its high-cadence, full-disk, multi-temperature observations will reveal the reorganizing field in the initial phases of flares and of filament eruptions, as well as the later evolution as the field relaxes into its new state. Particularly promising is the inclusion of four EUV pass bands that will observe the evolution of the coronal plasma for the first time at arcsecond resolution for temperatures between 3 to 15 MK (94, 133, 211, and 335Å).

**Main tasks for Objective 3:**

1. **Unstable field configurations and initiation of transients**
2. **Evolution of transients**
3. **Early evolution of CME's**
4. **Particle acceleration**

Co-investigators Nitta and Golub are responsible for coordinating this research objective.

**Task 3A: Unstable field configurations and initiation of transients**

**Major goals and significance** We still do not know what type(s) of instability are involved in the rapid reconnection that we associate with solar transients. In fact, we do not even know what types of field evolution are involved in what types of transients: flux emergence, field shearing, and the evolution of distant, stabilizing fields all appear to be involved, and because they often go hand in hand, it has proven difficult to identify the key processes that would point the way to identifying the instability criteria. The

field evolution is further complicated by the potential role of helicity, either the redistribution of helicity within the corona or the injection of new helicity upon flux emergence.

Theory predicts the likeliest site for rapid reconnection to be at discontinuities of magnetic field linkage, i.e., at separatrices and their intersections, the separators. In order to understand the nature of the instability, it is important to monitor the areas around these magnetic field discontinuities well before the transient and to capture major changes in field geometry and connectivity. For extended eruptions such as CMEs, it is also important to monitor larger areas and to find out whether the instability resides in the surrounding and overlying large-scale structures or within smaller-scale flux systems.

Part of the tool kit with which to address this problem is the mapping the conjugate endpoints of particle propagation pathways, including those into the heliosphere (as inferred from particle measurements near Earth and L1), will allow further tests of 3-D models of the coronal and heliospheric field.

As observation and theory have advanced over the last decade, the distinction between the different types of transient phenomena has blurred [42, 43, 44]: the evolution of the large-scale surrounding field appears to be intimately coupled to rapid field destabilization. It remains to be explored whether this is a global response to a perturbation, or whether a global change triggers the instability. The decade of YOHKOH observations shows that field rearrangements during CMEs and flares often involve more than a quarter of the solar disk.

**Technical approach and methodology** The AIA EUV spectroheliograms, and derived temperature maps, are examined to locate the area of first brightening or motion that develop into full-blown transients. These are compared with computations of null points and separatrices/separators from extrapolation of pre-event HMI (or, e.g., SOLIS) vector-magnetogram data. Furthermore, we may apply stretching methods to magnetic fields [8] to match the observed loops at the wide temperature range.

**Science data requirements** Full sets of full-disk EUV images, and full-disk vector magnetograms, complemented with high-cadence ($2-5$ s) subregion image sequences in UV and EUV to observe the initial phases of the destabilizing field. When AIA is operated in its fast mode with partial readouts, the $\sim$ 2-s cadence for bright, flaring regions will for the first time image the initial phases of transients at a range of temperatures essentially simultaneously and at high spatio-temporal resolution.

If possible, complementary observations with the Solar-B XRT will add information on relatively high-temperature plasma.

**Science team roles and responsibilities** P. Demoulin (extrapolation), G. A. Gary (field deformation), C. Keller (chromospheric magnetograms), Kosovichev (photospheric flow maps), T. Metcalf (vector field), E. Priest (reconnection model), A. van Ballegooijen (MHD modeling).

**Required resources** Multiple techniques for computing helicity injection. Tools to study field topology.

**Task 3B: Evolution of transients**

**Major goals and significance** A flare often starts with the impulsive phase (sometimes preceded by the precursor phase) and evolves into the gradual phase. They are characterized, respectively, by intermittent non-thermal emission and buildup of slower thermal emission. Magnetic reconnection is probably responsible for both phases, but what do the different manifestations mean? Measurement of the time differences of

brightenings in the (EUV) corona and in the (UV/WL) lower atmosphere will help distinguish the energization mechanisms by differentiating between, e.g., effects of high-speed particle beams from slower thermal conduction. Where is energy first released? Where does that energy thermalize? What roles do particle beams play?

It is important to somehow determine the reconnection rates during the evolution of the transients. This can be attempted by, e.g., analyzing the (extrapolated and observed) magnetic field and the observed evolution of the foot points of reconnecting loops as they are seen to sweep over the magnetic field: the ultraviolet and white-light channels provide information on magnetic connections to flare sites during the impulsive phase as particle beams that travel along the field reveal the endpoints of these connections wherever they impact the high chromosphere [45].

Some flares may be dominated by the gradual phase even from the beginning, and it is these flares that are often associated with major CMEs. In the later evolution of CME-associated flares, we often see down flows above spiky arcades [14]. They are taken as reconnection outflows. By the time these down flows are seen, hard X-ray emission usually finishes. But there is a report that gamma-ray emission lasted well beyond the impulsive phase [46]. Moreover, major SEP events are often associated with type III bursts coincident with the gradual phase [47]. Therefore it is important to explore signatures of particle acceleration late in the gradual phase.

**Technical approach and methodology** A full set of EUV/UV image sequences and extrapolated magnetic field are used to calculate the reconnection rate at flare ribbons throughout the flare. They also provide information on topological changes. High-cadence UV images give connectivity, which changes with time. UV images show heating in the chromosphere and TR, and the time difference of brightenings in UV images from coronal brightenings in EUV images is used to identify the energization mechanism (particles or conduction). Low frequency radio images (FASR/LOFAR) are overlaid on AIA images and compared with STEREO SWAVES dynamic spectra to explore possible acceleration in the gradual phase.

**Science data requirements** Full EUV sets; UV images at high cadence; high-cadence subregion image sequences. The exposure duration of order 2.7 s and the 10 s cadence of the AIA channels allows observations of velocities up to 150 km/s in quiescent conditions, or up to 900 km/s in bright features, without motion blurring. The standard cadence of about 10 s, and the higher cadence of partial images for the high temperature channels, will enable us to see the changes in connectivity as the field evolves. We will also observe high-speed flows, jets, (shock) waves, and plasmoids induced by the reorganizing field, even those so fast that they lead to some image blurring. TRACE has revealed the ubiquity of such propagating irregularities, but the improved cadence, coverage, and exposure durations of the AIA will allow us to study these phenomena in detail.

**Science team roles and responsibilities** E. DeLuca (thermal analysis), A. Fludra (flare studies), D. McKenzie (flows associated with reconnection), N. Nitta (flare studies, radio), T. Tarbell (reconnection rate), H. Warren (connectivity studies)

**Required resources** Radio observations for particle acceleration in the gradual phase

**Task 3C: Early evolution of CMEs**

**Major goals and significance** It is widely agreed that CMEs are triggered by magnetic forces, but it has not been calculated to reproduce the observed CME dynamics. One difficulty of comparison between models and observations resides in a gap between EUV/X-ray and coronagraph images. AIA has a comparable FOV but much much better cadence than EIT (1.35 $R_\odot$) FOV, and generally a 15 min. cadence), so it will be easier to observe initial evolution and acceleration. If the work done by the driving forces does not suffice to open the field or to dominate the gravitational energy, we expect to see a failed CME, often seen in TRACE data as filament matter that rises and then fall again. In an opposite case, if the overlying field is removed by reconnection, either internally (flux rope) or externally (breakout), the magnetic field would be completely opened-up and we expect a fully-developed CME.

The field of the erupting filament with respect to the overlying corona may well be a key factor for elimination of the force that holds down the flux rope. For the filament field in the same direction as the overlying field, it is expected that a fast CME results, and observationally it corresponds to two-ribbon flares that separate with time (Zhang and Golub). If we understand the magnetic field of the flux rope and the surrounding field, we can essentially predict $B_z$, which is important for geomagnetic storms. It is also important to observe all the closed pre-eruption structures for those CMEs that start without precursors. It appears that most CME models predict at least some signatures (i.e., heating) prior to the CME.

CMEs are thought to be a means to shed magnetic helicity. In order to prove this, we need to calculate changes of helicity in all the areas that are affected by the CME.

The details of the evolution of the field involved in CMEs remain elusive. One aspect is the energy budget of the field: the relatively high energy state of the opened field needs to be countered by a lowering of energy elsewhere, possibly far away. For example, a CME may involve field from several arcades, most of which is not opened [48, the "breakout model"]; in some cases these associated flux systems even involve trans-equatorial loop systems [49]. Furthermore, we need to understand the distinction between the common constrained filament eruption and the less frequent fully-developed CME. We also need to understand how, and how much, flux escapes from the Sun during CMEs [50, 51]. Adding to these problems is the fact that the CME field often is not force free [52]. AIA's field of view and thermal coverage enable observation of much more of the field involved in the early phases of CMEs than is possible now with SOHO and TRACE. Moreover, the high cadence of AIA allows us to observe exactly how the field evolves from one state to another, which is important to assess helicity evolution and where and how much field is not force free.

**Technical approach and methodology** Use AIA thermal maps to monitor pre-eruptive closed structures at a high cadence. Study filament barbs to deduce the filament axial field. Magnetograms (and extrapolations) will give the orientation of the overlying field and the bipolar/multipolar nature of the surrounding field. Temperature Maps for flare ribbons are correlated with the relation between the filament field and the surrounding field, and with the CME speed profile from coronagraph data (LASCO, Mauna Loa, STEREO). Using various assumptions (TBD), calculate the hoop (curvature force) in comparison with the tension force to understand the confined or fully developed nature of the CME. In connection with geo-space, compare $B_z$ at the Sun with that at 1 AU. Possibly use the force-free flux rope model to infer the magnetic field structure of the ejection at the Sun.

In order to compute the helicity injection, we also need to obtain the photospheric velocity field from correlation tracking.

If possible, complementary observations with the Solar-B XRT will add information on relatively high-temperature plasma.

**Science data requirements** Magnetograms, Full EUV sets, high temporal and spatial H-$\alpha$ images

**Science team roles and responsibilities** Demoulin (computation of helicity), S. Fuselier (geoeffectiveness), L. Golub (flare studies), R. Harrison (CME studies), P. Martens (filament magnetic field), Metcalf(helicity), N. Nitta (flare/CME studies), Z. Mikic (global magnetic field extrapolation)

**Required resources** Various CME models, coronagraph data (LASCO, STEREO, Mauna Loa), different techniques for computing helicity injection.

**Task 3D: Particle acceleration**

**Major goals and significance** Energetic electrons accelerated in solar flares precipitate into the low atmosphere and produce soft X-ray and UV emission. Major solar energetic particle (SEP) events, in contrast, are now thought to originate primarily from the shock produced by fast CMEs. These particles are one of the severe space weather threats. The shock origin of gradual SEPs is supported by spectra, composition and charge state. Another category of SEPs (impulsive), which is small so not a space weather threat, is thought to come from stochastic acceleration in flares because of the anomaly in the ion composition (i.e., enrichment in $^3$He and heavier). But recent results from ACE indicate that the division is not so clear, i.e., possibly flare-accelerated particles contributing to gradual SEPs either directly or as seed particles. Furthermore, if heavy ions in impulsive SEP events get re-accelerated by CME shocks responsible for gradual SEP events, it can be a concern in some space weather applications. The so-called hybrid SEP events (impulsive + gradual) may reflect the particular relation of the shock with the magnetic field (i.e., quasi-perpendicular), which should be satisfied only close to the Sun (or near Earth). In order to establish the origin of SEPs, it is important to understand the relation between SEPs and flare-accelerated particles, especially electrons.

**Technical approach and methodology** Since we will not have RHESSI hard X-ray imaging during SDO, we need to rely on UV brightenings as proxy to precipitating electrons. Difference AIA images at different wavelengths will reveal more waves than EIT, and they will be compared with other waves in broadband soft X-rays (Solar-B XRT, GOES/SXI) and on-/off-band H$alpha$ images. TRACE observations do indicate early manifestations of CME shocks, which will be better observed by AIA. Their traced motions will be compared with the potential field extrapolations, which will reveal field lines connected to Earth and give the geometrical relation of the magnetic field with the shock normal. Radio observations (STEREO/SWAVES) will help us understand the nature of the shock.

AIA may also observe various flows and waves around the reconnection regions, which can be linked to how the turbulence grows for stochastic processes that are responsible for accelerating impulsive SEPs. The velocity dispersion of the first arriving SEPs as observed by ACE or STEREO energetic particle instruments will be used to obtain the release time on the Sun.

**Science data requirements** Full EUV sets, fast cadence UV images (proxies for precipitating electrons), high temporal and spatial H$\alpha$ images (both on- and off-band)

**Science team roles and responsibilities** L. Harra (EUV waves) , C. Keller (Moreton waves), D. McKenzie (resonant waves), Metcalf (Magnetic field extrapolation), N. Nitta (CME shocks, SEP analysis), R. Shine (UV proxy for hard X-rays)

**Required resources** In-situ SEP data from ACE (ULEIS/SIS/EPAM) and STEREO (IMPACT), metric and DH dymanic spectra (groundbased and STEREO/SWAVE).

### A1.1.4 Objective 4: Connections to geospace:
*material and magnetic field output of the Sun*

The solar wind, the embedded magnetic field, and eruptive perturbations in the form of CMEs drive the variations in the space surrounding the Earth and other planets. The dynamic connections between Sun and geospace are a cornerstone of the ILWS program. To understand how the Sun's variability affects life and society, we must understand how the products of this variability are transported into and through the heliosphere, and how they interact with the Earth's magnetic field and atmosphere. The AIA investigation is expected to make substantial quantitative advances in many areas relevant to this problem. At the foundation of this expectation lies the improved understanding of the global coronal field and its extension into the heliosphere. In objectives 2 and 3 we discussed this for the pathways for escape of energetic particles into the heliosphere, the irradiance that affects the ionosphere and below, and the triggering of flares and CMEs. Here we focus on the magnetized solar wind and its perturbations.

The solar wind flows out radially into the heliosphere dragging along the magnetic field lines that are forced "open" within the first few radii from the Sun. The successes of simple concepts such as the potential-field source-surface (PFSS) model suggest that more realistic and detailed models should explain why this is. What determines which field lines will open? Why does the PFSS work as well as it does? The latter is particularly interesting because the PFSS model does not incorporate field dynamics. How is field opened, and how is it closed again as the connections evolve? This must have something to do with the properties of the solar wind, which we know depends on the field geometry and strength (often parameterized using the field expansion between low atmosphere and where the field becomes essentially radial). But although that dependence is empirically constrained, we still need to learn what determines the physical properties of the solar wind.

The eruptive coronal mass ejections perturb the background solar wind. How do they evolve through the coronal field? How do they couple into, and propagate through the heliosphere on their way to the Earth and the other planets?

In parallel to the above research topics, the AIA data products are designed to make an immediate contribution to space weather studies; data, catalogs, analysis software, and archive will be easy to use. The easy-to-use data and software systems (based on our YOHKOH, TRACE and SOHO experience) will make the AIA observations very useful for the world-wide solar physics community. Moreover, this approach will enable scientists from other fields within the ILWS community to easily access and use AIA data in their analysis of heliospheric and geospace data. In addition, the AIA investigation will develop and maintain an event catalog that is updated as data are received. Rapid brightenings, early rises of CME filaments, and other activity diagnostics will be listed on the web within minutes. All images will be inspected visually within 24 h in order to (a) augment the event catalog with filament and sigmoid developments, flare properties, flux emergence sites, wave phenomena, and other products requested by interested parties, and (b) create experience and intuition in researchers that stimulates the exploration of new avenues and discovery of new phenomena in traditional solar physics areas as well as in the wider ILWS context. To achieve this, the AIA team will explore how to best include heliospheric and geospace data in the daily assessment of events.

**Main tasks for Objective 4:**

1. **Dynamic coupling of corona and heliosphere**
2. **Solar wind energetics**
3. **Propagation of CMEs and related phenomena**
4. **Vector field and velocity**

Co-investigators Fuselier and Mikic are responsible for coordinating this research objective. With input

from the user community, the AIA team team will help develop space-weather and solar-physics products relevant to the study of connections to geospace.

**Task 4A: Dynamic coupling of corona and heliosphere**

**Major goals and significance** The dynamic coupling of the closed corona to the open field reaching into the heliosphere can be observed using the sensitive AIA telescopes. On the scale of supergranulation, the network field is replaced every few days in a continual process of flux emergence in ephemeral regions flux and cancellation due to collisions between opposite polarities [53]. This process forces magnetic reconnection in addition to those associated with the smaller-scale granular driving. TRACE observations of the corona above quiet-Sun regions hint at a multitude of dynamic structures, particularly in exposures of minutes or more [1]. The sensitivity of the AIA will allow us to observe these structures with much shorter exposure times, and hopefully reveal how this field couples to the that in the heliosphere, particularly in the open-field configurations of coronal holes at the base of the fast solar wind.

**Technical approach and methodology** The combination of HMI, AIA, and (ground- or space-based) coronagraph observations with modelling efforts will deepen our understanding of the interface between corona and heliosphere. Currently, the heliospheric field is readily approximated by a source-surface potential-field model and Parker spiral. This involves various poorly-testable, pragmatic corrections [54, 55, 56]. Detailed observations of the field geometry, in particular in the first few tenths of the solar radius above the limb where the field is strong, will help us understand these corrections, and the role currents and field dynamics play. This will improve the fast but simple source surface modelling and guide the more advanced MHD modelling.

One key tool in this is a surface dispersal model (already developed by our team, [57]), that simulates the evolution of photospheric field near the limb where it is hard to observe, and on the backside of the Sun. Combined with HMI magnetograms of the visible hemisphere, and seismological proxies for flux on the backside of the Sun (with assigned polarities) this provides a good approximation of the entire surface field needed as a basis for global coronal modelling.

AIA and coronagraph data, combined with such models, will allow the study of evolving coronal holes as parts of the heliospheric field. Team members with expertise in MHD modelling and field geometry studies will address this coupling. Such modelling capabilities will be exercised and refined starting with the SOLAR-B and STEREO missions. They will yield their full potential during SDO, when full-disk data enable us to cover scales from active regions to the entire corona.

**Science data requirements** Needed are high S/N observations of all coronal EUV wavelengths, possibly taking extra long exposures to see the faint, high-arching structures. Sequences at a cadence of $\sim 30\,\mathrm{s}$ or better are needed to study the evolving field. Comparison with HMI magnetograms and full-sphere field models are needed to compare observed field geometries with models.

**Science team roles and responsibilities** S. Fuselier (magnetospheric and ionospheric physics, manager of the space-physics department at LMMS/LMATC), N. Hurlburt (data management), Z. Mikic (MHD modelling of corona-heliosphere coupling), P. Scherrer (field extrapolation, comparison with results from Wilcox Solar Observatory modelling), and C. Schrijver (global modelling of coronal field).

**Required resources** Force-free and other field models are needed as part of this task.

**Task 4B: Solar wind energetics**

**Major goals and significance** The solar wind is accelerated within approximately 10 solar radii. Comparisons with in-situ measurements in the heliosphere (usually near the Earth, but also from, e.g., the interplanetary spacecraft and the out-of-ecliptic Ulysses mission) suggest that the wind density and velocity are determined by the geometry of the field near the Sun. The wind velocity has been found to anti-correlate with the so-called expansion factor, i.e., with the ratio of field strengths near the solar surface and at the distance of the source surface [58, 59, 60]. It may be that other parameters are involved [61], but testing such dependences requires a combination of the near-Sun field models with a wind propagation model that includes stream interactions. That combination of models also will help validate the field models for the highest domains of the solar corona that are too faint to observe directly and must be studied indirectly by comparing the model geometries and wind properties to observations in the low corona and within the distant heliosphere.

**Technical approach and methodology** The findings from task 1A are to be combined with heliospheric models of the solar wind, and then compared to in-situ measurements of wind properties.

**Science data requirements** Required are high S/N images of the solar corona at all AIA EUV wavelengths, perhaps requiring extra long exposures to see the faint, high corona. Combination with ground- or space-based coronagraphs (including STEREO imagery) will help validate the coronal field models. In-situ measurements of the solar wind, at least near Earth (as in the Sun-Earth L1 point) are needed at low temporal resolution for comparison with models. Coupling of coronal-field and heliospheric-wind models is needed to test and validate the high-coronal field and solar wind models jointly, as they cannot be independently verified.

**Science team roles and responsibilities** S. Fuselier (magnetospheric and ionospheric physics, manager of the space-physics department at LMMS/LMATC), N. Hurlburt (data management), Z. Mikic (MHD modelling of corona-heliosphere coupling), P. Scherrer (field extrapolation, comparison with results from Wilcox Solar Observatory modelling), and C. Schrijver (global modelling of coronal field).

**Required resources** Successful work on this task requires heliospheric models for the solar wind and embedded field.

**Task 4C: Propagation of CMEs and related phenomena**

**Major goals and significance** The high-cadence AIA images will enable the study of CMEs and associated (shock, blast, and other) waves that are launched into the heliosphere. CME-related shock waves [62, 49] likely play a significant role in the generation of solar energetic particles from within the heliosphere [63]. The calibrated AIA images covering a wide range of temperatures will, moreover, enable us to estimate the mass involved in an ejection (as already applied to SXT, EIT and TRACE observations, [64, 49]), and - for prominence eruptions - provide the acceleration profile of CME-related structures to be compared with coronagraph data higher up. Combination with coronagraph data may allow us to estimate velocities and field-strength evolution in the initial phase of CMEs, both important to the severity of related geo-magnetic storms [65]. The AIA images will also elucidate whether the short-term coronal dimming during CMEs [66] is a consequence of a change in density (related to field evolution) or temperature (reflecting expansion or

modified heating) or both. Moreover, the AIA images not only better clarify the relation of dimming with flux ropes or magnetic clouds observed in-situ but also (combined with magnetic field extrapolations) reveal the origin of the magnetic field in interplanetary coronal mass ejections.

Another important aspect is that SOHO's LASCO frequently observes matter falling back to the Sun, even from eruptions that reach beyond 6 solar radii [67]. TRACE observations of erupting filaments often show such material falling back in dark, absorbing streams in the early phases of CMEs. What determines what fraction of the CME mass falls back? What does that mean for its geo-effectiveness? We will study these processes by combining observations of erupting filaments seen in emission in He II 304 Å, in absorption in the EUV channels, and in scattered light in available coronagraph data.

In order to study the potential geo-effectives of eruptions, we need to constrain the field orientation, the mass content, (evolution of) the speed, and any associated EUV irradiance changes.

**Technical approach and methodology** Compare eruptions with MHD (or other) models of the evolving coronal field. Combine the observations of the near-Sun conditions with models for the propagation of perturbations through the background solar wind, and compare the results with the in-situ observations of CMEs passing by the Earth's magnetosphere.

**Science data requirements** In order to estimate the evolution of the innermost parts of CMEs, the AIA must see all temperatures to provide maximum observational constraints on the field evolution. Such complete vision of the coronal hot plasma will be helpful to estimate the near-solar velocity and mass, to trace the field structure, and to study the CME energetics. High cadence ($\sim 10$ s), and high S/N to see the faint high structures is needed.

**Science team roles and responsibilities** S. Fuselier (magnetospheric and ionospheric physics, manager of the space-physics department at LMMS/LMATC), Z. Mikic (MHD modelling of corona-heliosphere coupling), N. Nitta (ICME studies), P. Scherrer (field extrapolation).

**Required resources** As under 1A, plus models of CME propagation through the heliosphere. In-situ solar wind plasma and magnetic field data, and magnetic field model for flux ropes.

**Task 4D: Vector field and velocity**

**Major goals and significance** Observations of the initial evolution of the field in a CME (including any unwinding of the large-scale helical field), will help modellers compute the further evolution through the heliosphere, including CME-wind and CME-CME interactions. Of particular importance here are the direction of motion of the CME front and the direction and magnitude of the heliospheric field with which it will interact en route to Earth. Important factors for heliospheric modellers include the initial velocity evolution of the CME close to the Sun, and the total mass contained within it, because these determine the interaction with the ambient heliospheric plasma. With this input, the heliospheric models need to estimate the $B_z$ magnitude of the compressed field at the front interface of the CME as well as whether a shock forms before it reaches Earth. These properties define the strength of a geomagnetic storm and the intensity of the arorae [68]. Also important is the field orientation throughout the interior of the beginning CME, because that determines the recovery phase, including any substorms, of the geomagnetic field after the initial front passes. In order to provide the required input to heliospheric models, the evolution of the CME-related field and plasma needs to be observed and analyzed in the innermost corona observable with the AIA.

In a few cases, it may be possible to combine AIA image sequences with spectroscopic measurements from, SOLAR-B's EIS: together they provide the vector velocity that enables an accurate forecast of the geo-effectiveness of a CME. AIA, available coronagraphs, and hopefully STEREO observations can be combined to estimate 3-D velocity vectors.

**Technical approach and methodology** Measurements of the velocity profile of erupting filaments (and the surrounding corona field) are possible only projected against the plane of the sky. Combination with STEREO measurements, or with model MHD computations based on HMI vector-field measurements, should be made to study the evolution in three dimensions.

Calibrated intensities help constrain the mass contained in the CME.

**Science data requirements** High-cadence ($\sim 10$ s) observations at all coronal AIA wavelengths and in He II 304 Å. High S/N ratios at all corona temperatures to observe the evolution of faint loops high in the corona and around any erupting filament. Coordination with Solar-B EIS. Combination with STEREO observations and with ground-based coronagraph observations.

**Science team roles and responsibilities** S. Fuselier (magnetospheric and ionospheric physics, manager of the space-physics department at LMMS/LMATC), Z. Mikic (MHD modelling of corona-heliosphere coupling), P. Scherrer (field extrapolation).

**Required resources** MHD model of at least the propagation of CMEs through the innermost heliosphere, preferably out to Earth or beyond. Vector-field extrapolation models.

### A1.1.5 Objective 5: Coronal seismology:
*a new diagnostic to access coronal physics*

Recent observations from SOHO and TRACE show a variety of oscillation modes in the transition region and corona. These observations opened up the promising new field of *coronal seismology*. By studying the properties, excitation, propagation and decay of these oscillations and waves, we can reveal fundamental physical properties of the solar transition region and corona, such as the magnetic field, density, temperature, viscosity, ...[69].

Examples of seismic responses of the corona have been found in large-scale coronal Moreton and EIT waves [70], in polar plumes, sunspot fields, upper transition region moss, and what appear to be ordinary loops. The whole gamut of MHD waves predicted by theoretical considerations has been observed. Perhaps most striking are the transverse oscillations seen by TRACE in association with $\sim 8\%$ of all C, M, and X-class flares observed [71, 72]. Longitudinal oscillations and waves have also been observed: in the upper transition region moss [73], and in coronal loops, both in cooler loops with TRACE [74] and in hot ($10^7$ K) loops with the SUMER spectrometer [75].

There are still many unresolved issues about these waves and oscillations. How do they get excited? Why does only a fraction of the observed flares lead to clear oscillations? Are longitudinal waves in coronal loops with 5 minute periods related to p-modes? How do any of these waves propagate? Which of the many possible theoretical mechanisms can explain the unexpectedly rapid decay of some of these waves? These are some of the questions that we need to answer before we can seismically probe coronal physics.

The AIA design will allow us to develop the necessary improved understanding of the properties and other unresolved issues of the observed waves. The high cadence of AIA will extend the parameter space to

higher frequencies (by a factor of 2-4 compared with TRACE). The broad simultaneous temperature coverage will allow us to study waves in parts of active regions that have not yet been seen. Guided by significant advances in the theory of these waves (from 3D MHD simulations), and complemented with spectroscopic measurements of densities and line-of-sight velocities (for example by Solar-B/EIS), and reliable magnetic field extrapolations (e.g., from SDO/HMI-AIA), AIA will thus be the first instrument that fully exploits the potential of coronal seismology.

**Main tasks for Objective 5:**

1. **Transverse waves: excitation, propagation and decay**
2. **Longitudinal waves: excitation, propagation and decay**
3. **Probing coronal physics with waves**
4. **The role of magnetic topology in wave phenomena**

Co-investigators De Pontieu and DeLuca are responsible for coordinating this research objective.

**Task 5A: Transverse waves: excitation, propagation and decay**

**Major goals and significance** The transverse oscillations discovered by TRACE [71, 72] are the most promising candidates for accurate coronal seismology. Many of the observed oscillations have been identified as fast kink MHD modes in the fundamental eigen-mode. This implies that the observed period is related to the loop length and Alfvén speed along the loop.

However, there are many unresolved and confusing issues about these oscillations. For example, observations show substantial deviations from a nice symmetric kink mode oscillation, asymmetric excitation, and systematic eigenmotion trends superimposed on the oscillatory displacements [72]. And why only certain field lines are affected by the excitation mechanism remains unclear. In addition, the oscillations suffer from strong damping, which brings them to a halt after a few periods. Because of a lack of detailed observations, at least four different theories ranging from non-ideal effects, wave leakage, phase mixing, and Alfvénic resonant absorption [76], appear able to explain the strong damping.

By resolving these issues, AIA will provide the pathway to accurate seismological determination of coronal parameters.

**Technical approach and methodology** The improvement in field of view, signal-to-noise, and in the temporal and temperature coverage of AIA over TRACE, will revolutionize our understanding of transverse oscillations. The large field of view of AIA will provide much better statistics and help elucidate how oscillating loops are related to the exciting agent. The latter has often been difficult with TRACE data because of its limited field of view. The superior signal to noise and cadence of AIA over TRACE dramatically increases the discovery rate of oscillations. It also allows the detailed study of damping times and mechanisms, as many oscillations are too weak and short-lived for TRACE to observe in detail, which has led to considerable uncertainty in the determination of damping times. In addition, the improvement in cadence provided by AIA will, for the first time, shed light on the propagation effects and phase delays seen between different parts of the oscillating loops, and on how much the observed oscillations differ from the idealized eigenmodes that have so far been assumed [72].

Oscillating loops often change significantly in brightness while oscillating. The extended temperature range covered by AIA enhanced with spectroscopic density measurements using Solar-B/EIS, will elucidate the cause(s) of these brightness changes and whether they are related to temperature or density changes (or both). In addition, AIA will study whether correlated oscillations occur at different temperatures and over

what temperature range. Both issues will help explain the mystery of how the exciting mechanism affects (only certain parts of) the coronal volume [71].

Much progress will be made on the feasibility of the resonant absorption damping mechanism. Resonant absorption critically depends on the density contrast between the interior and exterior of the oscillating flux tube, which has been difficult to determine accurately with existing instruments. The increased temperature coverage and well-calibrated AIA intensities and simultaneous spectroscopic density measurements with Solar-B/EIS will enable us to determine whether and when resonant absorption is a dominant damping mechanism, which will lead to information about the sub-resolution structure of coronal loops [76].

**Science data requirements** Required are full sets of the EUV images so that the full thermal range of the coronal volume is visible. This will assist efforts to understand the trigger and damping mechanism(s). To fully understand the exciting mechanism, and for improved statistics, full disk images are necessary.

After the initial excitation, a cadence of 10 seconds in all wavelengths is necessary to allow adequate coverage of temporal evolution. During the initial phase, even shorter cadences of $< 3$ s will be needed. Coordination with Solar-B EIS will enable the determination of densities, which are crucial for coronal seismology and understanding the damping mechanism(s). Angular resolution of $1 - 1.5''$ is a necessity to observe these oscillations (EIT, at a resolution of $5''$, has never seen transverse oscillations on coronal loops).

**Science team roles and responsibilities** B. De Pontieu (oscillation studies, corona- chromosphere interface), E. DeLuca (plasma physics, modelling), D. Hassler (spectroscopic constraints), E. Priest (plasma physics), and N. Hurlburt (field modelling).

**Required resources** Most of the transverse oscillations in TRACE data were discovered through inspection of image sequences *not* optimally suited to study the flare or eruption that likely excited the wave: the waves generally escaped notice in initial inspections because the cadence, cutout, or intensity scaling chosen to view the exciting event were far from optimal to display the wave phenomenon. The detection of such sparse, weak, short-lived transverse oscillations is not likely to be possible with any automated event-recognition software until we have learned much more about their properties and likely locations of occurrence. Until then, finding transverse oscillations will require an observer looking at movies that can be readily displayed at different scalings in space, time, and intensity.

**Task 5B: Longitudinal waves: excitation, propagation and decay**

**Major goals and significance** Longitudinal oscillations and waves have been observed in a variety of solar environments. TRACE observations show intensity oscillations propagating upwards in coronal loops and sunspot fans [74]. What is the source of these waves? Are the similarities in period between the coronal waves and the dominant period of oscillations at the lower atmospheric foot points indicative of propagation from photosphere/chromosphere into corona [77, 73]? If so, what are the consequences of this energy input for the corona? How are these longitudinal waves damped in the corona [78]? What role does the magnetic field geometry play in the apparent weakening of the signal along the magnetic field lines? How are longitudinal oscillations at slightly different temperatures related?

AIA will allow us to address all of these issues and will, for the first time, render longitudinal coronal waves useful for coronal seismology. Extended temperature coverage from 1 MK to 10 MK will allow seismology of the thermal structure of coronal loops. In addition, coordinated observations with Solar-B

FPP/EIS will provide breakthroughs in understanding how the many oscillation modes of the lower atmosphere (such as p-modes) affect the coronal volume.

Longitudinal oscillations are also present in hot ($10^7$ K) loops (seen with SUMER). How are these triggered? How does the coronal volume react to the trigger at different temperatures? What are the consequences of these oscillations on coronal loops? How can we use these waves for coronal seismology at higher temperatures?

**Technical approach and methodology** To study the source of the longitudinal waves seen with TRACE in sunspot fans and coronal loops, coordination with Solar-B/FPP and EIS is necessary. These instruments provide data about the lower atmospheric oscillatory input at varying temperatures. By looking for correlations with lower atmospheric oscillations, the longitudinal waves can be used as a tool for chromosphere/corona interface seismology.

The increase in sensitivity and cadence of AIA will not only improve the statistics of longitudinal oscillations, but also help characterize damping lengths with much higher precision. Currently, there is uncertainty about what is responsible for the relatively short damping lengths, with some theoretical approaches suggesting (artificially) "enhanced" thermal conductivity or "enhanced" compressive viscosity as the main damping mechanism [78]. Future 2D or 3D simulations taking into account gravity, curvature of the loop, background magnetic field, density profiles across the loop, will be necessary to bring theory and observations closer. In addition, reliable magnetic field extrapolations using HMI vector magnetogram data will allow us to study the effect of the magnetic field geometry on apparent "damping" lengths.

How do the dispersion relationships along loops with different temperatures vary? Existing data is inconclusive with respect to correlations between longitudinal waves along such loops of different temperatures. Some find clear correlation decreasing along the loop (perhaps indicative of phase mixing because of different propagation speeds) [79]. Others find no correlation and suggest they are sampling different shells of a sunspot fan [80]. Using the large temperature coverage of AIA we will be able to exploit, for the first time, longitudinal waves as seismic probes of the thermal structure of coronal loops. In addition, AIA will provide the first detailed observational data of phase mixing in the coronal volume.

The longitudinal standing waves discovered by SUMER in hot loops, apparently triggered by (micro)flares, show that longitudinal oscillations are ubiquitous in dynamic environments at many different temperatures [81]. Simultaneous observations of AIA with spectra from Solar-B EIS (for the velocity signal) will elucidate the trigger mechanism(s) and the coronal response to these waves. Magnetic field extrapolations will allow better determination of loop lengths, adding these standing waves as another tool for coronal seismology at high temperatures.

**Science data requirements** Full thermal coverage from 10,000 K (lower atmospheric oscillations) to 10 MK is important for a better understanding of the role longitudinal waves play in the corona, and for their use a reliable tool of coronal seismology. Accurate magnetic field extrapolations (based on HMI magnetograms) will be necessary to disentangle geometric effects from physical damping mechanisms, as well as to determine loop lengths for standing waves. Signal to noise ratios of $\approx 100$ will be crucial to determine damping parameters of these relatively weak oscillations ($\delta I/I < 0.05$) with better accuracy. Coordination with Solar-B FPP/EIS is required to study the source of the longitudinal waves in sunspot fans.

Recent suggestions of high frequency intensity oscillations in the TRACE UV 1600 Å passband with periods as short as 10 s, are difficult to confirm using TRACE data because of signal to noise limitations. The higher cadence and sensitivity of AIA will enable unambiguous determination whether these signals are solar or instrumental artifacts. In addition, the capability of AIA for cadences as low as 4 seconds in

selected passbands will open up a new frequency domain for oscillations in the corona as well as in the lower atmosphere.

**Science team roles and responsibilities** B. De Pontieu (oscillation studies, corona- chromosphere interface, lower atmospheric modelling), E. DeLuca (oscillation studies, modelling), D. Hassler (spectroscopic constraints), A. Kosovichev (effects of $p$ modes), Z. Mikic (lower atmospheric MHD modelling), T. Metcalf (field extrapolation), and T. Tarbell (FPP coordination).

**Required resources** The force-free and non-force-free models of the coronal field developed for Task 1B will be very useful for this task. To study the lower-atmospheric source of longitudinal waves, we will also need more realistic 2D or 3D MHD models covering the photosphere into the lower corona. As with the transverse oscillations, automated event recognition will need to be developed to scan the AIA data for significant longitudinal oscillations. Such tools can also be used to find so-called "EIT" waves.

**Task 5C: Probing coronal physics with waves**

**Major goals and significance** Coronal seismology based on (nearly) resonant modes offers the possibility of measuring the mean Alfvén speed along loops. This requires the measurement of the period and the loop length (from 3-D field reconstructions). The measured Alfvén speeds can be tested against estimates based on other methods, such as field extrapolations and density estimates from brightness data or spectroscopy. Such independent consistency tests make these measurements very valuable.

The high cadence and short exposure times of AIA not only will show many more cases of oscillations, but promise to also uncover other types of MHD waves. These waves can be used, via dispersion relations for specific modes, to deduce basic properties of the coronal plasma such as its field strength and dissipation characteristics that are key to any modelling effort, but are hard to measure otherwise. Note that the 171 Å and 193 Å channels are so sensitive that they allow access to frequencies as low as 0.25 Hz using a dedicated 2-s exposure cycle with partial readouts.

The detection of waves in loops of different temperatures (in particular the active region loops in FeVII, 131Å; Fe XIV, 211Å; and Fe XVI 335Å ) will allow us to study the dependence on temperature of the wave periods, amplitudes and damping times (if any). If the damping is due to small turbulent structures within the loops [82, 83] one might expect more rapid damping for higher temperature loops (assuming that the turbulent structures are related to the loop heating in some way).

**Technical approach and methodology** Determining physical properties requires a combination of accurate measurements, reliable field line extrapolations and detailed plasma physics simulations. The most straightforward physical measurement is of the Alfvén speed. To extract a local magnetic field strength from this measurement, requires an accurate measurement of the period, wavelength and density in the loop. Lower limits to the electron density can be derived from the emission (or from a DEM inversion if the loop in question is visible in multiple wavelengths). Observations from Solar-B/EIS before or after the oscillation would be helpful in constraining the observations if density-sensitive line ratios are observed.

Understanding the physics of the rapid decay times in transverse loops opens the possibility of measuring the Reynolds number of coronal plasma, a key parameter in detailed numerical simulations. To date there have been conflicting views on the reason for the decay [80, 82, 84, 85, 86, 83, 87]. If decay is due to structures with in the corona (say resonant absorption layers) then loop oscillations provide a direct probe

of this structures. Studying more loops and loops at different temperatures will provide a definitive answer to this question.

**Science data requirements** Observations of active regions with the standard full AIA data set and associated HMI magnetic field measurements will provide the basic data for this study.

At some point we will search for higher frequency waves by running a special program with a limited FOV. The high frequency program will be run on 171 Å and 195 Å wavelengths and for AR at different disk positions. Support from Solar-B/EIS is useful in constraining the local plasma density.

**Science team roles and responsibilities** B. De Pontieu (oscillation studies, corona- chromosphere interface), E. DeLuca (plasma physics, modelling), D. Hassler (spectroscopic constraints), and E. Priest (plasma physics).

**Required resources** Measurements of physical parameters are dependent on tools that accurately project the magnetic fields into the corona (for wavelength determination). Tools that can identify the intensity contribution from a particular loop, will allows us to constrain the local density in the loop, subject to the value of the subresolution filling factor. Detailed plasma physics simulations will be compared with the observations to interpret the measurements and describe the underlying physical processes.

**Task 5D: The role of magnetic topology in wave phenomena**

**Major goals and significance** The magnetic topology and structuring of the coronal volume plays an important role in triggering, guiding, refracting and reflecting wave phenomena. One striking example is that transverse oscillations of coronal loops often appear to be near a large-scale magnetic separator [71]. The reason remains a mystery.

Another example is given by a fast magnetosonic wave phenomenon, referred to as “EIT waves”, which are often associated with Moreton waves observed in the lower atmosphere, and which propagate in the corona over significant distances (fraction of the solar disk). In the process they are refracted and deflected away from active regions, and also influence the magnetic field in the active regions. The propagation front of such waves depends on the local conditions in the corona, and it becomes distorted as the wave front propagates through regions of varying fast magnetosonic phase speed. Detailed, high cadence AIA observations covering a wide range of temperatures, coupled with advanced 3D MHD modelling, will allow analysis of the three-dimensional interaction between EIT waves and active regions. Such studies can serve as powerful diagnostics of the active region coronal magnetic structure [88].

A final example are oscillations which have been seen in filaments from ground-based studies. The combination of He II 304 Å and EUV passbands will allow us to study, for the first time the relationship of the filament oscillations to the surrounding coronal magnetic structure, and to search for associated oscillation in the coronal plasma.

**Technical approach and methodology** In all three cases, we require accurate magnetic field extrapolations using vector magnetograms by HMI (and guided by AIA EUV images of coronal loops as constraints). They will provide the necessary background magnetic field model to allow detailed comparisons of the observed wave excitation and propagation with that in numerical MHD models.

The wide temperature range of AIA will provide us with a better understanding of what fraction of the coronal volume undergoes the transverse oscillations, and indicate whether the proximity to magnetic separators is significant or not.

The temperature coverage of AIA will also provide a new window on the triggering mechanism, propagation characteristics and dispersion of EIT waves as they propagate through the multi-thermal coronal volume. In addition, the high cadence and full disk continuous coverage of AIA will not only improve statistics of EIT waves, but also allow for detailed comparisons with wave phenomena in the lower atmosphere (e.g., from ground-based SOLIS H$\alpha$ data). Comparisons of these observations with full 3D MHD numerical models of an active region corona (derived from field extrapolations) triggered by fast magnetosonic waves, will enable not only seismic probing of the coronal magnetic structure, but also provide independent confirmation of the reliability of the magnetic field extrapolations.

**Science data requirements** The observations of both the transverse oscillations and the fast magnetosonic waves require wide temperature coverage from 1 to 10 MK, high cadence ($\sim$ 10 s) and good S/N $\sim$ 100 to improve detectability. In addition, continuous photospheric vector magnetograms (from HMI, SOLIS or Solar-B) in combination with coronal loop data from AIA will be used to derive coronal magnetic field models. Such field extrapolations will be fed into 3D MHD models of the corona to determine the magnetic topology and structure, and its interaction with fast magnetosonic waves.

**Science team roles and responsibilities** B. De Pontieu (oscillation studies, corona- chromosphere interface), E. DeLuca (plasma physics, modelling), D. Hassler (spectroscopic constraints), C. Schrijver (magnetic field topology), T. Metcalf (field extrapolation), C. Keller (full disk chromospheric H$\alpha$ images).

**Required resources** We will need extensive improvements in theoretical modelling including less idealized coronal loops, taking into account curvature, density profiles perpendicular to the loop axis. To understand how exciting mechanisms function, full 3D MHD simulations will be necessary. In addition, reliable magnetic field extrapolations based on HMI vectormagnetograph data will be required to understand the relationship between oscillating locations and magnetic topology.

Table A2: Overview of the AIA science investigation. The final column lists as required resources both special characteristics of the data processing ('data') and the software tools needed to complete the objective; this listing differentiates between the 'core' software that the AIA team plans to develop or will stimulate with highest priority, and 'external' software that is either already pursued by other teams, or that requires funding to complement the limited AIA science budget.

| Main tasks | Specific Goals | Technical approach | Science data requirements | Co-I team | Required resources |
|---|---|---|---|---|---|
| 1: Energy input, storage, and release | | | | | |
| 1A: 3D configurations of the solar corona | End-to-end connectivity; twist, writhe, and braids; field strength along field; global and local separators | Temperature Maps; stereoscopy; flow vectors | Full EUV sets, $<$ 1/min. cadence or better if fast flows are studied, continuous over up to 3 few days | Brosius, Demoulin, Keller, Metcalf, Priest, Title | Core: DEM inversions; global surface field model; field extrapolations; image-to-model fitting. External: loop modeling; topology models; stereoscopic techniques |
| 1B: Mapping magnetic free energy | Free energy in active-region emergence; free energy build up by photospheric stressing motions; role of reconnection; scale couplings | Potential-field model; field-deformation model; MHD models | Sequences of vectormagnetograms and EUV and H$\alpha$ images at $\sim$ 1 hr cadence | Van Ballegooijen, Demoulin, Gary, Hurlburt, Keller, Kosovichev, Martens, Mikic, Metcalf | Data: H$\alpha$ images. Core: force-free field model; global surface field model; visualization tools. External: non-force-free field modeling, including MHD models. |
| 1C: Evolution of the corona towards unstable configurations | conditions for reconnection; dissipation of stresses and currents at a range of scales; balancing stress and relaxation; helicity evolution | connectivity studies; free-energy evolution | long-term continuous obs.at all coronal temperatures, & surface flows and fields | van Ballegooijen, Hurlburt, Kosovichev, Martens, Mikic, Priest, Weiss | As under 1A&B, plus: External: MHD or magneto-frictional models. |
| 1D: The life-cycle of atmospheric field | Retraction and expulsion of flux from the corona; latitude-dependence of flux subduction | Field-connectivity evolution | 10 s cadence at all coronal EUV wavelengths; HMI (vector)magnetograms at least every few minutes; H$\alpha$ observations | Hurlburt, Martens, Mikic, Title | As under 1B. Data: H$\alpha$ |

Table A2: Overview of the AIA science investigation (cntd.).

| Main tasks | Specific Goals | Technical approach | Science data requirements | Co-I team | Required resources |
|---|---|---|---|---|---|
| **2: Coronal heating and irradiance** | | | | | |
| 2A: Contributions to solar (E)UV irradiance by types of features | quantify contributions to spectral irradiance change from a variety of features (ARs, ephemeral regions, flares, quiet network, ...) | AIA/EVE comparisons; determine contributions for different solar regions and feature populations; isolate contributions by rotation tracking | calibrated EUV data (full-disk images and full-disk irradiance) at all coronal temperatures; 10 s cadence during flares, slower allowed otherwise | De Pontieu, Martens, Schrijver, Shine, Warren | Data: precise knowledge of AIA spectral response and other instrumental properties. Core: feature recognition and tracking |
| 2B: Physical properties of irradiance-modulating features | thermal distribution of coronal plasma; properties of coronal heating, and dependence of field and its topology | Core: DEM analysis to estimate full spectral irradiance; detailed variability studies and distribution functions; coronal heating properties; loop and field modeling | full-resolution, full-disk EUV images and HMI vector-magnetograms at at most 60 s cadence | Brosius, De Pontieu, Fludra, Golub, Gurman, Hassler, Lemen, Martens, Nordlund, Schrijver, Shine, Warren | DEM inversion code; loop identification; field modeling and visualization |
| 2C: Physical models of the irradiance-modulating features | dynamics of loop atmospheres in response to heating changes | MHD modeling of loop atmospheres; comprehensive forward modeling of (sections of) solar corona | | Brosius, De Pontieu, Fludra, Golub, Gurman, Hassler, Lemen, Martens, Nordlund, Schrijver, Shine, Warren | External: loop models, MHD and other field-modeling codes |
| 2D: Physics-based predictive capability for the spectral irradiance | predict spectral irradiance | forward model of full coronal emission, comparison with AIA and EVE data, iterative improvement by validation of results | see 2B,C | Brosius, De Pontieu, Fludra, Golub, Gurman (coronal physics), D. Hassler, Lemen, Martens, Nordlund, Schrijver, Shine, Warren | Core: coronal rendering, force-free field model. External: coronal heating model |
| **3: Transients** | | | | | |
| 3A: Unstable field configurations and initiation of transients | identification of the instability that directly leads to transients; locating the instability; locating reconnection with respect to separatrices and separators; computation of helicity | Thermal maps; correlation tracking; field extrapolation; separator models; helicity injection models, reconnection theory | Full EUV sets, full-disk vector magnetograms; high-cadence subregion image sequences. | Demoulin, Gary, Keller, Kosovichev, Metcalf, Priest, van Ballegooijen | External: techniques to compute helicity injection and field topology |
| 3B: Evolution of transients | Rapid changes of field; dynamic connectivity; location and rate of reconnection; relation between impulsive and gradual phase energy release; high-energy activity in the post-eruption phase; implications of motions (e.g., down flows) | Thermal maps; connectivity studies; flare-ribbon tracing; field extrapolation | Full EUV sets; UV images at high cadence; high-cadence subregion image sequences | DeLuca, Fludra, McKenzie, Nitta, Tarbell, Warren | Data: radio observations for particle acceleration in the gradual phase |
| 3C: Early evolution of CMEs | computation of Lorentz forces involved; characterization of adjacent and overlying field; CME speed profiles; fully open-up vs failed ejections; origin of $B_z$ | Thermal maps, CME models, field extrapolation, tracing filaments | Magnetograms, Full EUV sets, high temporal and spatial H-$\alpha$ images | Demoulin, Fuselier, Golub, Harrison, Martens, Metcalf, Mikic, Nitta | Data: coronagraph data (LASCO, STEREO, Mauna Loa). External: various CME models, different techniques for computing helicity injection |
| 3D: Particle acceleration | relation between downward and upward moving particles; computation of electric field; identification of flare and CME shocks; geometrical relation between shock front and magnetic field; waves resonant with particular ions | Thermal maps; difference images, dispersion relation from in-situ SEP data, potential field model | Full EUV sets, fast cadence UV images (proxies for precipitating electrons), high temporal and spatial H$\alpha$ images (both on- and off-band) | Harra, Keller, McKenzie, Metcalf, Nitta, Shine | Data: in-situ SEP data from ACE (ULEIS/SIS) and STEREO (IMPACT), metric and DH dymanic spectra (groundbased and STEREO/SWAVE) |

Table A2: Overview of the AIA science investigation (cntd.).

| Main tasks | Specific Goals | Technical approach | Science data requirements | Co-I team | Required resources |
|---|---|---|---|---|---|
| **4: Connections to geospace** | | | | | |
| 4A: Dynamic coupling of corona and heliosphere | interface between corona and heliosphere; geometry of open and closed fields, and its evolution | compare high S/N observations to force-free or PFSS models of the coronal field | observations at all AIA EUV wavelengths; coronagraphic image sequences | Fuselier, Hurlburt, Mikic, Scherrer, Schrijver | Core: force-free field models. External: MHD models of high corona & heliosphere. |
| 4B: Solar wind energetics | what determines the acceleration of the solar wind; why is field geometry apparently important | compare field models and observed coronal-hole boundaries with wind-propagation model to in-situ sensors in the solar wind | As 4A; in-situ wind measurements, preferably at multiple locations in the heliosphere | Fuselier, Hurlburt, Mikic, Scherrer, Schrijver | As in 4A, plus: External: propagation model for wind and field throughout the heliosphere out to available in-situ sensors |
| 4C: Propagation of CMEs and related phenomena | propagation of CMEs through background wind; determination of mass flows (outward and inward); energetics of field and plasma | model CME propagation using observed initial evolution | 10 s cadence in all AIA EUV channels; coronagraphic observations | Fuselier, Mikic, Nitta, Scherrer | External: coronal MHD, and heliospheric MHD models. |
| 4D: Vector field and velocity | initial evolution of the field associated with CMEs and filament eruptions | analyze high-cadence observations of field evolution during CMEs, combine with spectrographic observations whenever possible, combine with model computations | high-cadence observations of low corona, uninterrupted for hours at least to study the evolution of the writhing field; vector-field measurements | Fuselier, Mikic, Scherrer | External: MHD models of inner corona during eruptive processes |
| **5: Coronal seismology** | | | | | |
| 5A: Transverse waves: excitation, propagation and decay | wave excitation, propagation, decay | movie viewing to discover oscillations; measurement of properties; comparison to field and field topology and loop-atmosphere properties | 10 s cadence full-disk movies at all coronal temperatures and UV/WL | De Pontieu, DeLuca, Priest, Hurlburt | Observer to inspect movies. Data: Solar-B/EIS coordination. Core: field models. External: coronal atmosphere models |
| 5B: Longitudinal waves: excitation, propagation and decay | movie viewing to discover oscillations; measurement of properties; comparison to field and field topology and loop-atmosphere properties | wave excitation, propagation, decay | 10 s cadence full-disk movies at all coronal temperatures and UV/WL | De Pontieu, DeLuca, Hassler, Kosovichev, Mikic, Metcalf, Tarbell | Observer to inspect movies. Data: Solar-B/EIS coordination. Core: field models. External: coronal atmosphere models |
| 5C: Probing coronal physics with waves | use of dispersion relations, decay rates, etc., to quantify properties of coronal plasma and field | compare oscillation properties to field models and loop-atmosphere models | high-frequency, high S/N images at all temperatures | De Pontieu, DeLuca, Hassler, Priest | Core: field models, DEM profiles along loops. External: MHD simulations |
| 5D: The role of magnetic topology in wave phenomena | why are transverse oscillations seen only near magnetic separators, what is the imaged counterpart of high-temperature oscillations | field models and topology analysis | see 5A,B | De Pontieu, DeLuca, Hassler, Schrijver, Metcalf, Keller | External: advanced loop and field modeling based on HMI data and plasma-physics simulations |

## A2 Implementation of the AIA science investigation

The highest-level requirements derived from the Science Investigation, including the specific objectives, tasks, methodology, required data, and co-investigator teams, as discussed in Sect. A1, are summarized in Table A2. These requirements have implications for instrument design and operations, the data flow and products, the science investigation, and the coordination with other observatories both on the ground and in space. The subsequent sections, discuss these requirements and the top-level methods of ways to meet them; other Appendices to the AIA Concept Study Report describe the details of these implementations.

After detailed discussions within the AIA science and engineering teams, we concluded that the requirements on the instrument design and operations, discussed in Sects. A3 and A4, are compatible with the design discussed in the original proposal. Hence, the subsequent sections in this document should be viewed as more extensive rationales for the proposed instrument rather than that they require substantial design modifications.

The science requirements formulated in Sec. A1 also address issues that are related to the data-analysis part of the AIA Science Investigation, ranging from data flow to daily operations, and from data archive to scientific data-analysis tools. It is clear, however, that even the set of highest-priority tasks as formulated in Sec. A1 and summarized in Table A2 forms a formidable task that encompasses many fundamental problem areas in solar, heliospheric, and solar-terrestrial physics.

The AIA team realizes that only a part of the overall research program can be funded through the AIA contract. Sections A6 and A7 reflect what the AIA Science Team feel are the highest priorities for data and analysis management, based on the research interests and needs deduced from the SDO mission requirements and the (I)LWS program requirements.

In addition to the core tasks outlined in Sects. A6 and A7, the co-I team will actively pursue supplementary funding through, e.g., the LWS TR&T program, and will closely coordinate with other programs, including other space missions (Solar-B, STEREO, ...) as well as research funded through grants of both NASA and NSF. Coordination with other instrument and spacecraft teams is discussed in the following sections. Coordination with other research programs will be pursued by the co-I team members, who will regularly meet to discuss progress and re-evaluate prioritizations of the the AIA Science Investigation.

The research budget available within the AIA program itself will be used primarily for:

1. Evaluation of the science quality of the AIA data,
2. Inspection of the data for the purposes of discovery, education, cataloging,
3. Analysis of a subset of the data and the publication of scientific results from AIA that are at the core of the AIA Science Investigation,
4. Development and validation of key software tools, including visualization, calibration, alignment, intercomparison with other resources, and derivation of high-level data products such as temperature maps, variability, wave properties, and coronal field modelling,
5. Development of a science facility, closely connected to the operations center, with dedicated hardware for data analysis and interpretation,
6. Preparations for, and implementation of, a series of Science Team meetings (open to all interested parties), to discuss new developments, needs, and problem areas,
7. Outreach and interaction to other branches of the (I)LWS program and relevant related research programs,
8. Education and public outreach (discussed in a dedicated appendix).

Clearly, each of these goals in itself presents us with questions and problem areas. First, we will need to concentrate on the very fundamental questions of how we can best utilize the stream of image data for quantitative advances in our understanding of solar activity and its consequences for space weather. We shall

need to learn to answer such an apparently trivial question as how to make a fit of, e.g., a non-potential field model to the observed coronal configuration; we can, by eye, assess whether such a fit is at least in principle acceptable, but a quantitative measure by which multiple models can be compared to a given data set are yet to be developed. As another example, we note that we will also need to utilize computer resources to simulate large coronal volumes even when analyzing the evolution of loop atmospheres, because there is invariably line-of-sight confusion, and the few loops that stand out clearly against their surroundings over their entire length are obviously not characteristic of the bulk of the coronal loops.

The above questions, relating to the comparison of model and observations, become even more demanding of resources if they are to be implemented as tools for further analysis rather than research projects in their own right. How do we make coronal modelling a routine part of data-modelling comparisons? How do we optimally visualize and render coronal observations and model data? How to best implement and use modelling of the evolving thermal structure of the solar corona? The co-I team plans to make such questions that deal with the science infrastructure and methodology part of their series of team meetings prior to and during the operation of AIA on SDO. Some of the tools required will be discussed in Sects. A6.1 and A7.5.

Also of immediate concern are issues related to the utilization of AIA data within the LWS program. Examples, discussed in some detail in later sections, include:

1. Adequate pipeline processing speed from the archived level-0 data ("as-recorded image files") to level-1 data ("useful for scientific publications"), related to issues of capacity of hardware, software control (optimization, access, benchmarking). These are discussed in Sect. A6.1.
2. A user-friendly, comprehensive event catalog: useful contents, accessibility, searchability, (automated) feature recognition; see Sect. A6.2
3. Science capacity: pre-launch investments (data systems, analysis tools, catalogs), project coordination (within SDO, Solar-B, STEREO, FASR, SOLIS, ATST, ...), team work (from operations to observations to publications).

Integration across (I)LWS boundaries will prove to be essential to the success of the AIA (and SDO)

Table A3: AIA science timeline. Goals: maintain scientific flexibility, keep operations simple, and collect data suited to pipeline processing.

| Phase | Action | **Function** |
|---|---|---|
| pre-launch | Science theme development | **Define goals** within contexts of SDO, ILWS, solar physics |
| L+1 month | Launch and commissioning | |
| L+3 months | Science team meeting I:<br>• Discoveries<br>• Initial evaluation | **Learn from the early observations**, refine observing programs, streamline data flow, develop calibrations, ... |
| L+5 months | Early AIA operations<br>• Observations<br>• Analysis workshops<br>• Redefined operations modes | Begin of **coordinated observing** with other instruments and observatories, immediately followed by analysis workshops; evaluate observing modes |
| L+12 months | Science team meeting II:<br>• Presentations<br>• Definition of next year's observing strategy | **Ensure communication of findings** with other science teams and stimulate quick publication of results |
| Yrs. 2−... | Continued operations | **Optimized observing** in a simple & flexible mode |

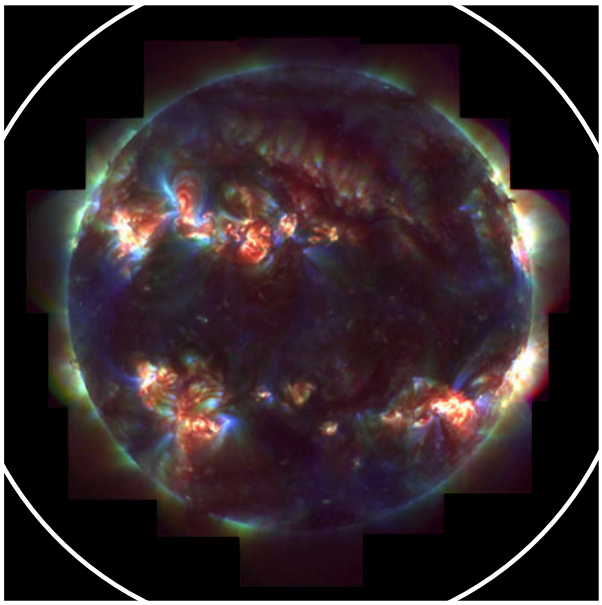

Figure A3: *AIA observes in 4 (E)UV channels simultaneously, alternating to cover up to 10 channels, imaging a 46′ circular area (vignetted by the filter wheel, as indicated by the circle, and cut to 41′ at the detector edges) with 0.6″ pixels. It will provide the first panoramic view of the dynamic corona at all temperatures at a ∼10-s cadence;* TRACE *needed* $\sim 2400$ *s for this 3-channel mosaic.*

programs. For one thing, coordinated observing and analysis must be the default. In terms of facilitating the science, we point out such projects as:

1. Analysis and visualization facility, and accommodation for "long-term" visiting scientists; section A7.3,
2. multi-observatory analysis and modelling.
3. "Whole-fleet months" in which planning teams of multiple space- and ground-based observatories decide to implement observing programs tailored to specific science needs; such programs of SOHO/TRACE (as "whole-Sun months") have proven very successful, and expanding them to other observatories appears highly promising.
4. University programs in solar physics and space weather. The co-I team recognizes the importance of such programs as one of the top priorities, but also among the more difficult. Discussions in the phase up to SDO's launch will be organized at co-I team meetings to identify (collaborative) opportunities, and to discuss strategies and progress.
5. Summer programs for (post-)graduate programs. Such programs may be developed as a collaborative effort within the SDO project, as well as part of existing efforts, such as the Center for Integrated Space-Weather Modelling (CISM). Details are to be developed over the coming years.

We appreciate the need to make a flying start with the science investigation (cf., Table A3). Apart from preparing the data flow and analysis tools prior to launch, this means a rapid convergence to standard operations and data flow very early in the SDO mission. Table A3 outlines our basic plan: The science goals need to be formulated early (as we are doing in this document). After an initial commissioning phase following launch, we plan to explore the Sun with the new diagnostics provided by AIA: full thermal coverage, high cadence, large field of view, and large dynamic range. Within a few months, we plan to evaluate whether the observing modes are compatible with the needs, and to distill early discoveries from

the data. This is all to be evaluated in one of a series of planned, open science team meetings. Within some 5 months after launch, the observing mode will have stabilized, and extensive coordinated observations with other instruments, on SDO and elsewhere, will begin. Within a year from launch, early results will be presented at a dedicated science meeting, either for SDO as a whole or for only AIA-related science.

## A3 Summary of AIA science requirements on instrument design

### A3.1 Field of view

The AIA field of view (FOV) is a compromise between the needs for high resolution and the requirement for full-Sun observing (see Fig. A2). *TRACE* observations show fine structure down to the 1.0 arcsec resolution, clearly requiring AIA to achieve a resolution comparable to that of *TRACE*. On the other hand, the 3 MK corona as seen by, e.g., YOHKOH/SXT extends well above the limb; the density scale height for a hydrostatic corona is 0.21 $R_\odot$ at 3 MK.

Fig. A4 shows the fraction of the X-ray irradiance for a circular field of view for a range of diameters. Our choice of a FOV with a diameter of $41 - 46$ arcmin enables us to observe $\approx 96\%$ of the total X-ray irradiance, out to $2.6 - 4.0$ emission scale heights (or half that in density scale heights). That means that the AIA observations miss at most $\sim 2\%$ of the expected SDO/EVE signal (compare Fig. A4) for the signal with the largest scale height. Emission from lower temperatures, as well as from the hottest, brightest phases of flares, is confined to well within the AIA FOV, and therefore fully captured in the telescopes.

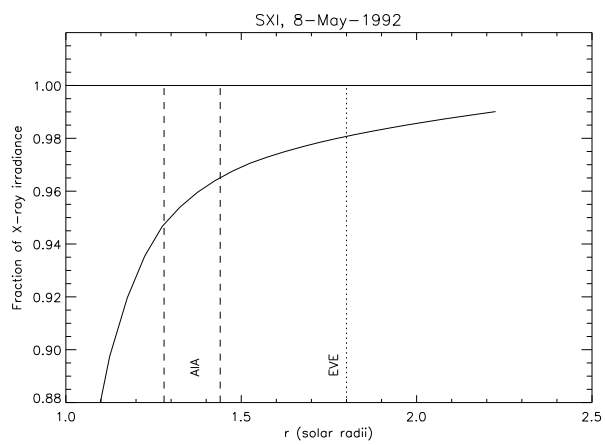


Figure A4: *The estimated fraction of the total X-ray irradiance, as measured by the YOHKOH/SXT telescope, for 8 May 1992, as a function of the height above the solar limb. The minimal and maximal AIA dimensions for the horizontal/vertical and diagonal fields of view (41 and 46 arcmin, respectively), are indicated by dashed lines. The dotted line shows the FOV of the SDO irradiance monitor, EVE.*

A $4096 \times 4096$ detector allows a field of view on the horizontal and vertical axes of $2.13\Delta\phi$, for pixels of $\Delta\phi$ arcsec. In order to match the EVE FOV of 1.8 $R_\odot$, for example, the pixel size would have to exceed the chosen value of 0.6 arcsec by $\sim 40\%$; such a decrease of resolution is not warranted given the substantial uncertainties in spectral-line properties, ionization balances, mirror and detector efficiencies of the AIA and EVE instruments, and the uncertainties intrinsic to absolute calibrations, combined with the need for high spatial resolution derived from TRACE observations.

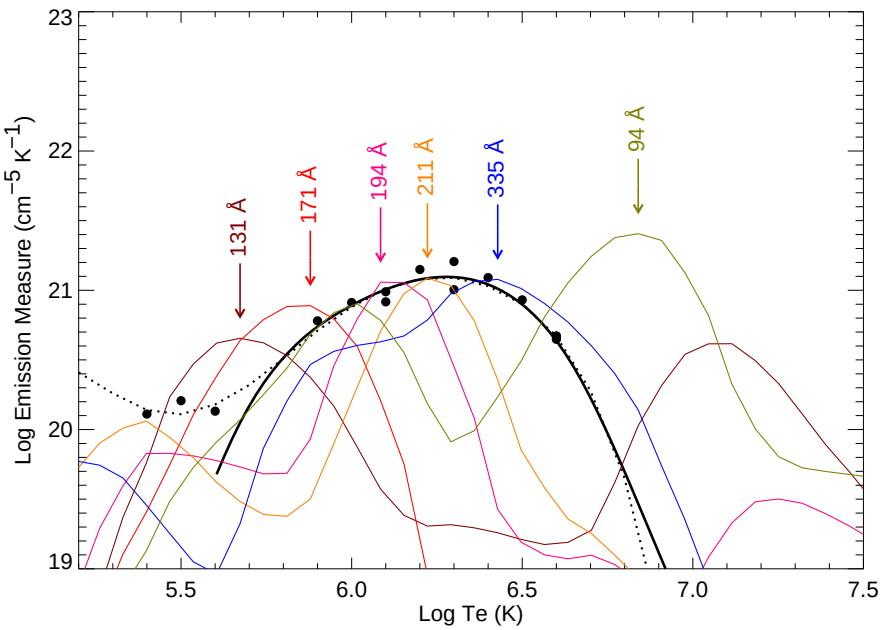


Figure A5: *The temperature coverage of the AIA allows us to derive the thermal structure within a pixel. This is demonstrated by the successful DEM reconstruction for a wide variety of features, demonstrating the complete view of the evolving plasma. Dots show the net DEM derived from 12 small SOHO/CDS rasters and 4* YOHKOH*/SXT filter images. The black curve is the recovered DEM based on simulated AIA data. The responses of the individual coronal AIA channels are shown normalized to the DEM where each product of response and DEM peaks. N.B. This figure has been updated from the proposal with the current response curves.*

### A3.2 Wavelength set

The AIA proposal included a set of 6 EUV channels to observe the solar corona. The guiding principles for the selection of that wavelength set were

1. the full set should cover the full range in temperatures from $\approx 1.$ MK to $\approx 16$ MK,
2. the number of channels should be compatible with the achievable temperature resolution given the physical constraints,
3. the lines should be emitted by ions of a single element to avoid a dependence of the relative abundances in the coronal plasma.

The required number of channels is derived by combining the required thermal coverage with the typical temperature interval over which a given ion dominates in the ionization balance (assuming thermal equilibrium). This limitation to the thermal resolution reflects the fact that the ionization partitioning provides a smooth weighting kernel to the Fredholm problem that describes DEM inversions which fundamentally limits the resolution of the inversion to about the width of that kernel in temperature space.

The thermal range of a factor of 16 spans four ionization intervals of a factor of approximately 2. In order to achieve the optimal resolution in temperature of a factor of 2, the thermal interval should be oversampled, ideally by a factor of two, suggesting 8 channels. Instrument constraints led us to choose 6 channels; modelling demonstrated that this is adequate to resolve the thermal structure, and certainly provides enough overlap that coronal volumes can be observed even if the coronal plasma evolves in temperature. An example of a DEM inversion is shown in Fig. A5 based on CDS observations of a quiescent active region; for

comparison, the figure shows the response curves of each of the channels to plasma at various temperatures. If the number of channels is reduced, the success of the inversion scheme rapidly deteriorates. Fig. A6 compares DEM inversions for a flare-like plasma for the optimal 6-channel case (right) to a 4-channel case (left); the reconstructed DEM in the latter case bears no resemblance to the structure of the input plasma.

The wavelength set originally proposed was carefully evaluated before and during the October 2003 AIA science team meeting. The lack of high transition-region lines (i.e., between 0.2 MK and 0.8 MK) was felt to be a deficiency, both by the team and by the broader community, including the EVE team. The AIA team considered the use of a narrow-band UV filter to select, for example, a region between 1302 Å and 1356 Å in which all strong lines are formed around $10^4$ K, while the continuum is weak throughout. Alternatively, EUV lines in the range of several hundred Ångstroms were considered.

The inclusion of a TR wavelength in the UV or EUV would adversely affect the capabilities of the AIA as proposed, because

1. A filter-based design would not enable the required observations in the UV: filters cannot be made narrow enough to adequately eliminate continuum contributions or contributions from neighboring lines. Imaging in the EUV with normal-incidence optics is not possible at the required passbands and sensitivity. Hence, inclusion of such transition-region lines would require a major redesign of the optics (as reflected in the grating-based imager included in SHARPP).
2. Given the current constraints on the instrument package, the inclusion of a mid-TR line would require the omission of one or more of the Fe lines in the EUV channels. That would reduce the thermal information to be derived from the AIA coronal data so significantly that the thermal coverage would no longer be complete, and the thermal information seriously compromised (cf., Fig. A5).
3. The current AIA design includes only iron lines to study the corona; inclusion of a non-iron TR line would introduce the substantial problems associated with changes in the composition of the coronal-TR gas depending on local conditions.

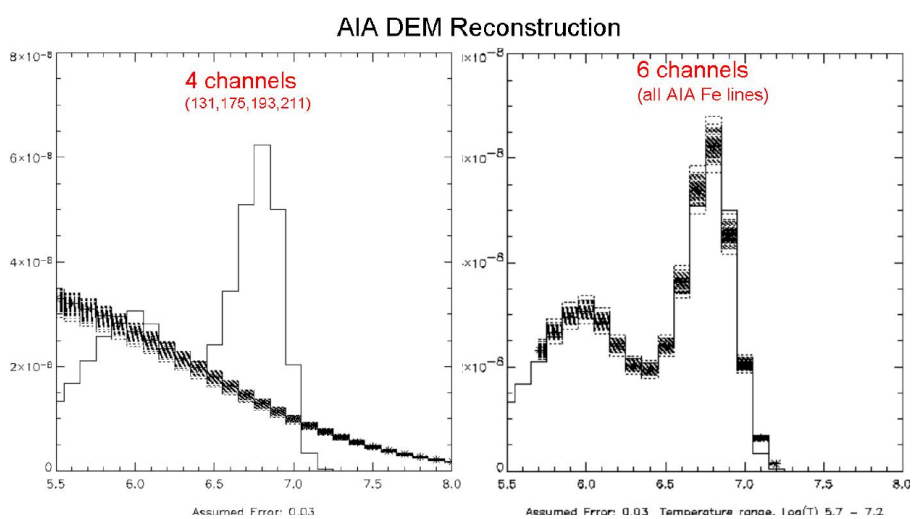


Figure A6: *The successful reconstruction of the thermal structure of the corona along the line of sight within a pixel depends strongly on the number of channels used: the input thermal weighting (thin histogram) of a flare-related plasma can be reproduced faithfully using the 6 Fe-line channels of AIA, but not at all if only 4 channels were available. The multiple histograms building up the reconstructed curves provide information on the inversion uncertainties.*

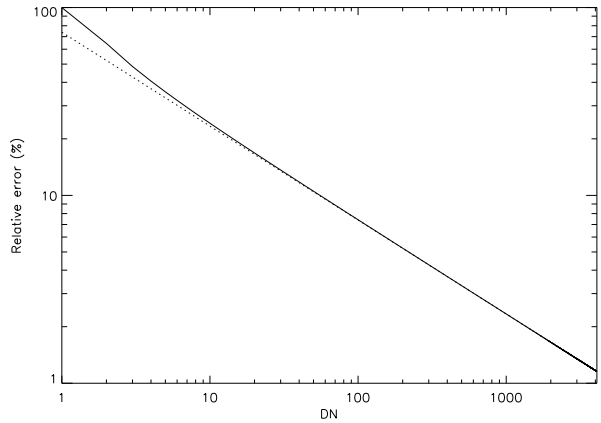


Figure A7: *Estimated relative uncertainty (in %) for a 14-bit A-D conversion, dropping the least significant two bits (leaving 4096× dynamic range), at 150,000 electrons full well, and an expected readout pedestal of 25 electrons. The AIA images will be photon-noise dominated even for low DN levels, as shown by the proximity of the expected uncertainty to the photon noise only (dotted line).*

In conclusion, the wavelength set as given in Table A1, was found to be well optimized for the primary science goals of ILWS and SDO. The set of Fe-line EUV channels provides the minimum set for which successful, relatively unambiguous thermal analyses (for example by DEM inversions) can be made for plasma temperatures ranging from that of quiet Sun to flares.

### A3.3 Dynamic range

The brightness contrast between active regions and quietest solar region is at least a factor of 10 to 100 for 1 MK to 4 MK plasma. During flares, that contrast can increase markedly, particularly in the highest-energy channels and in the TR channel that includes the C IV 1550 Å doublet.

The relative uncertainty in the signal at a given DN level, $S$, equals $\sigma = ([D\,S - P]/A)^{-1/2}$, for a readout pedestal (including dark current and readout noise of $P$ electrons (we expect $P \approx 25$) at $A$ electrons/photon and at $D$ electrons per DN. For photon energies equivalent to 200 Å, $A \sim 20$ (scaling inversely with wavelength). A full-well level of $150,000$ electrons implies a maximum dynamic range of 7,500, requiring a maximum resolution of 12.9 bits/pixel. With the above expression for $\sigma$, we find that at 12 bits/pixel, the noise reaches 100% at 1 DN (for a readout pedestal $P \sim 25$, and with $D = 36.6$ to reach full well at 4096 DN) - see Fig. A7.

### A3.4 Data aquisition system

The following essential capabilities were identified by the AIA science team for the on-board data acquisition system:

- start exposures in all cameras quasi-simultaneously, i.e., within a fraction of the exposure duration; starting exposures in a set within $\sim 1/10$th of a second appears adequate.
- read the full 4096x4096 image in under 2.5s
- perform partial readouts to speed up the cycle time; reading two strips on either side of the horizontal detector center is possible with the current camera design, and is adequate; it should be possible to specify the strip positions (top and bottom) to multiples compatible with the compression algorithm,

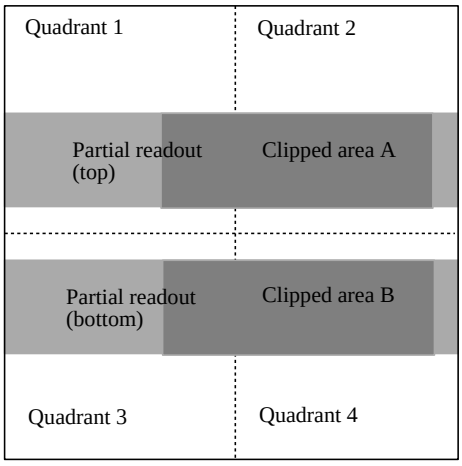


Figure A8: *The camera provides the following readout options: (1) The full detector (four quadrants) can be read out in approximately 2s. (2) By flushing parts of the detector information, partial fast readouts can be made of horizontal strips, symmetrically about the center of the detector. Subsequent clipping can select two rectangular areas on the detector; one or both of these can be sent into the telemetry stream. The automatic exposure control for a given wavelength and cutout combination functions on whatever part of the detector passes through the compressor into the telemetry stream.*

or perhaps as low a resolution as 32 pixels. Subsequent data processing should allow 'clipping' such partial fields to a specified width, again compatible with compression requirements, and not necessarily better than to 32 pixels. Note that the CCD orientation must be such that the rows are essentially aligned with the solar equator.

- have independent AEC systems for each "frame" instruction (i.e., wavelength and area), plus limiters to be specified for shortest and longest exposure.
- make intensity histograms for the region specified to be compressed into the telemetry stream.
- AEC to act on next exposure at the same wavelength and cutout combination.
- AEC algorithm to allow either stepping along a specified 'table' of exposures, or to jump to an estimated optimal exposure time to allow fast response to rapid brightenings, with explicit limiters at the low and high end of an allowed range.
- expose for specified duration in steps no coarser than a factor of 1.2
- have tunable compression schemes, including lossless and uncompressed, allowing compression up to at least a factor of 10.
- must not limit wavelength selections among the four telescopes when cycling through a set of nested loops.

Desired capability, subject to further study:

- Flare locator based on a low-resolution short exposure.

### A3.5 Telemetry

For a baseline observing mode that produces 8 $4096 \times 4096$ images per 10 s interval with 12 significant bits per pixel, the total uncompressed science telemetry need is 161 Mbps. Compared to this data stream, the volume of the housekeeping telemetry is negligible.

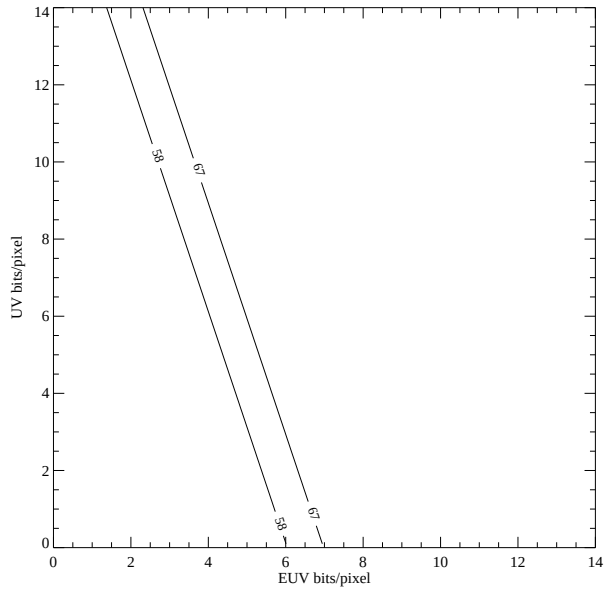


Figure A9: *Estimated telemetry rates for compressions to the specified number of bits per pixel for the 6 EUV (horizontal) and 2 UV/WL (vertical) images per set of 8. Two contours show where compression settings combine to a total (science plus housekeeping) telemetry rate of 58 and 67 Mbps, respectively. Optimal combinations with the least image compression for both are found near the diagonal*

Data compression by a factor of 2.29 to 2.65 brings that total down to 67 Mbps or 58 Mpbs, respectively. This net compression amounts to 4.5 to 5.2 bits per pixel. The UV/WL images are expected to compress better than the more structured EUV images (that also include a relatively larger number of particle hits). In order to meet the compression to 67 Mbps, the 6 EUV images could be compressed by a factor of $\sim 2$ and the 2 UV/WL images by a factor of $\sim 4$. Fig. A9 shows all possible combinations of compression factors (assuming a 12-bit AD conversion) that result in either 58 Mbps or 67 Mbps.

## A3.6 Exposure times

The science requirements of the AIA necessitate short exposure durations in all the EUV and UV channels for two complementary reasons: (1) in order to avoid blurring or ambiguity in the images due to evolution of the target *during* the exposure, and (2) to hasten the cadence of images to avoid loss of information *between* exposures. Motion during an exposure can be due to explosive phenomena, waves, or ejections), and short-time-scale transient heating events, like micro- and nanoflares. Blurring due to evolution of the target occurs according to the angular resolution of the images and the characteristic speeds of the anticipated variations. In the corona, disturbances traveling at a sound speed near 100 km $s^{-1}$ will appear blurred in the AIA 0.6-arcsecond pixels within 4 seconds, whereas changes that occur at the coronal Alfvén speed can blur portions of the image in less than half a second. The cadence of images is affected by the CCD readout rate, the mechanism move times, and any latency due to setup for the image.

Conversely, shorter exposures can impact the precision of the photometry, particularly for fainter plasma. The requirement of shortness of exposure must be balanced against a minimum allowable precision (i.e., maximum allowable uncertainty) in photometry, since much of the quantitative analysis to be performed with the AIA requires knowledge of the radiative output.

The SDO Science Definition Team report indicates a desired image cadence of 10 seconds (i.e., 10 sec-

onds between successive complete sets of images in all wavelengths). Additionally, the SDT report specifies a level of photometric precision of "about 10%...for these images to be useful as a tool for...determining the sources of the spectral irradiance..." and for "making useful ratios of the images to determine physical characteristics of the atmospheric features." With the relative signal uncertainty as described in Sect. A3.3, a precision of 10% in the photometry of a single image requires that the minimum exposure duration collects 100 photons per pixel.

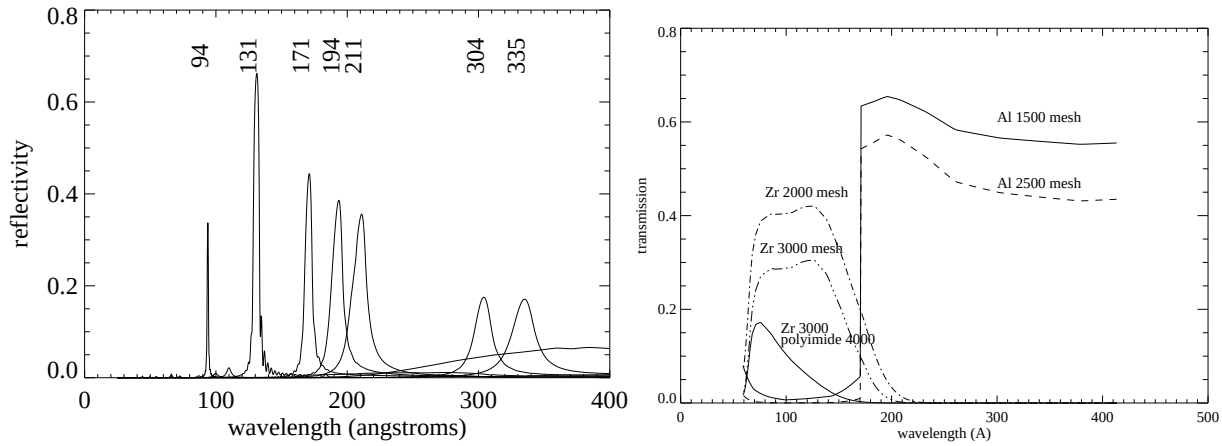


Figure A10: Left: *Reflectivities of the AIA EUV mirrors. The slowly rising curve at wavelengths longer than 230 Å is a secondary peak in the 94 Å channel; it is entirely rejected by the Zr filters.* Right: *Transmissivities of the entrance and focal plane filters of the AIA EUV channels.*

### A3.6.1 EUV sensitivity

The reflectivities of the AIA EUV mirrors are plotted in the left hand panel of Fig. A10, and the transmissivities of entrance and focal plane filters are shown on the right. The AIA filters are "thin aluminum" (1500 Å Al on 80% transmissive mesh), "thin zirconium" (2000 Å Zr on mesh), "thick aluminum" (2500 Å Al on mesh), "thick zirconium" (3000 Å Zr on mesh), and "Zr+poly" (3000 Å Zr supported by 4000 Å polyimide). The entrance filters are thin aluminum and thin zirconium, whereas the focal plane filters can be selected to be either the thin, thick, or Zr+poly (for 131 Å channel only), as desired. Countrates for the respective EUV channels are given in Table A4 for a variety of solar targets. These countrates are arrived at by assuming a solar EUV output spectrum (generated from the CHIANTI database [40] based on the coronal abundance given by [89], with ionization equilibrium given by [90]. This solar spectrum, as a function of temperature and wavelength, is convolved with the mirror reflectivities, the filter transmissivities, and CCD efficiency to yield the temperature-dependent response functions plotted in Fig. A11. The countrates for a given solar target in Table A4 are derived by convolving these response functions with published differential emission measure (DEM) estimates for that type of target. The particular DEM used (except for the microflare) are plotted in Fig. A12, with representations of the photon countrates for each of the EUV channels. The microflare simulation assumes a DEM of $2 \times 10^{28}\mathrm{cm}^{-5}$, with temperatures set to the peak response for each channel.

With CCD readout contributing 2.3 seconds to image cadence, the targeted 10-second image cadence allows 2.7 seconds of exposure duration per image (i.e., 2 channels per telescope $\times$ 5 seconds per channel). Changing of the focal plane filters and/or aperture selector is carried out simultaneous to the CCD readout (with the shutters closed), and therefore does not contribute to image cadence. Table A4 demonstrates that

Table A4: Predicted EUV Countrates, in photons per pixel per 2.7 s exposure, or time to full well ($< \ldots >$) if that is reached in less than 2.7 s, for various solar features and for the thin and thick focal plane filters in the top and bottom halfs, respectively.

| Channel | Quiet Sun | Active Region | M flare | Microflare |
|---|---|---|---|---|
| 94 Å | | 35 | $< 0.10s >$ | 170 |
| 131 Å | 22 | 240 | $< 2.8ms >$ | 3,400 |
| 171 Å | 1,100 | $< 2.1s >$ | $< 57ms >$ | $< 0.19s >$ |
| 193 Å | 810 | $< 1.6s >$ | $< 7.1ms >$ | $< 0.30s >$ |
| 211 Å | 250 | 6,600 | $< 74ms >$ | $< 1.1s >$ |
| 304 Å | 2,500 | 8,100 | $< 10ms >$ | |
| 335 Å | 61 | 2,700 | $< 97ms >$ | 5,200 |

| Channel | Quiet Sun | Active Region | M flare | Microflare |
|---|---|---|---|---|
| 94 Å | | 25 | $< 0.14s >$ | 120 |
| 131 Å | | 23 | $< 29ms >$ | 330 |
| 171 Å | 960 | $< 2.5s >$ | $< 67ms >$ | $< 0.22s >$ |
| 193 Å | 700 | $< 1.8s >$ | $< 8.2ms >$ | $< 0.34s >$ |
| 211 Å | 220 | 5,700 | $< 85ms >$ | $< 1.3s >$ |
| 304 Å | 2,000 | 6,400 | $< 13ms >$ | |
| 335 Å | 48 | 2,100 | $< 0.12s >$ | 4,100 |

even for the Quiet Sun, EUV channels imaging plasmas between 50,000 K and 2 MK (i.e., the 304, 171, 193, and 211 Å channels) will achieve the minimum-requirement 10% precision well within 2.7 seconds. (Indeed, the Quiet Sun countrates in those channels yield relative uncertainties on the order of 2–6%.) For active regions, only the 94 Å channel falls short of the prescribed 100 photons/pixel within the allotted time (yielding 17% relative uncertainty in our simulation); and for many flares, the CCD reaches full well quickly in all channels, indicating the need for a fast shutter mechanism.

The expected exposure times require that the shortest shutter-expose time should not exceed 5 ms. In order to calibrate the exposures to a normalized integration time, actual exposure durations should be measured and entered into the image 'header' in telemetry.

### A3.6.2 UV sensitivity

The UV channel of AIA is a simplified version of the highly successful TRACE system, which has been operating in space for 4 years now with very little if any optical degradation. These simplifications are possible because TRACE had additional requirements for 1216 Å and narrow-band C IV 1550 Å imaging. The most valuable TRACE UV channel has proven to be "1600Å," a 200 Å-wide high transmission band that includes the C IV lines (100,000 K), various chromospheric lines, and UV continuum formed in the temperature minimum. The high throughput allows very short exposures and high cadence, while the presence of C IV gives it great sensitivity to transient energy releases. During flares, footpoints, loops and ejecta are often all visible, sometimes causing confusion in footpoint locations. Therefore, a second UV channel (TRACE "1700Å") is included, which shows the temperature minimum and low chromosphere but very little plasma at transisiton region temperatures.

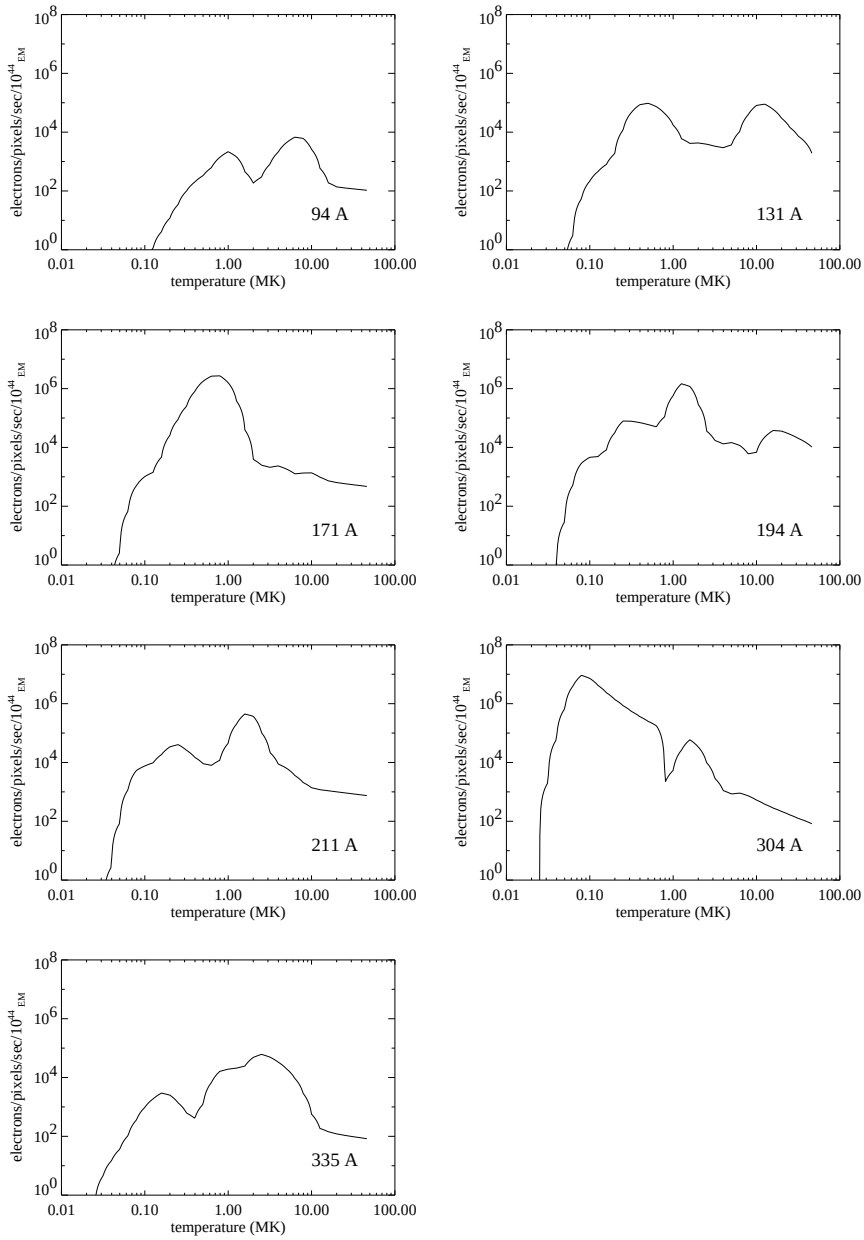


Figure A11: *Response functions of the EUV channels for AIA. Plotted is the signal in units of electrons per pixel per second per* $10^{44}$ *of emission measure, as a function of plasma temperature.*

AIA uses filters and coatings in key components similar to TRACE as follows:

- **Front Window**: $MgF_2$ with an interference filter coating to reject visible light ($\leq< 10^{-4}$ transmission) while passing UV ($>$ 20% transmission), identical to TRACE except smaller diameter (8 cm vs. 12 cm).
- **Primary and Secondary Mirror coatings**: Al with $MgF_2$ overcoat for protection, identical to the TRACE secondary. The TRACE primary had a dielectric mirror coating to maximize reflectivity at 1500 AA, but this is not needed for AIA. The simpler coating allows us to have one vendor apply

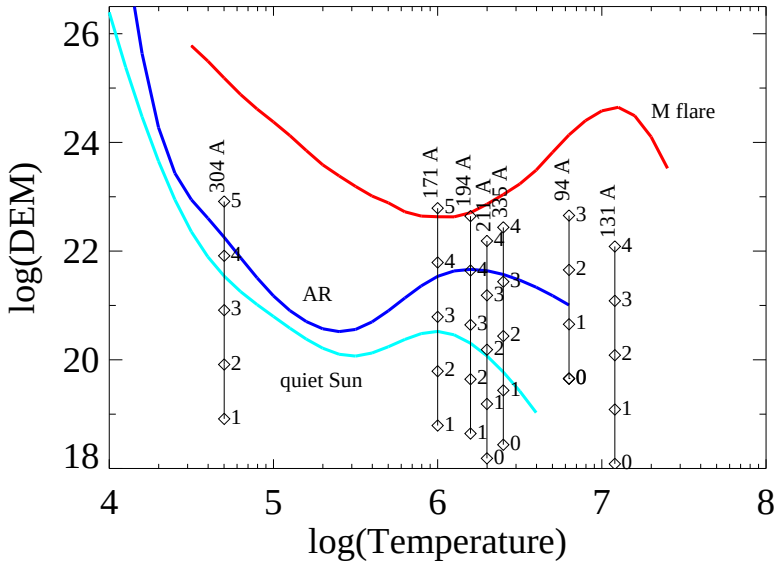


Figure A12: *Countrates, in detected photons per second per pixel, for each of the EUV channels. The vertical bars are plotted at the temperature of peak response for each channel, and display the log of the photon countrate as a function of emission measure. For comparison, DEM estimates for various solar features are shown, indicating the countrates to be expected from each kind of solar feature. The DEM used are those provided in the CHIANTI database, version 4.2.*

all mirror coatings, substantially reducing cost and risk of coating damage during handling.

- **1600 Å filter**: 200Å bandpass centered at 1600 Å, identical to TRACE; note this has high transmission (15%) for the C IV lines. The effect of the change in primary mirror coating on this channel has been simulated accurately using TRACE 1600 and 1700 Å images, demonstrating that none of the objectives are compromised.
- **1700 Å filter**: same design as 1600 Å filter but shifted 100 Å and applied to a fused silica substrate, which absorbs all light below 1600 Å, eliminating the C IV lines completely ($10^{-7}$ transmission). TRACE used a fused silica filter in series with its 1600 Å filter for this purpose (since it had 2 filterwheels); the AIA design has much higher throughput.
- **Visible filter**: 500 Å bandpass centered at 4500 Å, very similar to the TRACE guide telescope filter. A broad "white light" channel (as on TRACE) would require a very short exposure time, driving the shutter design. This filter permits images during ground testing and flight, in a well-defined wavelength band to allow image quality evaluation using phase diversity techniques.

No selector mechanism is required on this telescope because the Al filter in the filterwheel effectively blocks the UV/visible light from the EUV channel, and likewise the 1700 Å and 1600 Å filters block the EUV and UV/visible leakage through the front Al filter. This has been verified on TRACE by taking images with the quadrant selector uncovering roughly half of the 171 Å and UV quadrants simultaneously. After 4 years in orbit, the TRACE UV front window leaks only 20% more visible light than it did at launch. At the same time, the visible light leakage through the "worst" EUV front Al filter converts to a transmission of about $3 \times 10^{-6}$. With similar filter performance, the AIA wavelength bands will all have uncompromised spectral content, except for a diffuse scattered light level of about 5% in the visible band due to leakage

through the front Al filter. This can be estimated and subtracted if desired, using measurements of off-limb intensities.

### A3.7 Radiation and other image degradation

The AIA images in the UV and EUV pass bands will show high contrasts in measured intensity. This will be true particularly during eruptive or explosive events, but also in general during states of quiescence. The intensity gradients will be steep, with expected loop widths of a few pixels and below, with bright flare ribbons and kernels with scales near the telescopes resolution, and in 'mossy' regions in which chromospheric fibrils interact with the transition-region footpoints of hot coronal structures.

One source of image degradation will be the impact of high-energy particles on the detectors. These produce bright spikes localized almost entirely within single pixels. The shielding and telescope baffling is designed such that, except during particle storms, the number of particle hits is limited to several hundred per exposure. Experience with TRACE data processing demonstrates that such a dosage can be removed with acceptable image degradation and loss of information (several hundred pixels per image is equivalent to $\sim 0.001$ percent of the total).

Such particle hits, along with anomalously responding CCD pixels introduce strong gradients in the images. The image compression scheme needs to be able to deal with this. This is one of the reasons for choosing a pixel-by-pixel compression scheme: in a compression scheme like JPEG, the use of truncated Fourier series for patches of the image introduces substantial ringing around spikes, so that even after apparently successful removal of particle hits, residual patterns show up in the images. TRACE images often exhibit such artefacts in high-radiation exposures; they are most clearly seen in regions of low intensity, but affect the image information everywhere, complicating the analysis of, for example, high-frequency waves.

The AIA compression scenario is based on a pixel-by-pixel lookup table, so that we are certain the particle hits and anomalous pixels to do not contaminate the signal from neighboring pixels. Cross talk between the four segments of each CCD being read out simultaneously will not adversely affect the science if at a level of less than 1 DN at most, i.e. at 1 part in 4,000; current detector design has a best-case scenario of 1 in 20,000, i.e. significantly better than the requirement.

### A3.8 Calibrations and instrumental effects

**Absolute calibration of AIA** The design and calibration of the AIA must reflect that the investigation aims to perform quantitative analyses of the solar corona and its energy budget. Note that there are two aspects to the calibration needed by the scientific community: (a) the set of instrument properties that allow the calibration of the observed quantities to photons/cm$^2$/s in each passband, after deconvolution with the instrument's MTF and correction for other instrumental effects, and (b) the sensitivity curves that allow modellers to transform computed spectra to photons/cm$^2$/s in each passband. The latter transformation includes the radiative properties of a plasma, affected by abundances, densities, ionization states, line strenghts, possible radiative-transfer effects, and possible deviations from thermodynamic equilibrium. The constraints formulated below result in calibration procedures for which the instrument uncertainties are less than the uncertainties associated with the plasma properties, so that AIA data will remain valuable even when new, more accurate models of the radiative properties of the coronal plasma become available.

We identify the following requirements, in order of decreasing priority:

1. *Relative effective area within each passband:* In addition to the main spectral line (or few lines) listed in Table A1, each EUV passband contains contributions from multiple other lines (with negligible continuum emission, except during strong flares). Their contributions are relatively weak compared

to the main lines for the Fe-line channels. This relaxes the need for high accuracy on the determination of the wavelength dependence of each passband. Nevertheless, the sensitivities of the instrument to each of these lines must be known to a precision of a few percent relative to the dominant line(s) in order to not significantly affect thermal studies based on the full set of Fe-line images, and in order to enable adequate in-flight cross-calibration with EVE spectra. The latter, in fact, imposes the strictest contraints, as EVE observes only a subset of the lines observed by AIA, but uses other spectral lines from the same ionization states. Since, in general, the line strengths and ionization balance of a plasma are known to accuracies no better than of order 10%, a relative precision within the AIA passbands of order $3 - 5\%$ is adequate.

2. *PSF, scattered, diffracted, and stray light:* We expect high-contrast images in all but the near-photospheric passbands. This will be true in general, but particularly so during the early phases of flares. The wings of the PSF, and any scattered and stray light (including, for example, the light diffracted by the filter support grids), will contaminate light from the faint areas on the disk with light from the brighter regions.

   Information on the PSF could be obtained from a planet transit. Unfortunately, a disk transit of Mercury will not happen until 9 May 2016. A Venus transit will occur on 5 Jun 2012, which is within the primary phase planned for SDO; this will provide useful information, but earlier data on the telescope's properties are clearly needed. We are developing a plan that includes pre-launch studies of the telescope properties, and a combination of offset pointings and lunar eclipses during flight.

   We will investigate efficient methods to deconvolve images with the telescope's MTF to produce level-1 data; we plan to investigate the advantages and difficulties of different methods, including simple, but fast FFT filtering or the slower maximum-entropy methods that can deal better with noise and image artefacts. Design considerations to facilitate this most efficiently include alignment of the supporting wire grids of the segments of the front filter assembly to avoid multiple diffraction patterns. The deconvolution works best if multiple orders can be observed (optimally at least 10); even when reading out strips of the CCD for fast-mode operations, this places no significant constraint on the orientation of the filter grids relative to the detector as long as at least a 5-arcmin. wide strip is read out, or a $> 500$-pixel wide strip of an activity belt. The readout time of such a strip is expected to be $\sim 0.5$ seconds, or will at least be significantly less than the 2 s cadence planned for fast-mode operations. We therefore do not anticipate reading out even narrower strips that might require a particular orientation of the diffraction pattern.

3. *Absolute calibration of exposures in the EUV Fe-line channels to photon fluxes:* The relative effective areas of the Fe-line EUV channels needs to be known to a precision of approximately 10% (see SDO/SDT requirements). That precision is higher than uncertainties in expected signal strengths given uncertainties in oscillator strengths and ionization balance, and is therefore expected not to contribute significantly to thermal studies. Provided that the pass bands are well characterized (see under item 1), in-flight cross calibration with EVE can be performed to a precision of a few percent, which is a small fraction of the overall solar irradiance variability in the UV and EUV.

   Note that this issue also involves knowledge of the actual exposure durations to better than 1% (cf., Sect. A3.6.1).

   If SOHO or TRACE are still operating when SDO is launched, care should be taken to cross-calibrate the EIT, TRACE, and SDO 171 Å and 193-195 Å channels.

4. *System flat-field and CCD background level:* Ray-tracing studies will provide a baseline for the flat-field correction (including vignetting). Once in flight, repeated offset pointings can be performed to measure this in more detail, and to determine any degradations over time. Long-term averages of all the images in a single wavelength will be used to quantify flat-field gradients along the direction of solar

rotation. Occasional rotation of the SDO S/C for several weeks at a time would allow determination of the flat-field gradients in the y-direction of the detectors. This possibility, and alternative methods to determine flat-field properties, continue to be studied as their impact on the SDO investigation are clarified.

5. *Absolute calibration of exposures in the EUV He II 304 Å channel:* The calibration of the He II 304Å channel is primarily important for solar (E)UV irradiance studies, because the optically thick nature of the line severely limits its usefulness in the analysis of radiative losses to learn about the structure of the solar atmosphere. An absolute precision of order 10% is required (SDO/SDT report). If SOHO is still operating when SDO is launched, care should be taken to cross-calibrate the EIT and SDO 304 Å channels.

The AIA team will face a complex task to carry out the calibration to the required precision, but past experience suggests that it can indeed be done: using the CHIANTI database of atomic physics parameters for the spectral lines in the SOHO EIT multilayer bandpasses, it is possible to determine an in-flight, absolute calibration of instrumental response to much better than 10% [91]. This is crucial if we are to understand the spatially resolved, long-term EUV irradiance record - that is, the sources of variability in solar EUV output.

We note that AIA calibration will be further aided by comparison with observations by the SOLAR-B EIS spectrograph and the XRT X-ray imager. This will allow point-by-point relative calibrations, as well as in-flight assessment of the contributions from different lines to the pass bands.

Lowest priority issues regarding calibration include

1. *Absolute calibration of exposures in the UV/WL channels.* The AIA WL channel will be primarily used for image alignment with the HMI and other observatories, although some flare studies will use the higher-cadence flare-ribbon information that can be derived from the AIA images. No quantitative studies involving the WL channel require its absolute calibration.

The AIA UV channels will be used to analyze wave properties in the UV continuum and strong TR resonance lines like the C IV doublet around 1550 Å. The passbands are too broad to be able to separate the various contributions, however, so that the UV channels will be used primarily for differential studies focusing on the intensity evolution. A calibration accuracy of 10%, as for the other channels, allows the use of AIA UV images in comparison with UV irradiance instruments on other satellites.

**AIA intercalibration with other instruments** The current NASA Sun-Earth Connections theme plan is to overlap at least some SOHO instrument observation for up to one year with SDO operations. In particular, overlapping of EIT and AIA full-disk observations will allow the construction of an accurately calibrated time series of such data over at least a solar cycle and a half.

The database for the intercalibration effort will consist of observations normally obtained by both EIT (”synoptic” observations every six hours in all four EIT bandpasses) and AIA (the baseline observing program is described in Sec. A4). The broader range of temperatures covered by AIA should allow a substantially better determination of the coronal temperature structure over a large range of solar features of a variety of spatial scales.

The change in EIT throughput over time has been tracked with the use of visible-light calibration lamp images that allow the determination of the EUV flat field as a function of time [92]. One way to track flat-field changes accurately will be by AIA-EIT intercalibration during mission overlap, combined with comparison with the integrated solar EUV spectra obtained by EVE on SDO. One or more LEDs within each AIA telescope will provide supplemental information. We emphasize that the response of the AIA CCDs are expected to change much more slowly than the less mature detectors that were used in EIT.

Over more limited areas of the solar surface, Solar-B EIS spectra could be used to help calibrate similar areas of AIA images, and we could derive a calibration for the AIA data set from this source as well. In practice, this requires an accurate, absolute, photometric calibration for EIS, presumably provided by rocket underflights (are any planned?), but even with such rocket support, SOHO CDS intercalibration with EIT has proven of limited value - no single CDS or EIS observation contains all the lines in all the multilayer telescope bandpasses.

In order to insure progress on these and related intercalibration issues, we will propose to the SDO SWG the formation of an SDO intercalibration working group, to be charged with drawing up an intercalibration plan, executing it, organizing scientific workshops on this work, and publishing their proceedings.

## A4 Observing plans, and requirements on ground operations

**Operations Concepts** Simple mission operations and a uniform data product are primary goals for AIA. For comparison, we note that operations will be slightly more diverse than those for HMI but still require only minimal staffing. Communications to the MOC will be via dedicated workstations at LMSAL. They will be located in an area that meets NASA data systems IT-2 security requirements.

**AIA Commissioning Phase** After checkout and outgassing, AIA will enter a commissioning phase for approximately one to two months. This time will be used for calibration and testing of each channel and to determine the best exposures and cadence for the science programs. Compression parameters and AEC (automatic exposure control) will be checked and adjusted as necessary. Parameters for the baseline program will be tuned and other programs, such as high cadence series, will be explored for possible use in campaigns. A list of high priority science objectives will be prepared for special attention during this phase to guarantee early science return.

Commissioning phase activities will be conducted from the JSOC facility at LMSAL and will not require AIA personnel at the SDO MOC except in the event of unexpected problems.

We will also be testing and tuning our data access, processing, and analysis systems during this period.

**Initial exploratory phase** In the transition phase from commisioning to nominal, or standard, operations, we plan to explore the solar corona using all the capabilities of the AIA. We plan on using fast cadences, long exposures, potential off-points, etc., to allow discoveries to be made in the new spatio-temporal-thermal domain opened up by AIA. This period, of at least one to two solar rotation, is likely to see changes in observing modes from day to day, as we learn to interpret the new imagery.

**Standard operations** Nominal operations will begin once the baseline program is finalized, the exploratory phase ended, and some early science objectives and necessary calibrations accomplished. Our plans are essentially the same as described in the proposal.Once we begin nominal operations, we expect to have the data system working to provide near real time data products to the community.

The principal requirement for the AIA on SDO, as formulated by the Science Definition Team, is to produce one full set of EUV observations per 10 s interval. An example of such a mode, compatible with exposure time estimates in Sect. A3.6, is given at the top of Fig. A13. In this proposed baseline mode, the full EUV set is completed in 10 s intervals, while the full UV set is completed in 1 min./ intervals. The latter allows the use of the white-light (WL, or 4500) Å channel for photospheric flow tracking and multi-instrument alignment, while providing moderate-cadence 1700 Å UV continuum information to complement

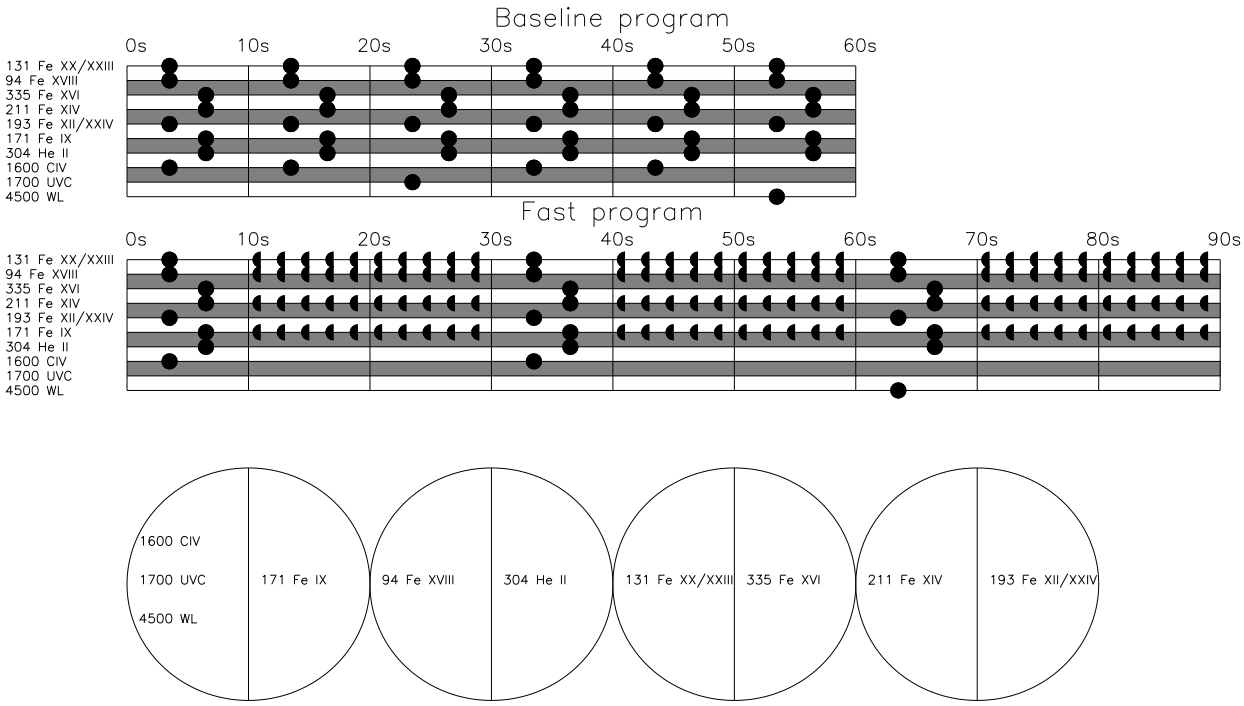


Figure A13: *Representations of AIA observing modes.* Top: *baseline AIA observing program, with each full-Sun image represented by a filled dot on a timeline bar; note that the observations are taken in sets of four ("chords" of essentially simultaneous exposures), which are paired to cover all desired wavelengths. These pairs constitute the "beats" on the bars, that are repeated with minor modifications as needed (see the 1600 Å, 1700 Å, and WL channels).* Center: *a sample special (flare) mode to observe at high cadence using partial images (half disks) in combination with full-disk observations (filled dots); if the images are smaller than 1/5th of the full detector, this sequence can be sustained indefinitely. A switch from the standard mode at the top to this special mode may be made by the planner for a substantial period, or may occur in response to a threshold-based flare flag that is under discussion.* Bottom: *The arrangement of the wavelength channels on the four telescopes.*

the more frequent observations in the 1600 Å channel measurements in which continuum and C IV lines (and others) strongly contribute.

**AIA Campaign Operations** Most of the time we expect to run AIA continuously and nearly autonomously using the baseline program. Certain classes of phenomena evolve even faster than resolvable with a 10 s cadence, as witnessed by observations in the visible, radio, and highest-energy X-ray channels. The initial, impulsive phase of flares and filament destabilizations (frequently part of a CME), for example, frequently exhibits processes on significantly shorter time scales. Oscillatory phenomena, part of the studies of coronal seismology, may also occur at higher frequencies. In order to observe and understand these phenomena, in their own right and as contributors to the spectral irradiance as measured by SDO's EVE instrument, we plan special observing modes to run during limited periods. Such modes should meet the constraints that

1. the net image frequency is significantly enhanced, while
2. the full-Sun synoptic program should not be discontinued entirely at any time, while
3. the full-Sun synoptic program should run without modification most of the time.

The above constraints are met by the following strategy:

1. during a period of no more than three months per year, the baseline program may be replaced by one or more special (custom) programs, that
2. enhance the cadence in certain wavelength channels significantly, by significant reductions in the field of view,
3. while slowing the cycle rate for the full set of full-Sun EUV observations to no slower than once per 30 s and for the WL/UV observations to no slower than once per 90 s.

Consultation with the SDO/EVE team let us conclude that the reduced full-Sun cadence from 10 s to 30 s in the above example does not significantly compromise the EVE science goals, and in fact are likely to prove helpful as the higher temporal resolution during flares allows a more detailed interpretation of the causes of the X-ray and EUV irradiance changes during such events.

To reduce cost and complexity, the onboard central processer will not perform image processing but some onboard responses and AEC can be accomplished using the count level accumulators. Scripts for special campaigns might include partial readouts from one or more CCD's for improved cadence. The location of the readout would have to be predefined for an onboard response. The subarea could be the location of an AR thought likely to flare or groundbased analysis of the data could be used to define an area (or correct it) if an observer is monitoring the quick look data. A cadence of 1 s to 2 s is feasible for a $1024 \times 4096$ readout (about 0.8 s for CCD readout and necessary mechnism moves leaving about 1 s for the exposure time) for a single wavelength. An interesting flare script might have the high temperature channels on telescopes 2 and 3 running at a 2s cadence while the other telescopes cycle through more slowly with the full FOV. The other wavelengths on these two telescopes could either be omitted or sampled at longer intervals to avoid interupting the high cadence set.

An example of such a program (details subject to further discussion) is shown in the second bar in Fig. A13. This mode of operations is readily implemented in the onboard software because near-synchronicity of the channels is maintained, and requires no changes to existing camera capabilities.

**AIA Eclipse-Season Operations** Loss of signal from the pointing systems during solar eclipses by the Earth are the primary concern for AIA. There may also be temperature pertubations degrading and/or off-setting the stabilization for a period after the eclipse. Stored commands in the AIA timeline will be used to open the image stabilization loops for each telescope prior to the predicted eclipse and turn off the S/C pointing feedback from the trackers. Stabilization during eclipse will be inertial, combined with a star tracker. The observing program will be suspended or modified for eclipse specific observations. After the eclipse, a programmed RTS will verify signal from the limb sensors, perform any required S/C re-pointing to put the image stabilization sensors within range and then re-engage the image stabilization loops for all telescopes.

## A5 Coordination with other instruments

The scientific capabilities of SDO and of the ILWS program will be greatly enhanced by coordination with the international fleet of solar and geospace spacecraft, and ground-based observatories. This will enable extensive coverage of Sun, heliosphere, and geospace. PI's or Co-I's from many of these instruments are on the AIA team, as identified in Fig. A14; they are committed to making optimal use of this intimate linkage to achieve the ILWS goals.

Starting from the premise that efficient coordination is essential to achieving the AIA science goals, the AIA science team will continue to develop a plan to coordinate. Because the AIA will be operating

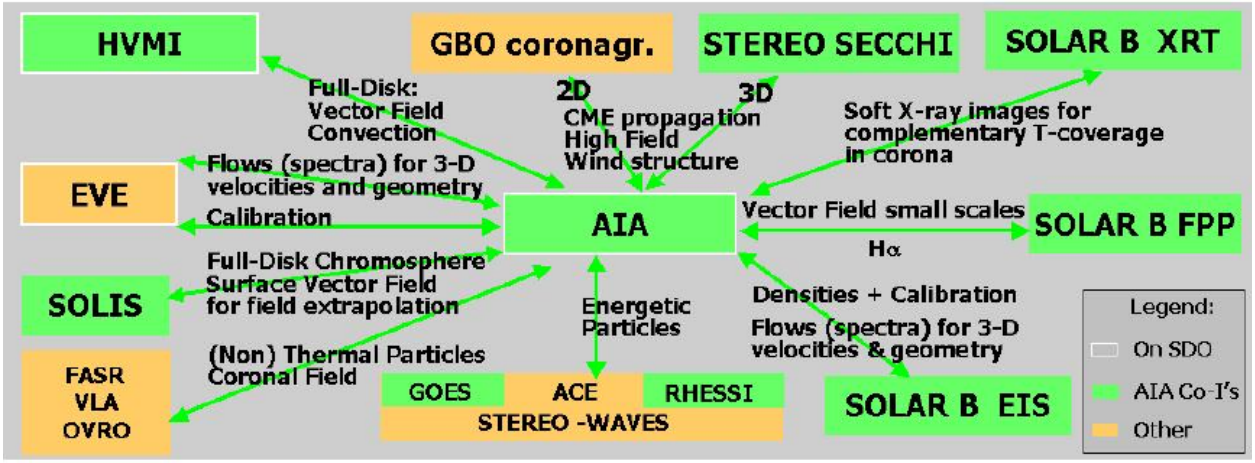


Figure A14: *The AIA team will closely coordinate with other science teams, both for instruments on SDO and others. This panel shows some of the science connections, and indicates which of the other science teams have PI's or co-investigators on the AIA team.*

in a standard mode much of the time, such coordination consists mostly in convincing other partial-disk instruments to coordinate on specific targets; fast communications and display of interesting regions on the AIA website will be essential for this.

The science goals discussed in preceding section made it clear that H$\alpha$ images and supplemental vector measurements are of highest priority. Coordination with Solar-B, and with SOLIS and other GBOs, will be defined prior to SDO's launch. Co-I's for both Solar-B and SOLIS are committed to making this succeed.

Of importance to the success of the (I)LWS program as a whole is coronagraphic information. In the absence of a coronagraph on SDO, coordination is needed with GBOs, such as HAO's observatory at Mees on Mauna Kea.

## A6 Observations, data bases, products, and requirements on data systems

For clarity in the descriptions below, we distinguish betwen 'pipeline software' (described in this section), 'browsing software,' and 'supporting software' (discussed in Section A7.5:

- *Pipeline software* is used to process each image, or a large fraction of images, to produce data products that are needed on a near-real-time to next-day basis. Such data products include quick-look image products (e.g. despiked images, browsable movies) and catalog entries (e.g. event listings). The data products produced by pipeline software will be regularly available, but the software itself will not be widely distributed.
- *Browsing software* describes the software that is used for rapid compilation, display, and comparison of movies, with coarse corrections for, e.g., exposure times and CCD readout pedestals, to enable easy inspection of substantial amounts of data, e.g. for daily inspection or to peruse sets of events; see Sect. A7.5.1.
- *Supporting software* encompasses software that is so often used that anyone engaging in detailed scientific research using AIA imagery will almost certainly need it. Examples include field-line extrapolation algorithms, loop-tracing algorithms, and thermal-analysis software.

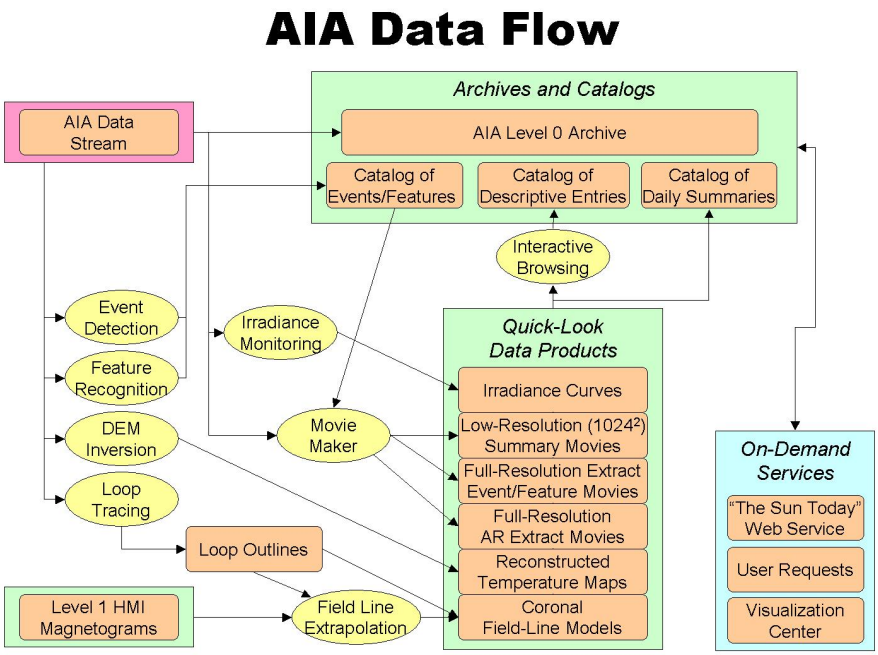


Figure A15: *Concept of the flow of AIA data for daily processing and evaluation.*

## A6.1 Data products

### A6.1.1 Near-real time

We anticipate that the following data products will be made available on the web within no more than 5 minutes following the receipt of the data at the Science Operations Center, based on automatic feature recognition software. This software will continuously query relevant external data sources, in particular the NOAA active-region and event listings.

1. Flare, filament eruption, CME, and other event listings.
2. Irradiance curves for each of the wavelength channels.

We plan to support an automated email distribution list to which interested parties can subscribe. The subscriber would select the types of events to which he would like to be alerted. When such an event is detected by the "sentinel software," email alerts will be automatically sent in parallel to the updating of the web summaries, based on the examples in Figs. A16 and A18.

### A6.1.2 Other products

Within a day of observations, the following products are expected to be generated, based on the entries into the event catalogs either by the automated feature recognition software, or the "observer of the day," or "duty scientist" (cf., Fig. A15):

1. Low-resolution summary movies of the entire FOV ($512 \times 512$)
2. Full-resolution cutout movies of all identified active regions ($5 \times 5$ arcmin).
3. Summary movies of other identified events, including filament destabilizations, CMEs, ....
4. "The Sun today" summary page (archived) which provides access to all generated movies.

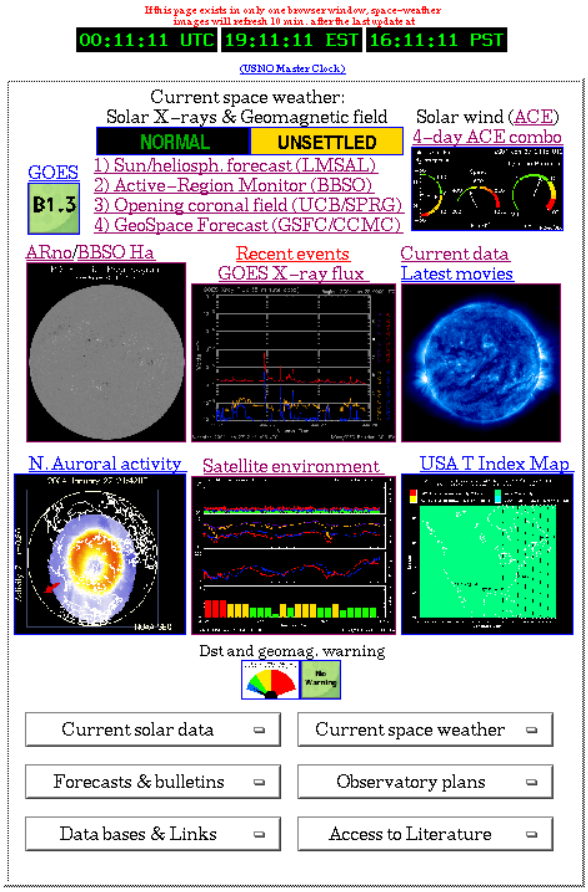


Figure A16: *Solar and space weather "station" (http://www.lmsal.com/solarsites.html). A similar page will be developed for the AIA data, including flare and other event flags, irradiance curves, full-disk images, and relevant space-weather related information. The contents of that page would be updated whenever new information becomes available, no slower than once every five minutes.*

Table A5: AIA data products.

| Level | Access | Description | Public release |
|---|---|---|---|
| | | **Observations** | |
| 0a | Team | Raw telemetry | N/A |
| 0b | Team | Science and engineering data with units separated by channel | N/A |
| 0c | Public | Quick-look image products (DN/s, despiked); sample movies | Near real time |
| 1 | Public | flat-fielded, despiked, deconvolved, calibrated image data | Next day |
| | | **Catalog data** | |
| 0 | Public | Automatically-generated event lists | NRT to next day |
| 1 | Public | Observer-annotated catalog entries | next day to week |

5. A few global differential emission measure inversions per day.
6. A few global potential-field models per day.

## A6.2 Catalogs

The AIA science team recognizes that the production of catalogs is of crucial value to the project. The catalog should enable the identification of particular phenomena based on quantitative search criteria; only if similar phenomena can be found in an archive can comparative studies be based on substantial samples of events.

The catalog needs to be generated by a combination of automated feature-recognition software and descriptive impressions entered by one or more observers. This need is a consequence of the high data rate: the observations need to be evaluated fast in order to keep up with the observations. Ideally, one SDO-wide catalog would be generated, basing results on magnetograms, seismograms, and (E)UV imagery.

The automated event-flagging and cataloging software needs to (1) take input from various web resources (e.g., the NOAA event listings and active-region listings), (2) combine that with the set of observations for a given time interval, and (3) compare that to earlier observations to establish differences, and - where possible - compare with model extrapolations to establish deviations from the expected images (for example, to detect emerging flux, or to flag the appearances and disappearances of sunspots or substantial changes in sunspot geometries). Examples are listed in Table A6.

On a day-by-day basis, all observations will be viewed by one or more observers. They will screen summaries of full-disk data and pre-made full-resolution movies based on the first pass through the event-flagging algorithms. A functioning prototype of such an interface to the data is run under SolarSoft IDL, and can be viewed http://www.lmsal.com/solarsoft/last_events/. The observations are also to be compared with model results, including model field extrapolations, coronal-hole modelling, and solar-wind models. A functioning prototype of this type of interface can be viewed http://www.lmsal.com/forecast/ under the links to under the heading 'Forecasts' and 'Summaries'. The AIA catalog can be queried to search for specific types of events, locations, times, or parts of the descriptive texts. A sample layout is shown in Fig. A17.

**Description of the event log generation:** Each day there will be 8 AIA movies running simultaneously containing the previous 24 hours of data, in parallel to an HMI magnetogram movie. All of these movies, and any additional windows described below, will be generated by an automated background script. We are planning to have partial-disk movies of the entire mission on line, so that the observer has the option to go back and look earlier developments. This process will ensure that all data are looked at and all events are recorded, including weekends and holidays.

These movies will have a standard control panel that will allow the observer to pause, rewind, fast forward and change the scaling of all movies as needed. Below the movie windows there will be a window which contains a general menu of typical solar type phenomena. The menu will consist of descriptors such as "coronal holes," "coronal mass ejections," "filaments/prominences," and "waves/oscillations" (Table A6). The list can be appended to as needed. The observer can click on the appropriate menu entry to produce a linking option. This linking option will allow the observer to then click on the phenomenon in one of the movie windows. The location will then be recorded, as well as the date and time, and cutout images centered on the position will automatically be generated as visual aids in the catalog.

All of this information will then be transmitted to an output log so that the observer can verify (and modify or delete) the entry. Comments can then be added. When all entries have been verified, the observer can use a button to automatically append the entry to the event log, which serves as the basis for generating web pages in response to queries.

The event log will be web accessible and will contain all the recorded events and comments. For each event and comment there will be a cutout thumbnail image in each channel, as well as the full-disk image for context, and the corresponding magnetogram information. When accessing the catalog, the user can specify

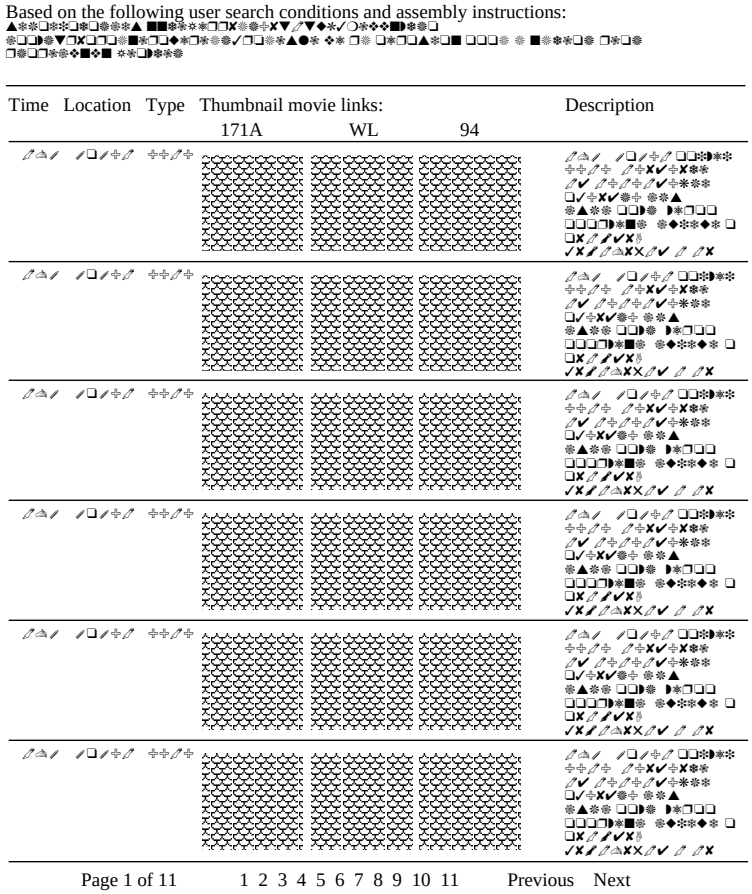


Figure A17: *Sample layout of a catalog search result: The AIA observing log can be queried to search for certain types of events, restricting locations, times, available wavelengths, etc. The results can be formatted by the user, including thumbnails of one or more wavelenghts that link to any existing movies in the daily summary pages.*

which channel(s) should show the thumbnail images.

Within the event log there will be an ”additional observations” button (with password protection, and an automatic entry of the user information with the log entry). Thus, data users can enrich the log, enter notes on supplementary data as well as publication records or other information. If desired, some images may be added to their entry, which will then also show up as clickable thumbnails linking to the higher-resolution originals.

In order to enable the generation of a useful and complete catalog, the following ingredients are essential, which are all being developed by separate projects associated with the AIA team. These include:

1. Automated interfaces to external web resources. The ability of the AIA datasystem to interact with others is a key ingredient for the overall LWS datasystem. The CoSEC project funded through the LWS TR&T program – and lead by AIA co-investigator, Neal Hurlburt – is developing a testbed environment for creating such a datasystem through the orchestration of web services. One of the tasks of this project is to work with the SDO instrument teams to guide their plans for connecting

Table A6: Partial list of AIA catalog entries; the list will grow in consultation with the AIA science team and scientific and space-weather user communities.

| Automated feature recognition | Observer annotation |
|---|---|
| Flares, ribbon patterns | Loop oscillation events |
| Flux emergence | Filament destabilizations/eruptions |
| CH boundaries (model vs. obs.?) | AR interconnection changes |
| AR thermal structure | Spot/pore evolution |
| AR/CH conjuctions | Unusual phenomena and field (re-)configurations |

to such a environment. In addition Co-I Joe Gurman is overseeing the development of the Virtual Solar Observatory and is available to assist in the integration of AIA catalogs into the larger solar community.

2. Feature recognition for sunspots and pores, flares, active regions, flux emergence, ... Leaders in these software tools are also members of the AIA Co-I team. Sam Freeland, through his NASA-supported work on SolarSoft, has deployed basic modules for identifying these features, and the European Grid of Solar Observations (EGSO) project, funded through an EU grant, has demonstrated that these modules can identify many of the required features. EGSO is based at MSSL, a Co-I institution and has partnerships with CoSEC and the Virtual Solar Observatory.
3. Advanced model for the photosphere- heliosphere coupling.
4. solar wind model to map wind at Earth (and STEREO?) back to the solar origins,

Several groups are pursuing these latter efforts, including the Solar MURI and the CISM projects, funded by the DoD and NSF respectively. Once again, members of our Co-I team, including Zoran Mikic, are intimately involved in these and related projects and will bring their results into the AIA plan.

### A6.3 Data archive

AIA data will be keep in an active archive managed by Stanford University in the Joint Science Operations Center (JSOC), which manages both the AIAand HMI datasystems. Full resolution AIA level-1 data will be stored near-line in a compressed format, with approximately the most recent 90 days and sub-sampled and clipped subsets of these data kept online. The images in these subsets will be processed preliminary level-1, using the best available calibration software at the time of data acquisition. All raw telemetry, level-0 data and calibration software will be backed-up onto high density tapes.

## A7 Required science infrastructure and a science operations center concept

### A7.1 Introduction

The successfull analysis of the AIA data requires close integration with the HMI investigation which provides the photospheric magnetic field maps. Together the two experiments generate about 112 Mbs (AIA: 67 Mbs, HMI: 50 Mbs), or 441 TB/yr. How can such a large amount of data be provided most efficiently to the science community?

The task of reducing and distributing the amount of data that SDO produces is significant. Fortunately we have experience developed over the past decade with Yohkoh, which produced 46 arc minute FOV soft x-ray images similar to some of AIA's EUV bands; eight years of EIT data, which produces full disk data

in many of the AIA spectral bands; six years of TRACE data, which produces EUV images with the same resolution as AIA over a much smaller field of view; and eight years of MDI data that produces line of sight magnetograms over the full Sun, but at lower resolution than HMI. All of these missions have made all of the data available via the web without constraint and have web based systems for distribution of software for data analysis and calibration. The archiving, software management, and data distribution as well as the local data analysis, have been done within the budgets allowed.

Whereas the total data volume appears very large, we realize that a much smaller subset of it is likely to be subjected to substantial analysis. We can derive an order of magnitude estimate based on the following arguments. Many processes of interest occupy only a small fraction of the solar surface and/ or occur only occasionally. To give some idea of the events that span the AIA investigation we consider the data implications for solar flares, which are reasonably local events, and coronal mass ejections (CME), which cover a significant fraction of the solar surface but occur less frequently. Flares occur in a range of sizes: C-class flares occur daily while giant-X flares occur only a few dozen times in a decade. The data system needs to be sized to manage the C-class flares because of their frequency. SDO with its high data rate and continuous coverage, will capture virtually all of these flares, while HMI will provide the associated magnetic data.

Small flares are usually contained in a $5 \times 5$ arcmin field of view, equivalent to 1.5% of the AIA FOV. In parallel to having access to a subregion at full resolution, scientific analysis will benefit from also having full-Sun coverage to check for large scale reordering of the loop structures. However, uses of the full disk data would usualy be satisfied with lower resolution images in a limited range of spectral bands. Even allowing for small flares to be in progress for 10% of the time, the full resoluton data plus full-disk context data would require at most significant data analysis of 0.2% of the AIA data set.

To provide access to the flare data we will expand upon a system currently in use. SolarSoft, our IDL-based software analysis package, has web pages that shows EIT movies for any given day and the GOES fluxes for the same day. All of the active regions are annotated on the solar images (see Fig. A18). For AIA primary support for active region studies could be a web page that provides images in all eight of the AIA bands, and corresponding line-of-sight and vector magnetograms from HMI taken within the last hour. In addition, annotated GOES and EVE plots for the past 24 hours could be displayed. By clicking on any of the AIA images, a $512 \times 512$ movie of the past 24 hours in that wavelength would be displayed. In addition, level-1 data for any of the active regions currently on the Sun will be available, and accessible, from the on-line archive. The active-region data would be centered on the active region and be tracked to the solar rotation rate at the center position. Line-of-sight magnetograms matched to the AIA data will also be available. The web page would allow the user to select any date and time period for both the Quick Look full disk movies and the active region extractions.

If we assume that on average 8 active regions are tracked, then 14% of the total AIA data will need to be stored to cover the evolution of all of these active regions. We believe that at least 90% of all active-region and flare studies can be carried out based on this subset of the full archive. If 10% of the active-region data were ”interesting” enough to warrent further study, this would represent less than 2% of the total AIA data, even with the full-disk context information included. In other words, less than 6 TB would be subjected to substantial analysis.

CME’s often cover about $50^\circ$ solid angle, and there are about 20 per month at solar maximum, ranging in in velocity between 200 and 600 km/s. Taking 200 km/s as the characteristic propagation speed, a CME takes about 3000 seconds to expand across the entire AIA field of view. If we require that we need access to all the AIA data during this time, then that requires about an hour at the full AIA data rate. At 20/month at cycle maximum, this amounts to about 2.8% of the total data volume, and substantiall less during solar minimum.

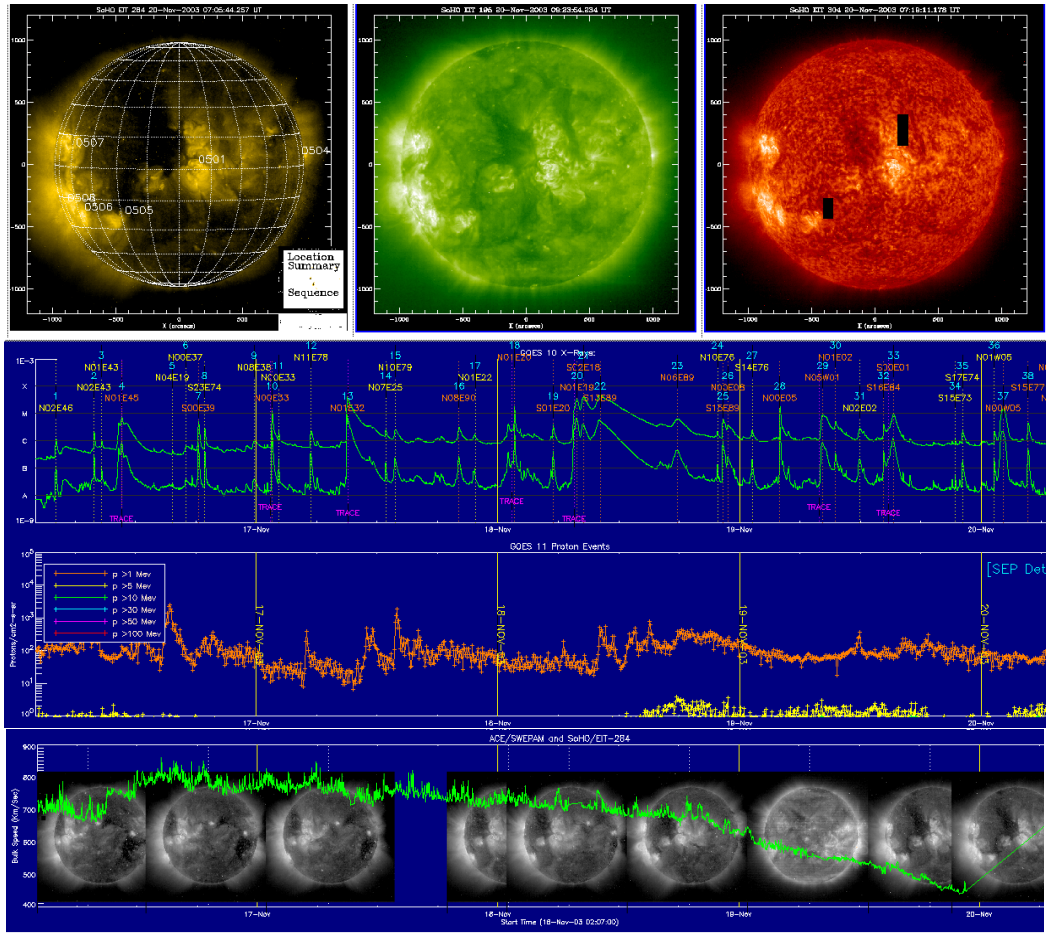


| Event# | EName | Start | Stop | Peak | GOES Class | Derived Position (SXI-GOES12 or EIT High Cadence Wavelength) |
|---|---|---|---|---|---|---|
| 1 | gev_20031116_0400 | 2003/11/16 04:00:00 | 04:13:00 | 04:07:00 | C1.1 | N02E46 |
| 2 | gev_20031116_0749 | 2003/11/16 07:49:00 | 07:58:00 | 07:54:00 | C1.9 | N02E43 |
| 3 | gev_20031116_0834 | 2003/11/16 08:34:00 | 08:43:00 | 08:39:00 | C1.0 | N01E43 |
| 4 | gev_20031116_1010 | 2003/11/16 10:10:00 | 11:16:00 | 10:39:00 | C7.0 | N01E45 |
| 5 | gev_20031116_1537 | 2003/11/16 15:37:00 | 15:44:00 | 15:40:00 | B4.7 | N04E19 |
| 6 | gev_20031116_1656 | 2003/11/16 16:56:00 | 17:25:00 | 16:59:00 | B6.5 | N00E37 |
| 7 | gev_20031116_1808 | 2003/11/16 18:08:00 | 18:21:00 | 18:16:00 | C4.9 | S00E39 |
| 8 | gev_20031116_1850 | 2003/11/16 18:50:00 | 18:58:00 | 18:53:00 | C2.6 | S23E74 |
| 9 | gev_20031116_2335 | 2003/11/16 23:35:00 | 00:05:00 | 23:48:00 | B9.9 | N08E38 |
| 10 | gev_20031117_0128 | 2003/11/17 01:28:00 | 01:39:00 | 01:34:00 | M1.2 | N00E33 |
| 11 | gev_20031117_0210 | 2003/11/17 02:10:00 | 02:17:00 | 02:13:00 | C2.2 | N00E33 |
| 12 | gev_20031117_0518 | 2003/11/17 05:18:00 | 05:37:00 | 05:27:00 | C2.2 | N11E78 |
| 13 | gev_20031117_0855 | 2003/11/17 08:55:00 | 09:19:00 | 09:05:00 | M4.2 | N01E32 |
| 14 | gev_20031117_1247 | 2003/11/17 12:47:00 | 12:57:00 | 12:52:00 | C2.5 | N07E25 |
| 15 | gev_20031117_1341 | 2003/11/17 13:41:00 | 14:01:00 | 13:49:00 | C2.5 | N10E79 |
| 16 | gev_20031117_2001 | 2003/11/17 20:01:00 | 20:16:00 | 20:08:00 | C3.1 | N08E90 |
| 17 | gev_20031117_2130 | 2003/11/17 21:30:00 | 21:54:00 | 21:45:00 | C1.7 | N01E22 |
| 18 | gev_20031118_0134 | 2003/11/18 01:34:00 | 01:42:00 | 01:39:00 | M1.8 | N01E20 |
| 19 | gev_20031118_0525 | 2003/11/18 05:25:00 | 05:35:00 | 05:30:00 | C3.8 | S01E20 |
| 20 | gev_20031118_0723 | 2003/11/18 07:23:00 | 08:06:00 | 07:52:00 | M3.2 | N01E19 |

Figure A18: *A partial snapshot of a example of a "recent-events page" as currently available on the web (http://www.lmsal.com/solarsoft/last_events/. We envision a similar AIA structure, with active links to summaries of events, active regions, etc.*

If, in addition, we keep all of the AIA data on line for a week and one data set per minute for a month, this requires 3.3% of the yearly database, or about 10 TB. In other words, if we keep adequate data on line for all flares, active regions, and CMEs, and the above extensive subset for the most recent period, this would add up to an on-line archive of order 20% of the full archive, or 80 TB/yr, of which eventually only a fraction will be analyzed.

### A7.2 Data access

A high-speed connection into the JSOC is critical to adequately process and analyze the AIA data at the tremendous ingestion rate. Our current concept, based upon the Storage Architecture Network (SAN) is to have the online AIA data stored physically at Lockheed Martin, but be logically within the JSOC for data management. This will provide the highest bandwidth between the data and the AIA analysis center, while maintaining strict data managment control (including backup and restoration) by the JSOC at Stanford.

We plan to store the level-0 data in the archive. When data are requested, one option available will be to request data processed to level-1, i.e., to data that are flat-fielded, deconvolved, and normalized; certain other steps will be implemented at the user's discretion, including correction for radiation hits on the CCD (de-spiking). The other option is to receive level-0 data, and use the processing software implemented as part of the IDL-SolarSoft package. An issue of concern, to be investigated further, is whether the IDL environment offers the required speed and security that all pipeline processing can be embedded within it. If not, dedicated C code will be developed, and run on the archive computer systems.

### A7.3 Analysis and visualization center

Within the context of the AIA investigation, we envision an analysis and visualization center that would serve as a base for researchers to browse through data, familiarize themselves with the solar processes as well as with the analysis tools, and to interact with other researchers. This center would contain display and computer systems to allow a few researchers at a time the full benefit of the high-resolution data from the past weeks, plus fast access to the data on all active regions, CME's, flares, and other events for which movies were made throughout the SDO mission. The center would provide tools for the efficient comparison and overlay of AIA and HMI data, as well as results from numerical models, such as model field lines, expected coronal-hole boundaries, etc.

The analysis and visualization center serves a number of purposes, in which often the same tools can be used for operations and data inspection as for later scientific analysis:

1. generate catalog information that is attached to the level 1 data that aids in the recognition of physical phenomena on the Sun;
2. allow a near- realtime assessment of Solar Phenomena;
3. evaluate new image displays that highlight solar phenomena;
4. provide displays and visualization tools for scientific analysis;
5. access other data sets from ground and space to aid in scientific interpretation of LWS processes;
6. provide an environment for scientific analysis by the PI and Co-I teams as well as visitors from the science community;
7. provide a training venue for scientists who wish to develop additional skills in the utilization of the HMI/AIA data;
8. provide a center for showcasing the SDO data to the science community, the international media, and for educational outreach;
9. provide a development tool for "shows" for use in science exhibits, museums, and planetaria.

### A7.4 Visualization tools

To achieve the objectives of the Analysis center requires the development of several software tools. These include the automatic feature and event detection software discussed in Sec.A6.1. Tools for integration into the larger LWS datasystem are described in Sects.A7.7 and A7.8. Here we focus on the visualization tools which will augment both the realtime data analysts functions and the full exploitation of the AIA datasets.

The quick, visual capture of events and features will be aided first through the extensive use of recent movies. Software will automatically create and update the past 24-36 hours of incoming data, and present it to the analysts on a multi-screen HDTV display. When a feature is identified through automated means it will also be highlighted on the display for confirmation. The analyst will be able to select any of these movies at anytime for full screen analysis and the software will reconfigure the multi-screen display to create a single, 16 megapixel screen, and can pan and zoom to thoroughly analyze interesting regions. These techniques have already been demonstrated on solar data sets using linux-based clusters ([93]; http://www.nas.nasa.gov/Groups/VisTech/hyperwall) and similar approaches are being explored within Lockheed Martin [94].

To further aid the analyst, we require quick field extrapolations that can be merged and overlaid on the AIA data. Initially these will consist of potential field extrapolations from the HMI longitudinal magnetograms. These tools are already available and are being used as part of the Virtual Star Lab (http://www.lmsal.-com/forecast/; [9]).

Aside form the initial cataloging of the images, detailed scientific analysis of the most recent few months of data, and other selected times, will also make use of the visualization center. These research efforts will require similar, but more computationally-demanding analysis, such as field extrapolations based upon full MHD models of the field derived from HMI vector magnetograms and photospheric flow maps, and realistic renderings of these fields using various models of coronal heating. These tools are being developed by the AIA Co-I team and will be imported into the visualization center as they mature.

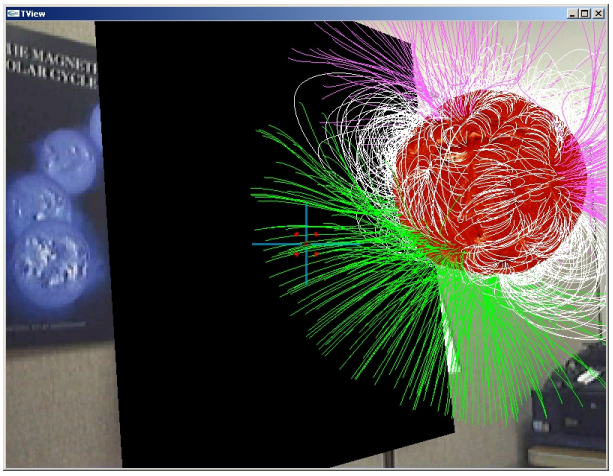

Figure A19: *An example of field visualization. A pilot project within LMATC involves rendering the 3D coronal field in an environment where a researcher can 'walk around' the Sun, or 'pick it up and turn it over', wearing goggles that display an object as if suspended within the room. Overlays, cuts, and combinations with other information can then be made.*

As part of the visualization system, we are studying whether a real-time 3D visualization system is helpful, for example, to understand the topology of the (evolving) magnetic field. An example is shown in

Fig. A19.

Table A7: Identification of software needs for AIA pipeline processing in the order of processing.

| | |
|---|---|
| 1) Decompression | 2) Artefact correction (“despiking”) |
| 3) Dark-current removal | 4) Readout pedestal removal |
| 5) Flat Fielding and normalization | 6) MTF deconvolution |
| 7) Lossless recompression | 8) Feature recognition and cataloging |

## A7.5 Supporting software

### A7.5.1 Data-browsing Software

Many ideas and insights arise from simply browsing through time series of data, and consequently it will be useful to have a way to quickly find, load, and animate blocks of data for interactive use. The capability to overlay distinct datasets is also expected to be of use. At LMSAL, the framework for such software already exists in the form of the ANA Browser, a GUI-based platform from which cubes of image data can be loaded into computer memory and then animated, sliced, and otherwise processed in a fast, interactive manner. ANA is also extensible, in that research-specific software can be written and interpreted by ANA; however, the science team suspects that the more established IDL will be utilized for this purpose instead of ANA. At present, ANA is unsupported outside of LMSAL. If it were to be used by the AIA community, it would require the development of AIA-specific routines, followed by software support and documentation.

Table A8: Identification of software needs for AIA data analysis past the pipeline processes. Priorities: P - highest, p - highly desirable, + - useful. Note that tasks B, C, or D often require that advances are made in preceding tasks. Software needs in bold face are considered part of the core AIA investigation; others are expected to be developed in parallel.

| | Objective 1 Energy input, storage, . . . | | | | Objective 2 Heating and irradiance | | | | Objective 3 Transients | | | | Objective 4 Connections to Geospace | | | | Objective 5 Coronal seismology | | | |
|---|---|---|---|---|---|---|---|---|---|---|---|---|---|---|---|---|---|---|---|---|
| | A | B | C | D | A | B | C | D | A | B | C | D | A | B | C | D | A | B | C | D |
| *CME prop. model* | | | | | | | | | | | | | | | P | | | | | |
| *Evolv. field (MHD)* | + | + | P | | | | P | | | P | P | P | P | P | | P | | P | p | P |
| **Feature recognition** | | | | | P | | | | P | | | | | | | | p | P | | |
| **Field surface dispers.** | P | P | | | | | | P | | | | P | P | P | P | P | | | | |
| *Field topology* | p | P | P | | | | | | P | | | | p | | | | | | | |
| **Field visualization** | P | P | P | | | | | | | | P | | P | | P | | | | P | |
| **Force-free field** | P | P | P | | | | | | | | P | P | P | | | | | P | p | P |
| *Helicity measurement* | P | P | P | | | | | | P | | | | | | | | | | | |
| *Loop atmosphere* | + | | | | | P | P | | | | | | | | | | | | | |
| **Loop fitting** | P | | | | | P | | | | | | | | | | | | | | P |
| **Movie “browser”** | P | P | P | P | P | p | | | P | p | P | | | | | | P | | | |
| **Potl-Fld Source-Surf** | P | P | | | | | | P | | | | P | p | | | p | | | | |
| *Solar-wind model* | | | | | | | | | | | | | | P | | | | | | |
| *Stereosc. inversion* | p | | | | | | | | | | | | | | | | | | | |
| **Thermal analysis** | P | | | | | P | | | | P | | | | | | | | | P | |

### A7.5.2 Supporting Analysis Software

Supporting software encompasses common data-processing routines that will be frequently used by diverse groups of researchers analyzing the AIA data. The ubiquitous nature of these algorithms coupled with the high data rate strongly suggest that such software be standardized and optimized for performance, and at the same time be widely available for use by the community. The supporting software will be kept up by the AIA science software team, and will be available to the general community via the AIA data center as part of the LWS data analysis system (see §6.6 and §6.7). In addition the source code will be made available through the existing SolarSoftWare (SSW) framework. We expect the following analysis routines to fall into this category:

- *Subregion tracking* routines will perform the extraction and remapping of localized regions of interest, enabling closer study of phenomena occurring on small scales.
- *Coronal loop recognition algorithms* are software routines that can trace the spines of obvious coronal loops in each EUV image. Loop locations will be useful for footpoint tracking studies, comparisons with model coronal magnetic fields, and loop oscillation and coronal seismology studies. The AIA team will develop at least an interactive (point-and-click) software tool to trace coronal loops within AIA images. The software allows the user to click on a loop within an image or set of images in different passbands. The program produces two curves outlining the loop from footpoint to footpoint. The user can manually adjust these curves by clicking on a point and dragging it to its desired position. We will attempt to develop more automated algorithms to automatically trace loops (possibly as initial guesses for the more interactive version described earlier). Either program will also measure loop photon count per pixel within each passband and correct the results for background emission (using a user-specified control region within each image).
- *Field-line extrapolation software* includes relatively straightforward, approximate methods that compute the magnetic field in the coronal volume using photospheric and chromospheric data as boundary conditions. Additionally, EUV data can be used as a constraint. Such magnetic fields will be useful for topology evolution studies, comparisons to coronal loops, studies of eruptive events, mapping of magnetic free energy, loop heating and cooling studies, models coupling the corona to the heliosphere, etc.
- *Topological feature recognition algorithms* identify critical points and surfaces in a vector field. As applied to coronal magnetic field extrapolations, such software will locate field nulls, separator lines, and separatrix surfaces in the coronal volume, which are thought to be the locations of rapid field reconnection, energy transfer, and particle acceleration. In addition, MHD instabilities may manifest themselves more strongly in these regions, generating waves that propagate throughout the corona.
- *Computation of the coronal thermal structure* will enable a study of the structure and evolution of the thermal properties of the solar corona (see Sect. A3.2). The set of EUV iron lines selected for AIA covers the thermal region of interest, and although only a limited set of spectral windows can be used, the advantage of AIA is that this method can be applied to the entire corona at any given instant, whereas a spectrograph would have to raster. Such analyses will be vital to our understanding of coronal heating mechanisms and in simulating the irradiance of the corona. The DEM inversion can be applied to any segment of an image, including the paths of specific loops as selected, or even traced, by the user. This program will produce the pixel-by-pixel DEM information that best fits the background subtracted loop emission, according to a number of selectable criteria. The program will also give estimates of the undertainty in the thermal structure. A prototype of such a code was demonstrated at the October 2003 AIA science meeting.

- *Common visualization tasks*, such as field line drawing, topological surface rendering, and volume renderings of model emission, are also expected to be widely used by the research community, and thus would also fall into the supporting software category. As part of this task, the AIA team will develop software tools for the comparison of 3D magnetic models with solar image data (including AIA and HMI images). This includes (1) the tracing of magnetic field lines passing through user-defined "starting points" within the 3D model; (2) plotting field lines from arbitrary viewing angle to visualize the 3D structure; (3) overlay projected field lines onto AIA images for comparison with observed loop and filament structures; (4) locate and plot "dips" in field lines. It shall also be possible to overlay field lines onto movies of AIA images (correcting for solar rotation), and to visualize a series of 3D models representing the corona at different times.

The AIA science team intends to embed the data processing and analysis software within the SolarSoft environment of IDL. The very large data flow rate requires that the routine data processing codes are optimized and vectorized where possible; maintenance of an optimal performance requires strict control of the software within the SolarSoft environment: only very few individuals should be able to modify the codes.

## A7.6 Theory and modelling software

The scientific topics covered by the AIA investigation preclude that all desirable theory and modeling software be developed within the program. We envision that at least two such research paths be pursued, at least in part within the AIA project: loop-atmosphere models and magnetic field models.

### A7.6.1 Loop-atmosphere Models

The AIA team will develop a software interface with existing loop hydrodynamics codes (such as the NRL code which is currently being modified for public release). This interface program will allow the user to define the coronal heating rate and loop geometry. It will take input from a loop tracing code, or from a coronal-field model. The program will produce temperature, density, gas pressure, flow velocity and energy fluxes (conduction, enthalpy flux) as functions of position along the loop. The program will also predict photon count rates per pixel in each AIA passband, and compare the results with the observed count rates.

We envision that full forward modeling of (part of) the solar corona, using field models and loop-atmosphere models, will eventually be developed; in fact, initial such models already exist in groups at SAIC, UCB, LMATC, and Kopenhagen. But for high-fidelity modeling of large-area, high-resolution images such as provided by AIA, the speed of the loop-atmosphere codes will need to be increased by several orders of magnitude. This may be achievable through code improvements, computer advances, or - more likely - the use of many-processor devices. Whereas we see this as an important validation effort for AIA knowledge, this effort will likely have to be funded through other channels than the AIA project itself.

### A7.6.2 Magnetic Field Models

The AIA team will develop software tools for the construction of three-dimensional (3D) models of the coronal magnetic field, and for comparison of such models with AIA images. The models will be based on measurements of the photospheric or chromospheric magnetic field taken at one instant of time. Four types of models will be considered:

1. Potential field models based on the radial magnetic field at the coronal base; this will be a general utility, part of the 'supporting software.'

2. Nonlinear force-free models based on the vector field at the base. At present such models are viewed as 'research projects,' because they exist only in rudimentary form and are slow to run. If substantial progress in this area is made over the coming years, this type of modeling will be used as 'supporting software.' Otherwise, it will be viewed as a modelling effort, the pursuit of which would be a priority of the team, funded either directly or with funding sought via other channels. Note that we see this as one of the highest-priority modelling investements, which we will pursue prior to launch as much as possible given the tight budget.
3. Field-distortion models obtained by perturbing an existing magnetic model (e.g., potential field) until the field-line structure of the model agrees with the observed loop structures seen in AIA images. Early versions of this type of modeling exist [8] but substantial advances in methodology, speed, and assimilation of observed coronal configurations are required.
4. Models in which a magnetic flux rope is inserted along the neutral line to reproduce an observed filament.

The model construction software will accept magnetograph data from a variety of sources, including HMI. The software will allow the user to select a region of interest on the photosphere (image plane or longitude-latitude grid), extract the relevant magnetic data ($B_r$ or $\mathbf{B}$), correct for projection effects, and if necessary embed the data into a larger magnetic map of the entire sun (based on measurements taken at earlier times). The output will consist of the magnetic field $\mathbf{B}(\mathbf{r})$ on a 3D grid in longitude, latitude and radius, representing all or part of the solar corona.

Modeling the time-dependent structure of the coronal magnetic field $\mathbf{B}(\mathbf{r}, t)$ and velocity field $\mathbf{v}(\mathbf{r}, t)$ is beyond the scope of the AIA project. However, the AIA Team will define a flexible, standardized file format for the storage of 3D magnetic models, and will provide the basic software necessary for reading such files into IDL. This will allow any 3D magnetic model to be compared with AIA image data. The display software will include the capability to follow particular field lines in time (by moving the "starting points" of the field lines in accordance with the plasma velocity).

### A7.7 Web environment

All AIA data and documentation will be accessible on the web. The top-level SDO web page at LMSAL (at http://sdo.lmsal.com/) will provide access to

1. **solar and space weather area** that contains, e.g.,
   - "the Sun today," with movie summaries (also used by observation planners and data evaluators compiling the event catalog),
   - event lists and visualizations,
   - (access to) data products requested by the user community,
   - forecasts of photospheric, coronal, and heliospheric conditions,
   - E/PO information and links.
2. **science investigation areas** for AIA and HMI (and EVE?) that contain, e.g.,
   - science plans,
   - science presentations,
   - meeting announcements, information, summaries
3. **instrument areas** for AIA and HMI (and EVE?) that contain, e.g.,
   - descriptions and "manuals" of instruments, data, and software packages,
   - the data-analysis guide

4. **operations areas** for AIA and HMI (and EVE?) that contain, e.g.,
   - logs and visualizations of observing plans,
   - descriptions of observing modes,
   - descriptions of science plans for special purpose modes,
5. **data areas** for AIA and HMI (and EVE?) that contain, e.g.,
   - catalogs
   - data archive,
   - search tools
6. **results pages** with, e.g.,
   - science nuggets,
   - press releases,
   - (links to) publications,
   - (links to) images and movies of observations, models, and comparisons
7. password-protected **team areas** for AIA and HMI that provide access to, e.g.,
   - instrument documentation subject to ITAR or other restrictions on general distribution,
   - email exploders and archives,
   - instrument status pages and logs
8. **related links** to, e.g.,
   - VSO, COSEC, etc.,
   - other observatories,
   - other resources related to LWS and solar and heliospheric physics.

All pages should be user and system friendly, i.e., work with multiple versions of web browsers, with minimal overhead for transfer across slow connections.

The science team will make as much of the instrument documentation available as possible within legal boundaries.

## A7.8 External data interfaces

There will be two principal routes for external users of the AIA data: a Web interface for interactive data requests, and a Web service for interfacing with other systems on the Internet, e.g. the Virtual Solar Observatory (VSO).

### A7.8.1 Web interface

Interactive data requests through the Web interface will be able to select data based on time, wavelength(s), and event criteria. Events could include solar events such as flares, coronal mass ejections (CME's), and eruptive prominences; spacecraft events such as roll maneuvers, and other events as noted in AIA databases, such as observer's logs. Since solar events are likely to be noted in external databases, however, it is probably not efficient for the AIA team to attempt to duplicate those event databases, but rather to interface with them for a compound query. The most efficient method for doing so in the SDO era will be compound data services (see Sect. A7.8.2).

Simple Web interfaces for searching solar EUV imaging instrument databases already exist for TRACE (http://vestige.lmsal.com/TRACE/DataCenter?cmd=home&loc=west) and SOHO EIT (http://umbra.nascom.nasa.gov/eit/e catalog.html). With the exception of the larger number of wavelengths, the AIA interface could be nearly identical to either of these (see Fig. A20 and A21).

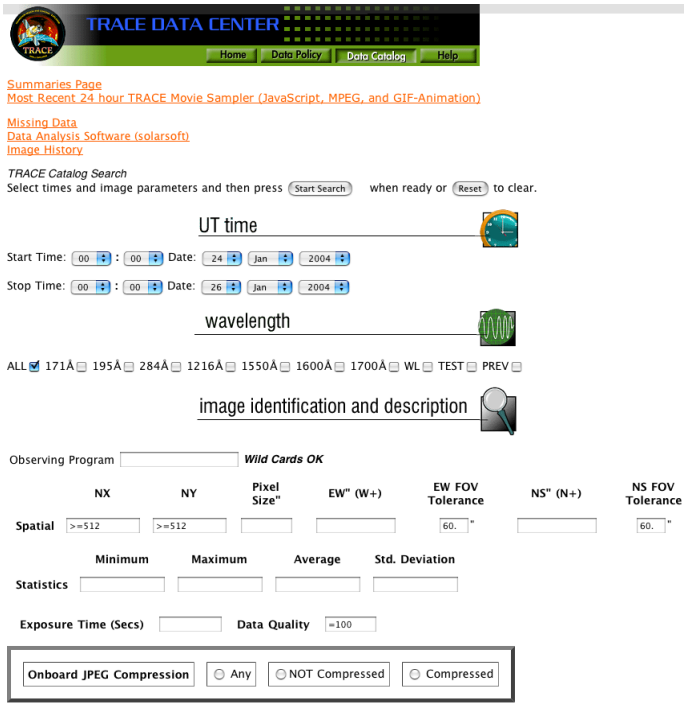


Figure A20: *The TRACE Data Center Web interface; simple yet exhaustive.*

The data delivery interface employed by both TRACE and EIT Web interfaces is a compressed archive (”tarball”) of the requested files, either downloadable or, if the requested volume is over some PI team-configurable limit, delivered on removable media. Clearly, data volume is a concern for the AIA data requests, but growing network bandwidth to most universities and government labs will offset much of the increase. Inexpensive removable media such as DVD(+/- R[W]) are also growing in capacity, and should allow the delivery of tens to hundreds of Gbyte of data in a timely fashion. Finally, continued drop in hard drive prices makes delivery of data on external hard drives with FireWire or USB 2.0 interfaces (or their successors) with volumes of 300 Gbyte and up may be a practical delivery model for occasional, large data requests.

### A7.8.2 Web service interface

Just as humans interact with the Web via the rendering of object in HTML documents, so machines can interact over the Internet by offering ”Web services” that allow communication between machines. This is the method, for instance, by which credit card authentication occurs, unseen by the human user, during a commercial transaction on a Website.

Web services are at the heart of virtual observatory efforts such as the Virtual Solar Observatory (VSO; funded by NASA), the European Grid of Solar Observations (EGSO; funded by the European Community, but with US and participation as well), and the Collaborative Sun-Earth Connector (CoSEC; funded by LWS

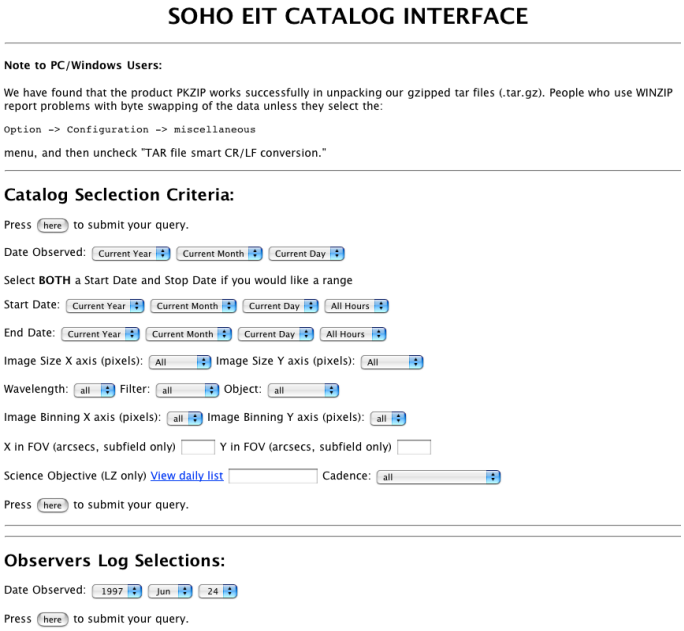


Figure A21: *The SOHO EIT Web catalog: a slight elaboration is the link to a local subset of an external science objective database. In addition, the observer's log can be searched for specific phenomena, but only by date.*

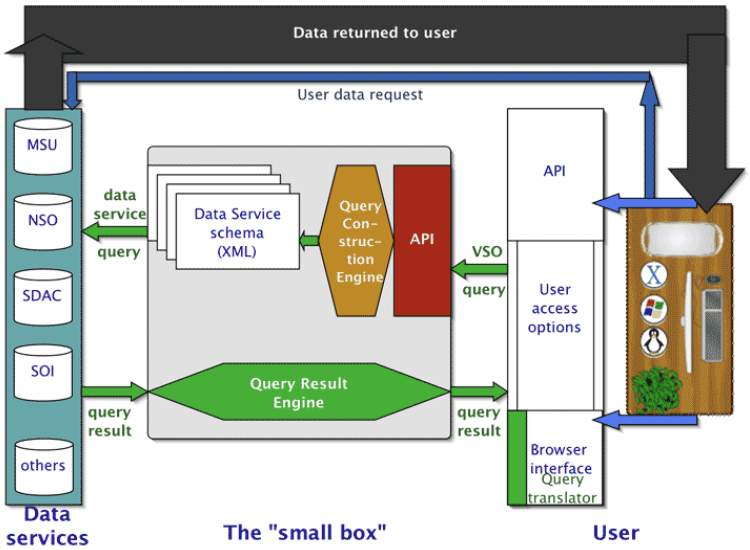


Figure A22: *A conceptual model of the Virtual Solar Observatory: a user (right) initiates a data request based on various metadata (time, wavelength, etc.), which the VSO ("small box" in center) farms out to the appropriate data service (left) - which will include the AIA archive in Phase E and beyond - and returns the responses to the user. After possible further refinement of the data selection, the user is able to request data directly from the data service.*

TR&T). The VSO further, is expected to be part of a wider, SEC-wide effort to implement first discipline-specific virtual observatories, then a meta-virtual observatory combining them to allow scientists in the various disciplines to access relevant data from sister disciplines without requiring intimate knowledge of

instruments and analysis methods.

The VSO, which is currently in initial beta testing, is a straightforward example of the use of Web services to allow the discovery, selection, and delivery of data.

Data delivery in the VSO occurs just as it would from a direct Web interface to the individual data service (see Sect. A7.8.1, above); thus, the AIA team will not need to implement any additional data delivery services to allow VSO users to access AIA data.

What the AIA team will need to implement to enable VSO access is a SOAP (Simple Object Access Protocol) server that is able to access the same database front-end as is accessed by the Web interface to the data. Such servers have already been implemented at the Solar Data Analysis Center (SDAC) at NASA Goddard, the National Solar Observatory (NSO) Digital Library, Montana State University, and Stanford University's solar archive, which includes tens of Tbyte of SOHO MDI data and related helioseismology and solar magnetogram field data. The SOAP servers are written in the widely used perl language.

Once these interfaces are in place, the AIA data center can participate in more complex forms of interactions, including virtual processing pipelines built from the core web services. The compound query mentioned in section 6.7.1 is one example of this. The CoSEC project has developed operational prototypes of such "orchestrated" web services (see http://cosec.lmsal.com). A more refined CoSEC testbed will be operational in 2005 and will be made to work with AIA web services.

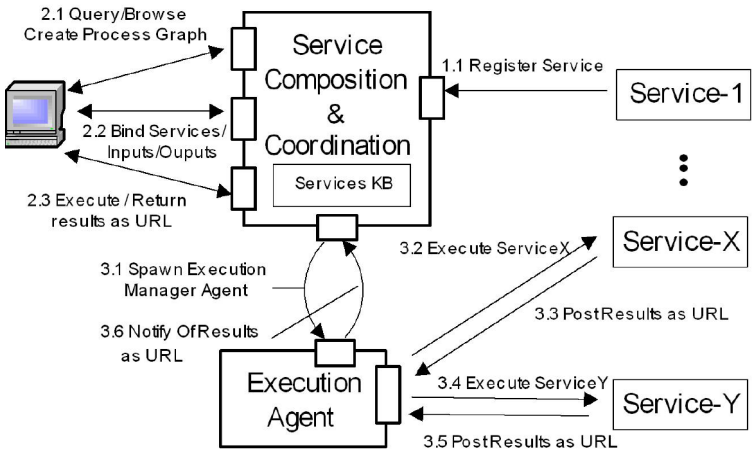


Figure A23: *CoSEC is based on a web-service model, building upon both commercial standards and DARPA-funded software agent technology. Software and data sources can publish their services through a service composition agent. This agent assists user to compose complex combinations of these services to locate, extract and process data for their research.*

## A8 References

[1] C. J. Schrijver, A. M. Title, T. E. Berger, L. Fletcher, N. E. Hurlburt, R. Nightingale, R. A. Shine, T. D. Tarbell, J. Wolfson, L. Golub, J. A. Bookbinder, E. E. DeLuca, R. A. McMullen, H. P. Warren, C. C. Kankelborg, B. N. Handy, and B. De Pontieu. A new view of the solar outer atmosphere by the Transition Region and Coronal Explorer. *SPh*, 187:261–302, 1999.

[2] M. J. Aschwanden, D. Alexander, N. Hurlburt, J. S. Newmark, W. M. Neupert, J. A. Klimchuk, and G. A. Gary. Three-dimensional Stereoscopic Analysis of Solar Active Region Loops. II. SOHO/EIT Observations at Temperatures of 1.5-2.5 MK. *ApJ*, 531:1129–1149, 2000.

[3] G. D. Holman and M. R. Kundu. The microwave structure of hot coronal loops. *ApJ*, 292:291–296, 1985.

[4] J. W. Brosius, E. Landi, J. W. Cook, J. Newmark, N. Gopalswamy, and A. Lara. Measurements of 3-D Sunspot Coronal Magnetic Fields From Coordinated SOHO EUV and VLA Radio Observations. In *American Geophysical Union, Spring Meeting 2001, abstract #SH32C-02*, page 32C02, May 2001.

[5] J. W. Brosius, E. Landi, J. W. Cook, J. S. Newmark, N. Gopalswamy, and L. Lara. Measurements of three-dimensional magnetic fields from coordinated extreme-ultraviolet and radio observations of a solar active region sunspot. *ApJ*, 574:453–466, 2002.

[6] X. Zhao and J. T. Hoeksema. Predicting the heliospheric magnetic field using the current sheet-source surface model. *Adv. Space Res.*, 16:181–, 1995.

[7] T. R. Metcalf, L. Jiao, A. N. McClymont, N. Alexander, R. C. Canfield, and H. Uitenbroek. Is the solar chromospheric magnetic field force-free? *ApJ*, 439:474–481, 1995.

[8] G. A. Gary and D. Alexander. Constructing the Coronal Magnetic Field By Correlating Parameterized Magnetic Field Lines With Observed Coronal Plasma Structures. *SPh*, 186:123–139, 1999.

[9] C. J. Schrijver and M. L. DeRosa. Photospheric and heliospheric magnetic fields. *SPh*, 212:165–200, 2003.

[10] P. Démoulin, J. C. Henoux, C. H. Mandrini, and E. R. Priest. Can we Extrapolate a Magnetic Field when its Topology is Complex? *SPh*, 174:73–89, 1997.

[11] T. Amari, T. Z. Boulmezaoud, and Z. Mikic. An iterative method for the reconstruction of the solar coronal magnetic field. I. Method for regular solutions. *A&A*, 350:1051–1059, 1999.

[12] J. Lee, S. M. White, M. R. Kundu, Z. Mikić, and A. N. McClymont. ”A Test for Coronal Magnetic Field Extrapolations”. *ApJ*, 510:413–421, 1999.

[13] T. G. Forbes and L. W. Acton. Reconnection and Field Line Shrinkage in Solar Flares. *ApJ*, 459:330, 1996.

[14] D. E. McKenzie and H. S. Hudson. X-Ray Observations of Motions and Structure above a Solar Flare Arcade. *ApJL*, 519:93–96, 1999.

[15] J. A. Klimchuk. Post-Eruption Arcades and 3-D Magnetic Reconnection. In *ASP Conf. Ser. 111: Magnetic Reconnection in the Solar Atmosphere*, page 319, 1997.

[16] B. Kliem, M. Karlický, and A. O. Benz. Solar flare radio pulsations as a signature of dynamic magnetic reconnection. *A&A*, 360:715–728, 2000.

[17] T. Yokoyama, K. Akita, T. Morimoto, K. Inoue, and J. Newmark. Clear Evidence of Reconnection Inflow of a Solar Flare. *ApJL*, 546:69–72, 2001.

[18] M. Berger and G. B. Field. . *J. Fluid Mech.*, 147:133, 1984.

[19] P. Démoulin, C. H. Mandrini, L. van Driel, B. J. Thompson, S. Plunkett, Z. Kovári, G. Aulanier, and A. Young. What is the source of the magnetic helicity shed by CMEs? The long-term helicity budget of AR 7978. *A&A*, 382:650–665, 2002.

[20] R. C. Canfield, H. S. Hudson, and D. E. McKenzie. Sigmoidal morphology and eruptive solar activity. *Geophys. Res. Lett.*, 26:627, 1999.

[21] E. R. Priest and T. Forbes. *Magnetic reconnection*. Cambridge University Press, Cambridge, U.K., 2000.

[22] T. R. Metcalf and D. L. Mickey. The Magnetic Free Energy in Active Regions. *American Astronomical Society Meeting*, 31:992, 1999.

[23] C. Zwaan. A dynamo scenario. *SPh*, 169:265–276, 1996.

[24] A. Balogh, R. G. Marsden, and E. J. Smith. *The heliosphere near solar minimum: The Ulysses perspective*. Springer, London, U. K., 2001.

[25] D. J. McComas, J. L. Phillips, A. J. Hundhausen, and J. T. Burkepile. Observations of disconnection of open coronal magnetic structures. *Geophys. Res. Lett.*, 18:73–76, 1991.

[26] J. W. Bieber and D. M. Rust. The Escape of Magnetic Flux from the Sun. *ApJ*, 453:911, 1995.

[27] A. A. Pevtsov, G. H. Fisher, L. W. Acton, D. W. Longcope, C. M. Johns-Krull, C. C. Kankelborg, and T. R. Metcalf. The Relationship Between X-Ray Radiance and Magnetic Flux. *ApJ*, 598:1387–1391, 2003.

[28] J. L. Lean and A. Skumanich. Variability of the Lyman alpha flux with solar activity. *JGR*, 88:5751–5759, 1983.

[29] R. R. Meier. Ultraviolet spectroscopy and remote sensing of the upper atmosphere. *Space Sci. Rev.*, 58:1–185, 1991.

[30] J. L. Lean, J. Cook, W. Marquette, and A. Johannesson. ”Magnetic Sources of the Solar Irradiance Cycle”. *ApJ*, 492:390–401, 1998.

[31] H.P̃. Warren, J.T̃. Mariska, and J. Lean. ”A new model of solar EUV irradiance variability. 1. Model formulation”. *JGR*, 106:15,745–15,757, 2001.

[32] R. A. Harrison and A. M. Thompson. A study in preparation for the SoHO mission. Technical report, Science and Engineering Research Council, Rutherford Appleton Laboratory, Childon, Didcot, Oxfordshire, England, 1992. RAL-91-092.

[33] M. J. Aschwanden. Do EUV Microflares Account for Coronal Heating? *SPh*, 190:233–247, 2000.

[34] C. E. Parnell and P. E. Jupp. Statistical analysis of the energy distribution of nanoflares in the quiet Sun. *ApJ*, 529:554–569, 2000.

[35] M. J. Aschwanden and P. Charbonneau. Effects of Temperature Bias on Nanoflare Statistics. *ApJL*, 566:59–62, 2002.

[36] J. Lee, A. N. McClymont, Z. Mikic, S. M. White, and M. R. Kundu. Coronal Currents, Magnetic Fields, and Heating in a Solar Active Region. *ApJ*, 501:853, 1998.

[37] P. Riley, J. A. Linker, and Z. Mikic. An empirically-driven global MHD model of the solar corona and inner heliosphere. *JGR*, 106:15,889–15,902, 2001.

[38] B. V. Gudiksen and Å. Nordlund. Bulk heating and slender magnetic loops in the solar corona. *ApJL*, 572:113–116, 2002.

[39] T. E. Berger, B. De Pontieu, C. J. Schrijver, and A. M. Title. Imaging the structure and dynamics of the solar transition region. *ApJL*, 519:97–100, 1999.

[40] K. P. Dere, E. Landi, H. E. Mason, B. C. Monsignori Fossi, and P. R. Young. CHIANTI - An atomic database for emission lines. Paper I: Wavelengths greater than 50 Å. *A&AS*, 125:149–173, 1997.

[41] P. Démoulin, E. R. Priest, and D. P. Lonie. Three-dimensional magnetic reconnection without null points 2. Application to twisted flux tubes. *JGR*, 101:7631–7646, 1996.

[42] D. Alexander and L. Fletcher. High-resolution Observations of Plasma Jets in the Solar Corona. *SPh*, 190:167–184, 1999.

[43] N. V. Nitta and H. S. Hudson. Recurrent flare/CME events from an emerging flux region. *Geophys. Res. Lett.*, 28:3801–3804, 2001.

[44] M. J. Aschwanden, A. I. Poland, and D. Rabin. The new solar corona. *ARA&A*, 39:175–210, 2001.

[45] L. Fletcher and H. Hudson. The Magnetic Structure and Generation of EUV Flare Ribbons. *SPh*, 204:69–89, 2001.

[46] G. Kanbach, D. L. Bertsch, C. E. Fichtel, R. C. Hartman, S. D. Hunter, D. A. Kniffen, P. W. Kwok, Y. C. Lin, J. R. Mattox, and H. A. Mayer-Hasselwander. Detection of a long-duration solar gamma-ray flare on June 11, 1991 with EGRET on COMPTON-GRO. *A&AS*, 97:349–353, 1993.

[47] H. V. Cane. Using Type III Radio Bursts to Track Solar Energetic Particles. In *American Geophysical Union, Spring Meeting 2002, abstract #SH21D-04*, pages D4–+, 2002.

[48] S. K. Antiochos, C. R. Devore, and J. A. Klimchuk. A Model for Solar Coronal Mass Ejections. *ApJ*, 510:485–493, 1999.

[49] J. I. Khan and H. S. Hudson. Homologous sudden disappearances of transequatorial interconnecting loops in the solar corona. *Geophys. Res. Lett.*, 27:1083–1086, 2000.

[50] D. F. Webb and E. W. Cliver. Evidence for magnetic disconnection of mass ejections in the corona. *JGR*, 100:5853–5870, 1995.

[51] M. K. van Aalst, P. C. H. Martens, and Ã. J. C. Beliën. Can Streamer Blobs Prevent the Buildup of the Interplanetary Magnetic Field? *ApJL*, 511:125–128, 1999.

[52] R. Wolfson and B. Dlamini. Cross-Field Currents: an Energy Source for Coronal Mass Ejections? *ApJ*, 483:961, July 1997.

[53] C. J. Schrijver, A. M. Title, A. A. Van Ballegooijen, H. J. Hagenaar, and R. A. Shine. Sustaining the quiet chromospheric network; A dynamic balance of flux emergence, fragmentation, merging, and cancellation. *ApJ*, 487:424, 1997.

[54] Y.-M. Wang and N. R. Sheeley. Solar Implications of ULYSSES Interplanetary Field Measurements. *ApJL*, 447:143–146, 1995.

[55] H. B. Snodgrass, J. M. Kress, and P. R. Wilson. Observations of the Polar Magnetic Fields During the Polarity Reversals of Cycle 22. *SPh*, 191:1–19, January 2000.

[56] M. Schulz, E. N. Frazier, and D. J. Boucher. Coronal magnetic-field model with non-spherical source surface. *SPh*, 60:83–104, 1978.

[57] C. J. Schrijver. Simulations of the photospheric magnetic activity and outer-atmospheric radiative losses of cool stars based on characteristics of the solar magnetic field. *ApJ*, 547:475–490, 2001.

[58] A. J. Hundhausen. *Coronal Expansion and Solar Wind*. Springer-Verlag, Berlin, 1972.

[59] Y.-M. Wang and N. R. Sheeley. Solar wind speed and coronal flux-tube expansion. *ApJ*, 355:726–732, 1990.

[60] K. Hakamada, M. Kojima, M. Tokumaru, T. Ohmi, A. Yokobe, and K. Fujiki. Solar Wind Speed and Expansion Rate of the Coronal Magnetic Field in Solar Maximum and Minimum Phases. *SPh*, 207:173–185, 2002.

[61] C. N. Arge and V. J. Pizzo. Improvement in the prediction of solar wind conditions using near-real time solar magnetic field updates. *JGR*, 105:10465–10480, 2000.

[62] R. Schwenn. Relationship of coronal transients to interplanetary shocks 3D aspects. *Space Sci. Rev.*, 44:139–168, 1986.

[63] M. A. Lee and L. A. Fisk. Shock acceleration of energetic particles in the heliosphere. *Space Sci. Rev.*, 32:205–228, 1982.

[64] T. A. Kucera, V. Andretta, and A. I. Poland. Neutral hydrogen column depths in prominences using EUV absorption features. *SPh*, 183:107–121, 1998.

[65] W. D. Gonzalez, B. T. Tsurutani, and A. L. Clúa de Gonzalez. Interplanetary origin of geomagnetic storms. *Space Sci. Rev.*, pages 529–562, 1999.

[66] B. J. Thompson, J. S. Newmark, J. B. Gurman, O. C. St. Cyr, and S. Stetzelberger. SOHO/EIT and SOHO/LASCO Observations of the April 1 1997 Event: Coronal Observations of a Moreton Wave. *Bull. Am. Astron. Soc.*, 29:01.30, 1997.

[67] Y.-M. Wang and N. R. Sheeley. Observations of Core Fallback during Coronal Mass Ejections. *ApJ*, 567:1211–1224, 2002.

[68] D. J. Webster, J. C. Samson, and G. Rostoker. Eastward propagation of transient field-aligned currents and Pi 2 pulsations at auroral latitudes. *JGR*, 94:3619–3630, 1989.

[69] B. Roberts. Waves and Oscillations in the Corona - (Invited Review). *SPh*, 193:139–152, 2000.

[70] B. J. Thompson, J. B. Gurman, W. M. Neupert, J. S. Newmark, J.-P. Delaboudinière, O. C. St. Cyr, S. Stezelberger, K. P. Dere, R. A. Howard, and D. J. Michels. SOHO/EIT Observations of the 1997 April 7 Coronal Transient: Possible Evidence of Coronal Moreton Waves. *ApJ*, 517:151–154, 1999.

[71] C. J. Schrijver, M. J. Aschwanden, and A. M. Title. Transverse oscillations in coronal loops observed with TRACE: I. An overview of events, movies, and a discussion of common properties and required conditions. *SPh*, 206:69, 2002.

[72] M. J. Aschwanden, B. De Pontieu, C. J. Schrijver, , and A. M. Title. Transverse oscillations in coronal loops observed with TRACE: II. Measurements of Geometric and Physical Parameters. *SPh*, 206, 2002.

[73] B. De Pontieu, T. D. Tarbell, and R. Erdélyi. Correlations on arcsecond scales between chromospheric and transition region emission in active regions. *ApJ*, 590:502–518, 2003.

[74] I. De Moortel, J. Ireland, R. W. Walsh, and A. W. Hood. Longitudinal intensity oscillations in coronal loops observed with TRACE - I. Overview of Measured Parameters. *SPh*, 209:61–88, 2002.

[75] T. J. Wang, S. K. Solanki, W. Curdt, D. E. Innes, I. E. Dammasch, and B. Kliem. Hot coronal loop oscillations observed with SUMER: Examples and statistics. *A&A*, 406:1,105–1,121, 2003.

[76] M. J. Aschwanden, R. W. Nightingale, J. Andries, M. Goossens, and T. Van Doorsselaere. Observational Tests of Damping by Resonant Absorption in Coronal Loop Oscillations. *Astrophysics*, 598:1,375–1,386, 2003.

[77] A. Fludra. Intensity oscillations in a sunspot plume. *A&A*, 344:75–78, 1999.

[78] I. De Moortel and A. W. Hood. The damping of slow MHD waves in solar coronal magnetic fields. *A&A*, 408:755–765, 2003.

[79] D. B. King, V. M. Nakariakov, E. E. DeLuca, L. Golub, and K. G. McClements. Propagating EUV disturbances in the solar corona; two-wavelength observations. *A&A*, 404:L1–L4, 2003.

[80] E. Robbrecht, E. Verwichte, D. Berghmans, J. F. Hochedez, S. Poedts, and V. M. Nakariakov. Slow magnetoacoustic waves in coronal loops: EIT and TRACE. *A&A*, 370:591–601, 2001.

[81] T. J. Wang, S. K. Solanki, W. Curdt, D. E. Innes, and I. E. Dammasch. Oscillating hot loops observed by SUMER. In *ESA SP-508: From Solar Min to Max: Half a Solar Cycle with SOHO*, pages 465–+, Noordwijk, The Netherlands, 2002. ESA.

[82] V. M. Nakariakov, L. Ofman, E. E. DeLuca, and J. M. Davila. TRACE observations of damped coronal loop oscillations: implications for coronal heating. *Science*, 285:862–864, 1999.

[83] L. Ofman and M. J. Aschwanden. Damping Time Scaling of Coronal Loop Oscillations Deduced from Transition Region and Coronal Explorer Observations. *ApJL*, 576:153–156, 2002.

[84] C. J. Schrijver and D. S. Brown. Oscillations in the Magnetic Field of the Solar Corona in Response to Flares near the Photosphere. *ApJL*, 537:69–72, 2000.

[85] B. De Pontieu, P. C. H. Martens, and H. S. Hudson. Chromospheric Damping of Alfvén waves. *ApJ*, 558:859–871, 2001.

[86] M. S. Ruderman and B. Roberts. The Damping of Coronal Loop Oscillations. *ApJ*, 577:475–486, 2002.

[87] M. Goossens, J. Andries, and M. J. Aschwanden. Coronal loop oscillations. An interpretation in terms of resonant absorption of quasi-mode kink oscillations. *A&A*, 394:39–42, 2002.

[88] L. Ofman and B. J. Thompson. Interaction of EIT Waves with Coronal Active Regions. *ApJ*, 574:440–452, 2002.

[89] U. Feldman, P. Mandelbaum, J. F. Seely, G. A. Doschek, and H. Gursky. The potential for plasma diagnostics from stellar extreme-ultraviolet observations. *ApJSS*, 81:387–408, 1992.

[90] P. Mazzotta, G. Mazzitelli, S. Colafrancesco, and N. Vittorio. Ionization balance for optically thin plasmas: Rate coefficients for all atoms and ions of the elements H to NI. *A&AS*, 133:403–409, 1998.

[91] J. S. Newmark, J. W. Cook, F. Auchere, J. D. Moses, and F. Clette. In-flight Calibration of SOHO EIT. *AGU Spring Meeting Abstracts*, pages 21–+, 2001.

[92] F. Auchére. *Contribution à l' Etude de l'H'elium dans la Couronne Solaire,*. PhD thesis, University of Paris - South, 2000.

[93] T. Sandstrom, C. Henze, and C. Levit. The hyperwall. In *International Conference on Coordinated and Multiple Views in Exploratory Visualization,*, pages 124–133. IEEE, 2003.

[94] R. A. Shine, N. Hurlburt, A. M. Title, and R. W. Nightingale. Visualizing and Interpreting Very High Resolution Solar Movies. *AGU Fall Meeting Abstracts*, pages A498+, 2002.

## List of Tables



## List of Figures

## List of acronyms and abbreviations

**AEC** Automatic exposure control
**AIA** Atmospheric Imaging Assembly
**AR** Active region
**ATST** Advanced Technology Solar Telescope
**CHIANTI** Atomic Database for Spectroscopic Diagnostics of Astrophysical Plasmas
**CoSEC** Collaborative Sun-Earth Connecter
**CH** Coronal hole
**CISM** Center for Integrated Space-weather Modeling
**CME** Coronal mass ejection
**DEM** Differential emission measure
**DoD** Department of Defense
**EGSO** European Grid of Solar Observations
**EIS** EUV imaging spectrometer
**EIT** Extreme-ultraviolet Imaging Telescope
**EUV** Extreme ultraviolet
**EUVI** Extreme-Ultraviolet Imager
**EVE** Extreme-ultraviolet Variability Experiment
**FASR** Frequency-Agile Solar Radio-telescope
**FOV** Field of view
**FPP** Focal plane package
**GOES** Geostationary Operational Environmental Satellite
**HMI** Helioseismic and Magnetic Imager
**IDL** Interactive data language
**ILWS** International Living With a Star program
**JSOC** Joint Science Operations Center
**LASCO** Large Angle and Spectrometric Coronagraph
**LMATC** Lockheed Martin Advanced Technology Center
**LOFAR** Low-Frequency ARray
**LWS** Living With a Star
**MEGS** Multiple Euv Grating Spectrograph
**MHD** Magneto-hydrodynamics
**MSSL** Mullard Space Sciences Laboratory
**MTF** Modulation transfer function
**MURI** Multidisciplinary University Research Initiative
**NASA** National Aeronautics and Space Administration
**NSF** National Science Foundation
**NSO** National Solar Observatory
**PSF** Point spread function
**SAIC** Science Applications International Corporation
**SDO** Solar Dynamics Observatory
**SDT** Science definition team
**S/N** Signal to noise ratio
**SOHO** Solar and Heliospheric Observatory
**SOLIS** Synoptic Optical Long-term Investigations of the Sun
**SOLSTICE** Solar stellar irradiance comparison experiment
**SSW** SolarSoftWare
**STEREO** Solar-Terrestrial Relations Observatory
**SUMER** Solar Ultraviolet Measurements of Emitted Radiation
**TRACE** Transition Region and Coronal Explorer
**TR&T** Targeted research and technology program of LWS
**UARS** Upper-atmospheric research satellite
**UCB** University of California, Berkeley
**UV** Ultraviolet
**VSO** Virtual Solar Observatory
**WL** White light, or visible light
**XRT** X-ray telescope